SAPIENZA
UNIVERSITÀ DI ROMA

SAPIENZA UNIVERSITY OF ROME

AND

UNIVERSITY OF ROME TOR VERGATA

PH.D. IN ASTRONOMY, ASTROPHYSICS
AND SPACE SCIENCE

CYCLE XXX

The dusty high redshift universe: the dust content and its effects in the first galaxies

Mattia Mancini

A.Y. 2016/2017

Supervisor: Prof. Raffaella Schneider

Coordinator: Prof. Roberto Capuzzo Dolcetta

Deputy Coordinator: Prof. Pasquale Mazzotta

[...] dà ancora uno sguardo fuori dalla finestra, una brevissima occhiata, per l'ultima sua porzione di stelle. Poi nel buio, benché nessuno lo veda, sorride.

[Il deserto dei tartari - Buzzati]

Abstract

The advent of the new Atacama Large Millimeter/submillimeter Array (ALMA) has opened a new window onto the high redshift Universe, shedding light on the cold interstellar medium (ISM) of normal star forming galaxies at redshift $z > 5$ [Capak et al., 2015, Watson et al., 2015, Knudsen et al., 2017, Barišić et al., 2017, Laporte et al., 2017b]. The information collected so far through observations that map the rest-frame emission in the ultraviolet (UV) and infrared (IR) have started to paint a complex picture: while the ALMA view of the Hubble Ultra Deep Field (HUDF) has detected the most massive star forming galaxies [Dunlop, 2016], with only one source at $z > 3.5$, reflecting the rapid drop-off of high-mass galaxies with increasing redshift, these sources may be simply the tip of the iceberg of a larger population of fainter dusty systems. These systems are very interesting as their star formation rates are comparable to those of UV selected galaxies. The comparison between faint dusty galaxies and the unobscured population may be key to understand the factors that determine the dust content in galaxies with comparable properties. Faint dusty star forming galaxies are difficult to detect, particularly at high redshift, and the only two sources that have been detected in their rest-frame IR continuum at $z > 6$ so far are gravitationally lensed: A1689-zD1, a magnified galaxy at redshift ~ 7.5 with an estimated dust mass of the order of $10^7 M_\odot$ [Watson et al., 2015, Knudsen et al., 2017], and the galaxy A2744 YD4 with $z = 8.38$ identified in the ALMA Frontier Fields, with an estimated dust mass of $\sim 6 \times 10^6 M_\odot$ [Laporte et al., 2017a]. These observations have shown that ALMA has the potential to detect dust emission at $z > 6$ and that future observations in conjunction with the upcoming *James Webb Space Telescope* will be able to trace the onset of chemical enrichment and the emergence of dust in the Universe.

In this original work, we have attempted to improve our understanding of the dust content and its effects in $z > 5$ galaxies. To accomplish this goal, we have combined the

information provided by multi-wavelength observations of high redshift galaxies with the results of cosmological hydrodynamical simulations [Maio et al., 2010, Dayal et al., 2014] coupled with a state-of-the-art chemical evolution model with dust [Valiante et al., 2009, de Bennassuti et al., 2014]. This semi-numerical model allows us to account for both dust production from stellar sources (Supernovae and Asymptotic Giant Branch stars) and for dust reprocessing in the ISM, including dust destruction in interstellar shock waves and grain growth in dense clouds.

In its first application, the model has been used to investigate the origin of the observed dust mass in the $z \sim 7.5$ galaxy A1689-zD1 [Watson et al., 2015, Mancini et al., 2015]. We find that while stellar sources dominate the dust mass of small galaxies, the higher level of metal enrichment experienced by galaxies with stellar mass $M_{star} > 10^9 M_\odot$ allows efficient grain growth, which provides the dominant contribution to the dust mass. Even assuming maximally efficient supernova dust production, the observed dust mass of the $z = 7.5$ galaxy A1689-zD1 requires very efficient grain growth. This, in turn, implies that in this galaxy the average density of the cold and dense gas, where grain growth occurs, is comparable to that inferred from observations of QSO host galaxies at similar redshifts [Valiante et al., 2009, 2012, 2014]. Although plausible, the upper limits on the dust continuum emission of galaxies at $6.5 < z < 7.5$ show that these conditions must not apply to the bulk of the high-redshift galaxy population. Indeed, more recent and deeper ALMA observations of A1689-zD1 suggest that the thermal dust emission comes from two spatial components, and that the morphological structure is similar to what is observed with HST, pointing to a perturbed dynamical state, perhaps indicative of a major merger or a disc in early formation [Knudsen et al., 2017].

We then extended the analysis to investigate how dust properties affect the appearance of galaxies in the redshift range $5 \leq z \leq 8$. Using a simple extinction model, we can relate the ISM dust content predicted for each galaxy by the model with direct observables [Bouwens et al., 2015, 2016], such as the number density of objects with a given UV magnitude (the UV Luminosity Functions, LF) and the magnitude dependence of their UV spectral slope β (the Color Magnitude Relation, CMR). In addition, our simple model allows us to estimate the infrared luminosity due to dust thermal emission. This provides additional constraints on the mass and properties of dust, given the possibility to compare

our predictions with the far infrared continuum emission from a sample of normal star forming galaxies at $z \sim 5$ [Capak et al., 2015, Barišić et al., 2017, Faisst et al., 2017].

We find that observations require a steep, Small Magellanic Cloud-like extinction curve and a clumpy dust distribution, where stellar populations younger than 15 Myr are still embedded in their dusty natal clouds. Investigating the scatter in the colour distribution and stellar mass, we find that the observed trends can be explained by the presence of two populations: younger, less massive galaxies where dust enrichment is mainly due to stellar sources, and massive, more chemically evolved ones, where efficient grain growth provides the dominant contribution to the total dust mass. Computing the IR/UV luminosity ratio (the so-called IRX) as a function of the UV colour β, we find that all but the dustiest model galaxies follow a relation shallower than the Meurer et al. [1999] one, usually adopted to correct the observed UV luminosities of high-z galaxies for the effects of dust extinction. As a result, using the Meurer et al. [1999] relation to infer the dust correction from a given value of β might lead to overestimate the star formation rate.

Finally, we compare our predicted IRX-β relation with observations of galaxies at $5.1 \leq z \leq 5.7$ by Capak et al. [2015], which have been argued to be significantly more dust-poor and less IR-luminous than lower z galaxies with comparable colours. We find that our simulated galaxies that follow a steep attenutation curve are marginally compatible with the ALMA detected sources by Capak et al. [2015], but that simulated galaxies with IRX compatible with the upper limits inferred for the ALMA undetected sources have significantly bluer colours than observed, consistent with their low dust content. Hence, our study confirms that it is difficult to explain the low IRX of the Capak et al. [2015] sources, unless their slopes have been overestimated or the dust temperature (hence the FIR flux) has been underestimated. Interestingly, both of these hypotheses have been recently confirmed by new observational works, that find systematically bluer colours [Barišić et al., 2017], and that normal high-redshift galaxies have a warmer infrared spectral energy distribution compared to average $z < 4$ galaxies that were used as prior in previous studies [Faisst et al., 2017]. These new data relieve some of the tension between theoretical predictions and observations [Mancini et al., 2016, Narayanan et al., 2017].

The thesis is organized as follows: in Chapter 1 we present some basic properties of the ΛCDM cosmological model, we review our current understanding of the formation of the

first stars and galaxies, and the best observational strategies that have been used to detect galaxies at $z > 5$ with current observational facilities. In Chapter 2 we present the semi-numerical model and we predict the dust content of normal star forming galaxies at $z > 6$. The results have been published in M. Mancini, R. Schneider, L. Graziani, R. Valiante, P. Dayal, U. Maio, B. Ciardi, L. K. Hunt, 2015, MNRAS, 451, L70. In Chapter 3 we compare the predicted evolution of galaxy colours at $5 \leq z \leq 8$ with existing data and infer important constraints on their dust properties and its distribution in the interstellar medium. The results of this study have been published in M. Mancini, R. Schneider, L. Graziani, R. Valiante, P. Dayal, U. Maio, B. Ciardi, 2015, MNRAS, 462, 3130. Finally, in Chapter 4 we draw our main conclusions.

Contents

Chapter 1

Introduction

The definition of what is a first galaxy is not trivial. In fact, there are different mechanisms that shape the properties of the interstellar medium and the conditions that enable star formation. These mechanisms are difficult to disentangle, particularly at very high redshifts. A necessary condition to allow the gas to cool and condense is the presence of a dark matter potential well. But the minimum dark matter halo mass required to host a first galaxy depends on our modelling of the star formation process.

To host long lasting star formation, the dark matter potential well should be deep enough to retain the gas that can be heated by photons emitted by the stars to temperatures higher than 10^4 K, that is the typical virial temperature of a Lyman-α cooling halo. It should be able to retain the gas accelerated by supernova (SN) explosions. And, finally, it should not be isolated from its environment, in order to be able to attract new gas from its surroundings.

The first requirement depends on our understanding of the formation and evolution of the first, Population III (Pop III) stars. In particular, the initial mass function (IMF) of these stars, that describes their mass distribution at their formation, is still highly debated ([Bromm and Yoshida, 2011]). The Pop III IMF is crucial to understand the impact that this first stellar population has on its environment and, more generally, on the formation and evolution of the first cosmic structures through mechanical and radiative feedback effects.

If the Pop III IMF is similar to the IMF that is observed in the Local Universe, we expect that mini-haloes (haloes with total mass $\mathrm{M} \sim 10^6\ \mathrm{M}_\odot$) may be able to host long lasting star formation ([Bromm and Yoshida, 2011]). However, many other theoretical studies suggest

that the Pop III IMF is biased towards higher mass stars, i.e. it is *top-heavy*. This is a consequence of the highly inefficient H_2 cooling, the only available cooling mechanism in the metal-free star forming gas (see Section 1.2 for a more detailed description). If the IMF of Pop III stars is *top-heavy*, radiative feedback is able to prevent the formation of additional stars, through the photo-dissociation of H_2 molecules and the photo-evaporation of the gas. Furthermore, mechanical feedback due to energetic SN explosions could deprive the halo of its gas, halting star formation (Bromm and Loeb 2003, Greif et al. 2007 but see also Whalen et al. 2008 for somehow different conclusions).

In this first Chapter, we briefly review our current understanding of the formation of the first cosmic structures, and the observational strategies used to observe the first galaxies.

1.1 The formation of the first haloes

The formation of the first cosmic structures is driven by the gravitational instability of the inhomogeneous density field emerging from the Inflationary epoch. Although there is still debate on what are the energy scales involved in this evolutionary epoch, and on how long has it lasted, it is commonly thought that Inflation only lasted for a brief period of time ($\mathrm{t} \sim 10^{-33}\mathrm{s}$) [Barkana and Loeb, 2001]. This event produced a semi homogeneous density field that is reflected in the homogeneity of the Cosmic Microwave Background (CMB) radiation. In this Section, we will briefly describe how the first cosmic structures have been formed from the growth of these primordial perturbations. For the sake of simplicity, we will restrict the formulation to a standard $\Lambda\mathrm{CDM}$ universe with the following cosmological parameters: $\Omega_\mathrm{M} = 0.30$, $\Omega_\Lambda = 0.7$, critical baryon density $\rho_\mathrm{b}/\rho_\mathrm{c} = \Omega_\mathrm{b} = 0.04$, and a Hubble constant $\mathrm{H}_0 = 70$ km/s/Mpc.

We define the density fluctuation δ over the mean field $\bar{\rho}$ as:

$$\delta(\mathbf{x}, \mathrm{t}) = \rho(\mathbf{x})/\bar{\rho} - 1, \tag{1.1}$$

where x is the comoving position. Under the assumption of small perturbations, the differential equation that describe the time evolution of the density perturbation can be written as:

$$\frac{\partial^2 \delta}{\partial \mathrm{t}^2} + 2\mathrm{H}\frac{\partial \delta}{\partial \mathrm{t}} = 4\pi \mathrm{G}\bar{\rho}\delta, \tag{1.2}$$

where we have neglected the pressure term since we restrict our study on the evolution of dark matter perturbations. We expect to have two solutions and, since $\mathrm{H(t)} > 0$, one of them will describe the 'growing' solution and the other will describe the 'dumped' one. Expanding Eq. (1.1) in Fourier components,

$$\delta_{\mathbf{k}} = \int \delta \, \mathrm{e}^{(-\mathrm{i}\mathbf{k}\cdot\mathbf{x})} \, \mathrm{d}^3\mathrm{x}, \tag{1.3}$$

it is possible to understand the scales of a growing or of a dumped density perturbation. This kind of formulation of $\delta_{\mathbf{k}}$ is very convenient since Inflation generates Gaussian perturbations of the density field, where all the modes are independent.

The mean amplitude of the modes is:

$$\langle \delta_{\mathbf{k}} \delta^*_{\mathbf{k'}} \rangle = (2\pi)^3 \mathrm{P(k)} \delta^{(3)}(\mathbf{k} - \mathbf{k'}), \tag{1.4}$$

where k and $\mathrm{k'}$ are the modules of the modes $\mathbf{k}$ and $\mathbf{k'}$, respectively. The standard Inflationary model predicts a power spectrum:

$$\mathrm{P(k)} \propto \mathrm{k^n} \tag{1.5}$$

with $\mathrm{n} \sim 1$. Unfortunately, the amplitude of the power spectrum is not predicted by any model of Inflation. Therefore, it has to be estimated through some observables.

To select only the scale at which the amplitude of the perturbations is measured, the field is usually convolved with a filter function. The most used one is a top hat filter, which is defined as:

$$\mathrm{W}(|\mathbf{x} - \mathbf{x'}|) = \begin{array}{cc} \frac{3}{4\pi \mathrm{R}^3} & \text{if } |\mathbf{x} - \mathbf{x'}| < \mathrm{R} \\ 0 & \text{elsewhere.} \end{array} \tag{1.6}$$

With this choice of the filter function we are measuring the mass fluctuation of spheres with a given radius R. The variance is therefore expressed as:

$$\sigma^2(\mathrm{R}) = \int_0^\infty \frac{\mathrm{dk}}{2\pi} \mathrm{k^2 P(k)} \left[\frac{3\mathrm{j_1(kR)}}{\mathrm{kR}} \right]^2, \tag{1.7}$$

where $\mathrm{j_1(x)} = (\sin(\mathrm{x}) + \mathrm{x}\cos(\mathrm{x}))/\mathrm{x}^2$. $\sigma_8 = \sigma(\mathrm{R} = 8 \text{ Mpc})$ is used to quantify the normalization of the power spectrum of the inflationary field and can be measured in independent ways. For instance, it can be determined by galaxy-galaxy correlation [e.g. Tegmark et al., 2004, Cole et al., 2005], fluctuations in the CMB [Spergel et al., 2003,

2007, Komatsu et al., 2009], gravitational lensing statistics[e.g. Hoekstra et al., 2006, Benjamin et al., 2007, Kitching et al., 2007], cluster mass function [e.g. White et al., 1993, Bahcall and Fan, 1998, Reiprich and Böhringer, 2002, Wen et al., 2010], Ly-α forest[Jena et al., 2005, McDonald et al., 2005] and galaxy peculiar velocities [Feldman et al., 2003].

The values of n and σ_8 published by the Planck Collaboration et al. [2016] are:

$$\begin{aligned} \mathrm{n} &= 0.9645 \pm 0.0049, \\ \sigma_8 &= 0.831 \pm 0.013. \end{aligned} \tag{1.8}$$

If we consider a homogeneous sphere with mass M and density equal to the current average matter density, ρ_{m}, its radius R would be:

$$\mathrm{R_M} = \left(\frac{3\mathrm{M}}{4\pi\rho_{\mathrm{m}}}\right). \tag{1.9}$$

Hence, it is possible to express the fluctuations of the density field as a function of the mass M of these spheres:

$$\sigma_{\mathrm{M}} = \sigma_{\mathrm{R}}(\mathrm{R_M}). \tag{1.10}$$

This function plays a crucial role in estimating the number of collapsed haloes.

It is possible to express the final perturbation amplitude as a function of the initial power spectrum as:

$$\mathrm{P_{fin}(k)} = \mathrm{T(k)} \cdot \mathrm{Ak^n}, \tag{1.11}$$

where $\mathrm{T(k)}$ is known as transfer function. The numerical solution of the equation provides a good fit for $\mathrm{T(k)}$ for a Cold Dark Matter model [Bardeen et al., 1986]:

$$\mathrm{T(k)} = \frac{\ln(1+2.34\mathrm{q})}{2.34\mathrm{q}}\left[1+3.89\mathrm{q}+(16.1\mathrm{q})^2+(5.46\mathrm{q})^3+(6.71\mathrm{q})^4\right]^{-1/4}, \tag{1.12}$$

where

$$\mathrm{q} = \frac{\mathrm{k}}{\Omega_0 \mathrm{h}^2} \mathrm{e}^{-\Omega_{\mathrm{b}}(1+\sqrt{2\mathrm{h}}/\Omega_0)}, \tag{1.13}$$

and the correction for the effects of the baryonic density has been taken into account [Sugiyama, 1995].

Since $\mathrm{T(k)}$ is an increasing monotonic function of $\mathrm{k} \propto 1/\mathrm{l}$, where l is the corresponding size scale of the mode k, it is evident that the growth of smaller scale perturbations is favoured over the larger scale in a ΛCDM universe.

As the Universe expands and cools, ionized hydrogen atoms start to capture electrons, hence becoming neutral (the process called *recombination*). During this evolutionary phase, matter is pulled by the gravitational force and pushed by the photons that interact with the partially ionized gas. At redshift $\mathrm{z} \sim 1200$, the photons dump baryonic perturbations, producing the so called *baryon acoustic oscillations* since they happen on a scale of the order of the sound horizon ($\mathrm{k} \sim 0.01\mathrm{Mpc}^{-1}$). On larger scales, baryonic perturbations grow following the power spectrum of dark matter fluctuations.

When the matter density perturbation δ becomes of order unity, the linear treatment is no longer suitable to describe the successive stages of structure formation.

It is possible to solve the problem in spherical symmetry, with an initial density set by the linear regime. This is a very brutal approximations, but it allows us to describe the physical conditions and the processes involved in the formation of the first haloes.

At the first stages of perturbation growth, it is possible to use a Newtonian equation, with an additional pressure term given by the dark energy:

$$\frac{\mathrm{d}^2\mathrm{r}}{\mathrm{dt}^2} = \mathrm{H}_0^2\,\Omega_\Lambda\,\mathrm{r} - \frac{\mathrm{GM}}{\mathrm{r}^2}, \tag{1.14}$$

where r is the physical radius, H_0 is the Hubble constant, M is the mass enclosed in the radius r, and the initial velocity field is given by $\dot{\mathrm{r}}_0 = \mathrm{H(t)r}$.

If the total energy on the right side is negative, the perturbed region eventually collapses to a point. However, a slight deviation from exact symmetry is to be expected. Hence the matter - instead of collapsing into a point - undergoes a violent relaxation process, that brings the halo into virial equilibrium. Considering the virial theorem $\mathrm{U} = -2\mathrm{K}$, where U and K are the potential and kinetic energies of the gas in the final state, the final overdensity can be expressed by the fitting formula

$$\Delta_\mathrm{c} = 18\pi^2 + 82\mathrm{d} - 39\mathrm{d}^2, \tag{1.15}$$

where $\mathrm{d} = \Omega_\mathrm{m}^\mathrm{z} - 1$ is evaluated at the redshift of collapse, so that:

$$\Omega_\mathrm{m}^\mathrm{z} = \frac{\Omega(1+\mathrm{z})^3}{\Omega_\mathrm{m}(1+\mathrm{z})^3 + \Omega_\Lambda + (1-\Omega_\mathrm{m}-\Omega_\Lambda)(1+\mathrm{z})^2}. \tag{1.16}$$

The virial radius of the collapsed halo is:

$$\mathrm{r_{vir}} = 0.784\left(\frac{\mathrm{M}}{10^8\mathrm{h}^{-1}\mathrm{M}_\odot}\right)^{1/3}\left[\frac{\Omega_\mathrm{m}}{\Omega_\mathrm{m}^\mathrm{z}}\frac{\Delta_\mathrm{c}}{18\pi^2}\right]^{-1/3}\left(\frac{1+\mathrm{z}}{10}\right)^{-1}\mathrm{h}^{-1}\mathrm{kpc}, \tag{1.17}$$

at which there is a corresponding circular velocity,

$$\mathrm{V_c} = \left(\frac{\mathrm{GM}}{\mathrm{r_{vir}}}\right)^{1/2} = 23.4\left(\frac{\mathrm{M}}{10^8\mathrm{h^{-1}M_\odot}}\right)^{1/3}\left[\frac{\Omega_\mathrm{m}}{\Omega_\mathrm{m}^\mathrm{z}}\frac{\Delta_\mathrm{c}}{18\pi^2}\right]^{1/6}\left(\frac{1+\mathrm{z}}{10}\right)^{1/2}\mathrm{km/s}. \quad (1.18)$$

It is also possible to define the virial temperature:

$$\mathrm{T_{vir}} = \frac{\mu \mathrm{m_p V_c^2}}{2\mathrm{k}} = 1.98\times10^4\left(\frac{\mu}{0.6}\right)\left(\frac{\mathrm{M}}{10^8\mathrm{h^{-1}M_\odot}}\right)^{2/3}\left[\frac{\Omega_\mathrm{m}}{\Omega_\mathrm{m}^\mathrm{z}}\frac{\Delta_\mathrm{c}}{18\pi^2}\right]^{1/6}\left(\frac{1+\mathrm{z}}{10}\right)^{1/2}\mathrm{K}, \quad (1.19)$$

where μ is the mean molecular weight, and $\mathrm{m_p}$ is the proton mass. μ depends on the degree of ionization of the primordial gas as well as on its composition. If the primordial gas is fully ionized $\mu = 0.59$, otherwise $\mu = 0.61$ in case of single ionization of the helium component. Finally, the binding energy is:

$$\mathrm{E_b} = \frac{1}{2}\frac{\mathrm{GM^2}}{\mathrm{r_{vir}}} = 5.45\times10^{53}\left(\frac{\mathrm{M}}{10^8\mathrm{h^{-1}M_\odot}}\right)^{5/3}\left[\frac{\Omega_\mathrm{m}}{\Omega_\mathrm{m}^\mathrm{z}}\frac{\Delta_\mathrm{c}}{18\pi^2}\right]^{1/3}\left(\frac{1+\mathrm{z}}{10}\right)^{1/2}\mathrm{h^{-1}erg}. \quad (1.20)$$

So far we focused on the integrated properties of dark matter halos and of their baryonic content. To understand how matter is distributed within a dark matter halo, it is necessary to carry out numerical simulations. A fitting function to simulation results was provided by Navarro et al. [1996, 1997], and it express the radial distribution of dark matter density:

$$\rho_\mathrm{DM}(\mathrm{r}) = \frac{3\mathrm{H_0^2}}{8\pi\mathrm{G}}(1+\mathrm{z})^3\,\frac{\Omega_\mathrm{m}}{\Omega_\mathrm{m}^\mathrm{z}}\,\frac{\delta_\mathrm{c}}{\mathrm{c_N x}(1+\mathrm{c_N x})^2}, \quad (1.21)$$

where $\mathrm{x} = \mathrm{r}/\mathrm{r_{vir}}$, $\mathrm{c_N}$ is the concentration parameter and the characteristic density δ_c is

$$\delta_\mathrm{c} = \frac{\Delta_\mathrm{c}}{3}\frac{\mathrm{c_N^3}}{\ln(1+\mathrm{c_N}) - \mathrm{c_N}/(1+\mathrm{c_N})}. \quad (1.22)$$

The concentration parameter depends also on the halo mass M and redshift [Barkana and Loeb, 2010].

Right after recombination, the gas temperature is locked to the CMB temperature by Compton scattering that arises from the residual ionization of the gas. Eventually, when the free electron fraction drops, at a redshift $\propto 1000\,(\Omega_\mathrm{b}\mathrm{h}^2)^{2/5}$, the gas temperature decouples from the CMB [Peebles, 1993]. After decoupling, the gas can collapse into DM halos and virialize. During the virialization, the gas undergoes various compressions and shocks that reheat it to the dark matter halo virial temperature. Hence, to understand the formation of the first stars, it is important to understand the gas cooling properties in these first collapsed structures.

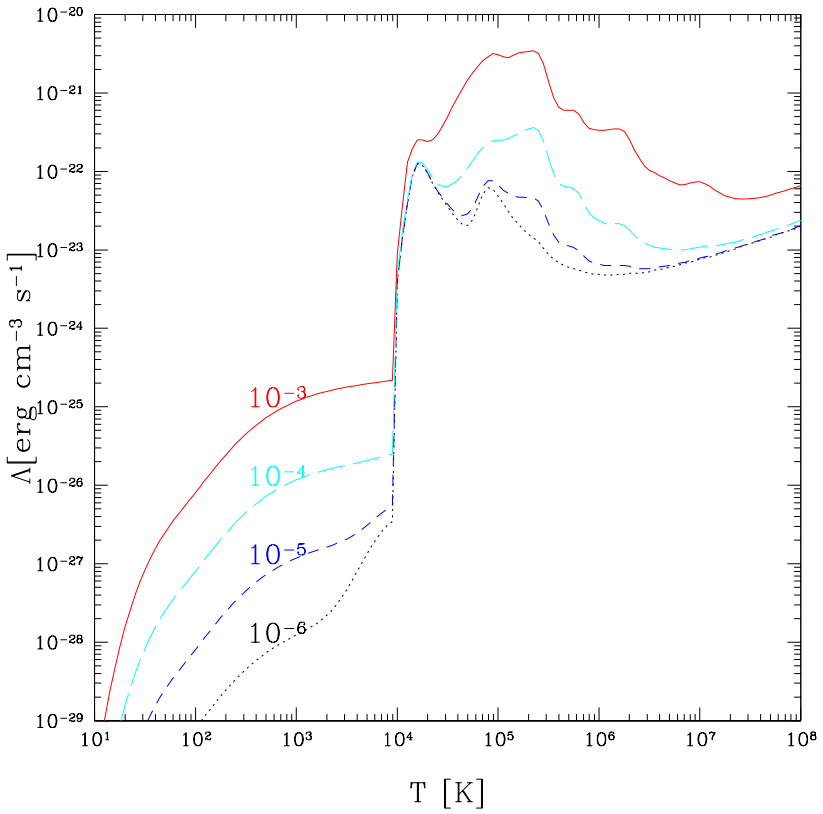

Figure 1.1. Cooling function accounting for hydrogen, helium, metals, H_2 and HD molecules as a function of temperature, for gas having a hydrogen number den.sity of $1\mathrm{cm}^{-3}$, the H_2 and HD fractions are fixed to a value of 10^{-5},10^{-8} respectively. The different lines represent different gas metal fractions. Adapted from Maio and Viel [2015].

The first requirement for a bound object to collapse is to have a mass higher than the Jeans mass:

$$\mathrm{M_j} = 3.08 \times 10^3 \left(\frac{\Omega_\mathrm{m} \mathrm{h}^2}{0.13}\right)^{-1/2} \left(\frac{\Omega_\mathrm{b} \mathrm{h}^2}{0.022}\right)^{-3/5} \left(\frac{1+\mathrm{z}}{10}\right)^{3/2} \mathrm{M}_\odot. \tag{1.23}$$

In a perturbation with mass greater than $\mathrm{M_j}$ the pressure force is not counteracted by gravity and the structure collapses. Thus $\mathrm{M_j}$ sets a threshold for the scales which can collapse. The second fundamental requirement is that the cooling timescale doesn't exceed the Hubble time.

In Figure 1.1, the cooling rate is shown as a function of temperature [taken from Maio et al., 2010]. The different colors and line styles represent different values of gas metallicity. For very metal poor gas, cooling is dominated by H_2 and HD cooling for temperature

$T < 10^4$ K while collisionally excited HI and HeII atomic lines dominate the cooling at higher temperatures. The sharp increase of the cooling efficiency at $T \sim 10^4$K is given by the hydrogen Lyman α line, while the feature at 10^5K is given by the HeII.

If we consider the virial temperature of the halos as a proxy for the temperature of the gas, the shape of the cooling function of the primordial gas allows us to identify two classes of dark matter halos: minihaloes, with $T_{vir} < 10^4$ K where the gas can cool only via molecular transitions (H_2 and HD) and Lyman-α cooling haloes with $T_{vir} \geq 10^4$ K.

1.2 Star formation in mini-halos

In the bottom-up structure formation scenario predicted by the ΛCDM cosmological model, the first haloes that virialize are the small-mass mini-haloes, with $T_{vir} < 10^4$K. Hence, the molecular content of these haloes is very important to compute the gas cooling timescale, and to assess whether cooling is efficient enough to allow the formation of the first stars.

At redshift $z \gtrsim 400$, H_2 is formed via the H_2^+ formation channel that leads to a cosmic mean abundance of $f_{H_2/H} \sim\approx 10^{-7}$. At redshift $z < 100$, the CMB radiation becomes so weak to allow the formation of H^-. These ions form H_2 molecules through this chain of reactions:

$$\begin{aligned} H + e^- &\rightarrow H^- + h\nu \\ H^- + H &\rightarrow H_2 + e^-. \end{aligned} \tag{1.24}$$

Consider both these formation channels, several studies the primordial cosmic abundance of H_2 to be in the range $10^{-6} \leq f_{H_2/H} \leq 10^{-4}$ [e.g. Lepp and Shull, 1984, Palla et al., 1995, Haiman et al., 1996, Anninos and Norman, 1996, Tegmark et al., 1997]. Thus, the fate of the virialized gas in a mini-halo crucially depends on its ability to rapidly increase its H_2 content during the collapse phase, allowing further gas cooling. Tegmark et al. [1997] estimated the evolution of the H_2 abundance in halos with different masses. For each virialization redshift, they found that there is a critical halo mass, M_{sf}, above which the gas can cool and form stars. At $z \sim 20$, $M_{sf} \sim 10^6\, M_\odot$, which corresponds to $T_{vir} \sim 10^3$ K.

The formation of the first stars requires the gas to collapse, increasing its central density, until the central region is able to form a first hydrostatic core, which then grows in mass by gas accretion. These processes are very complex and again rely on the balance between thermal (and eventually turbulent) support and self-gravity. In general, cooling is efficient

when the cooling time is shorter that than the free fall time [e.g. Schneider et al., 2002], and the gas temperature decreases with increasing density. Hence, the efficiency of gas cooling sets the characteristic mass scale of the newly formed stars. Pop III stars form in metal-free mini-halos, with a very low gas ionization fraction (of the order $\sim 10^{-4}$). Under these conditions, the only efficient coolant is H_2. Roto-vibrational lines allow the gas to cool down to a temperature of $T \gtrsim 200K$ and a density of $10^4 cm^{-3}$, when the level populations have reached their local thermodynamic equilibrium. This phase is generally referred to as the *loitering* phase [Bromm et al., 2002] and terminates when the mass of the innermost dense region exceeds the mass of the most massive stable hydrostatic gas cloud, the Bonnor-Ebert mass [Bonnor, 1956, Ebert, 1955, Abel et al., 2002],

$$M_{BE} \simeq T^{3/2} n^{-1/2} M_\odot. \tag{1.25}$$

For $n \sim 10^4 cm^{-3}$ and $T \sim 200K$ this mass has a value of $M_{BE} \sim 1000 M_\odot$. When this critical mass is reached, the protostellar cloud decouples for its environment, stopping further mass accretion, and continues to collapse until a central small hydrostatic core is formed, with a mass $\sim 0.01\ M_\odot$. The resulting stellar mass is set by the efficiency of gas accretion onto the central core (it is formed from the inside-out Smith e.g. 2012, Vorobyov et al. e.g. 2013, DeSouza and Basu e.g. 2015, Sakurai et al. e.g. 2016).

This picture has been confirmed by numerical simulations that start from cosmological initial conditions. Figure 1.2 shows the phase diagram of a gas cloud with primordial composition [Yoshida et al., 2006]. The labels identify important phases during the evolution. In (A) the gas density is too low for efficient cooling, while in (B) H_2 cooling sets in and it enables the gas to evolve to lower temperatures. In (C) the gas reaches the loithering phase and the corresponding mass scale is $\sim 10^3 M_\odot$. Thereafter, the prostellar cloud continues to collapse and - although its properties change along the evolution (through phase D - G) - no additional fragmentation episodes occurr in the simulations. More recently, however, higher resolution simulations that can evolve the collapsing cloud beyond the density limit shown in Fig. 1.2 have shown that instabilities can lead to fragmentation of the high density accretion disc that forms around the central hydrostatic core, opening the possibility to form low-mass Pop III stars [Stacy et al., 2010, Clark et al., 2011, Greif et al., 2011, 2012, Turk et al., 2012, Stacy et al., 2016].

Additional important processes may affect the mass value of the newborn Pop III star.

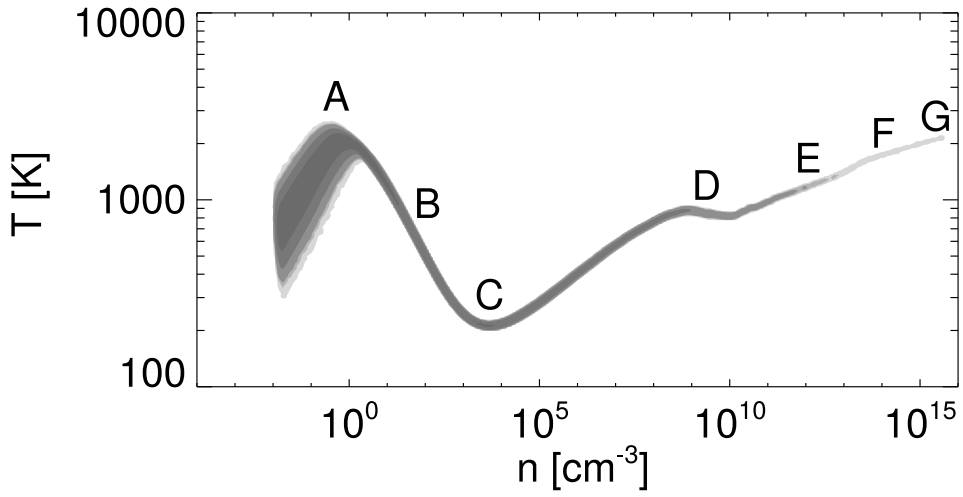

Figure 1.2. Gas distribution of gas temperature as a function of density for a cloud with primordial composition and a central density of $5{\times}10^{15}\mathrm{cm}^{-3}$. The letters represent some typical conditions that a cloud undergo in the collapse. (A) after the gas virialization the cloud has a temperature higher than $> 1000\mathrm{K}$ and H_2 molecules start to form. In (B) the H_2 molecules start to efficiently cool the gas to a temperature of $200\mathrm{K}$ until the point (C) is reached. In (C) the gas reaches the density independent local thermodynamic equilibrium. In (D) the H_2 is formed with three body reaction cooling further down the gas. In (E) the cloud density is high enough to start shielding the emission decreasing the cooling rate. In (F) the lines are excited by collisional processes and finally in (G) the temperature are high enough to start dissociate the molecular hydrogen. Adapted from Yoshida et al. [2006].

Among these, radiative feedback from the growing central protostar can limit further gas accretion, leading to masses of the order of a few tens of solar masses, [McKee and Tan, 2008, Hosokawa et al., 2011, Stacy et al., 2012, Susa, 2013, Susa et al., 2014, Hosokawa et al., 2016].

Our current understanding is that Pop III stars were predominantly massive but may have formed with a broad range of stellar masses, from $\sim$ 10s to $\sim 1000\,\mathrm{M}_{\odot}$. This is consistent with a detailed statistical analysis made by Hirano et al. [2014], Hirano and Bromm [2017] through complex multi-scale simulations starting from cosmological initial conditions and exploring the fate of hundreds of star forming mini-halos at very high redshift. Figure 1.3 shows the mass spectrum of Pop III stars that emerges from the simulations.

Since massive Pop III stars are short-lived, their environment will be rapidly enriched and it is foreseen that even the deepest observations with the *James Webb Space Telescope* (JWST) will tend to see low-metallicity Pop II systems [Rydberg et al., 2010]. Metal-free non-rotating stars with progenitor masses in the range $[140 - 260]\ \mathrm{M}_{\odot}$ are predicted to explode as powerful pair-instability supernovae [PISN Heger and Woosley, 2002]. Individual PISNe are bright enough to be detected with JWST, but the challenge will be their low surface density, such that a wide area needs to be searched multiple times to detect these transients [Hummel et al., 2012, Pan et al., 2012, Whalen et al., 2013, Wang et al., 2017]. If such a search were able to identify a high redshift PISN, this will constrain the high-mass end of Pop III stars. Alternatively, we may attempt to constrain the Pop III IMF and the nature of the first SNe by means of *stellar archeology*, i.e. interpreting the statistical distribution and surface enrichment pattern of the metal poor Galactic Halo stars [see e.g. Graziani et al., 2017, de Bennassuti et al., 2017, and references therein].

1.3 Star formation in Lyman-α cooling halos

In the bottom-up $\Lambda\mathrm{CDM}$ scenario, the number density of Lyman-α cooling halos is low at redshift $\mathrm{z} > 15$ and it starts to rise in the redshift range $\mathrm{z} \in [10, 15]$ [Miralda-Escudé, 2003, Gao et al., 2007]. At these redshifts the first generation of stars has already formed, emitting UV radiation, releasing the first heavy elements through powerful supernova (SN) explosions, and forming the first black hole remnants. This complex interplay of mechani-

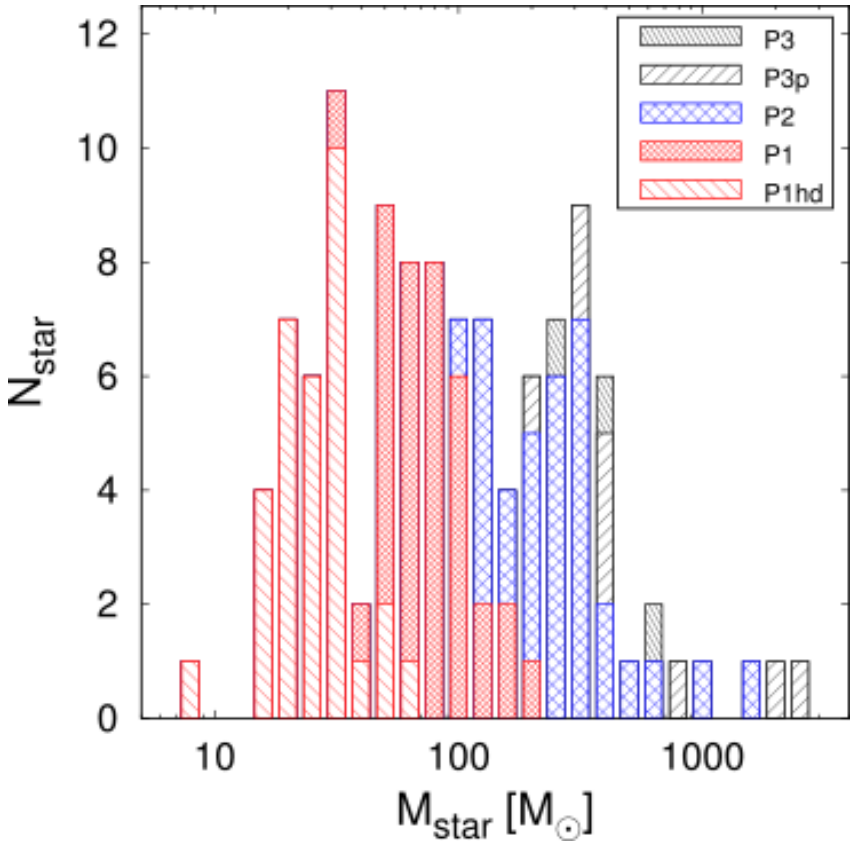

Figure 1.3. IMF of Pop III according to the 2D radiation hydrodynamics simulations of [Hosokawa et al., 2011], applied to 110 different mini-halos. The red, blue, and black histograms represent the different paths of proto-stellar evolution: P1 denotes Kelvin-Helmholtz contracting proto-star(red), P2 an oscillating proto-star (blue), and P3 super-giant proto-star (black). P1hd refers to the cases in which the gas clouds are formed by HD cooling and evolve on low-temperature tracks. P3p (predicted) indicates the same cases as P3, except that the final masses are calculated from a correlation between the properties of the cloud and the resulting stellar mass. Adapted from Hirano et al. [2014].

cal and radiative feedback processes [Ciardi and Ferrara, 2005] most probably delayed the formation of subsequent stars by $\sim 10^7 \mathrm{yr}$ [e.g. Johnson et al., 2007]. In particular, UV photons in the Lyman-Werner band photo-dissociate H_2 molecules thereby inhibiting primordial gas cooling. In these conditions, gas cooling and star formation is possible only if metals produced and released by a previous generation of stars have already enriched the star forming gas. In addition, Lyman-α cooling halos are likely the ones that have a large enough binding energy to retain or recollect the gas after the first SNe have exploded. Hence, we expect that Lyman-α cooling halos predominantly form Pop II stars [Bromm, 2013].

Unfortunately, it is still difficult to probe the physical properties of the interstellar medium and of the stellar populations hosted by galaxies at $z > 6$, even with the most advanced observational facilities. As we will discuss in Section 1.4, for the vast majority of normal star forming galaxies at $z > 6$ we must infer the star formation rate, the stellar mass and age through rest-frame UV data obtained through deep observations of the Hubble Space Telescope (HST). Hence, we have to rely on theoretical models to predict the properties of these first protogalaxies.

Very likely, the star formation in Lyman-α cooling halos occurs under physical conditions that are very different from the ones described above. Both in-situ (from stars formed in progenitor systems) and ex-situ (from stars formed in nearby systems) metal pollution may have enriched their interstellar medium (ISM) with gas phase metals and solid dust grains formed in the ejecta of the first SNe [Todini and Ferrara, 2001, Nozawa et al., 2003, Schneider et al., 2004, Bianchi and Schneider, 2007, Schneider et al., 2012a, Marassi et al., 2014, 2015]. In addition, the gas has been partially ionized by the UV radiation and by SN shocks. Star formation likely occurs in turbulent, chemically enriched, magnetized molecular clouds with a degree of complexity that is somehow similar to what we expect in the Local Universe [Bromm and Yoshida, 2011]. It is therefore very important to understand what chemical enrichment path these galaxies have followed.

Regarding the infall of enriched gas from the intergalactic medium (IGM), the picture is not yet clear, as recently reviewed by Finlator [2017]. Metals ejected from star forming mini-halos had surely polluted the IGM, as suggested by different simulations[Yoshida et al., 2004, Tornatore et al., 2007a, Greif et al., 2007, Xu et al., 2016c, Gnedin et al.,

2017], but observations indicate that the CIV abundance declines at redshift higher then 6, suggesting that most of the enrichment of this element has been done since $z \sim 6$ [Becker et al., 2009]. In more massive haloes, the heavy elements can still unload in the IGM by radiation pressure winds and SNe explosion [Madau et al., 2001, Mori et al., 2002, Wada and Venkatesan, 2003, Ritter et al., 2015, Jeon et al., 2015, Jaacks et al., 2017, and references therein]. In principle, it is possible to understand the chemical enrichment history comparing the metallicity evolution with the star formation history. The current data suggest a delayed enrichment from the IGM [Hultman Kramer et al., 2010]. Cosmological simulations of structure formation suggest that the distributions of metals into the IGM is very patchy leaving large volume of gas unpolluted [Bertone and Stoehr, 2005, Tornatore et al., 2007a, Pallottini et al., 2014]. Hence, simulations suggest that Pop III star formation may occur even at redshift $z < 6$ [Scannapieco et al., 2005, Johnson, 2010, Xu et al., 2016b].

However, chemical enrichment inside the galaxies occurs very rapidly after the first episode of star formation [Schneider et al., 2006, Salvadori et al., 2007], as confirmed by numerical simulations [Greif et al., 2010, Ritter et al., 2016, Jaacks et al., 2017, and references therein]. The presence of gas-phase metals and dust grains in star forming gas clouds have a large impact on the cooling efficiency of the gas and on the nature of the stars that are ultimately formed (the so-called chemical feedback).

Fig. 1.1 shows the temperature and metallicity dependence of the cooling function. The presence of metals provides a very efficient cooling channel at gas temperature $T < 10^4$K, in fact, it overcomes the cooling rate given by the H_2 and HD even at metallicities $Z \sim 10^{-5} Z_\odot$. Metal cooling is due to fine structure lines at low temperature (mostly OI, CII, FeII and SiII) and collisional ionization at higher temperatures.

Studies of the properties of star forming clouds at very low metallicities have proposed that the thermal evolution is dramatically affected by the presence of metals (through molecular cooling of OH, CO, H_2O or through fine structure emission of OI and CII) and that, when $Z \geq Z_{crit} \sim 10^{-4} Z_\odot$, low-mass Pop II stars can form [Bromm et al., 2001, Bromm and Loeb, 2003, Santoro and Shull, 2006].

In addition, it has been suggested that the presence of dust grains in star forming clouds increases the cooling efficiency by enabling H_2 formation on the surface of the grains and, at much higher densities, by opening a new cooling channel due to collision excitation

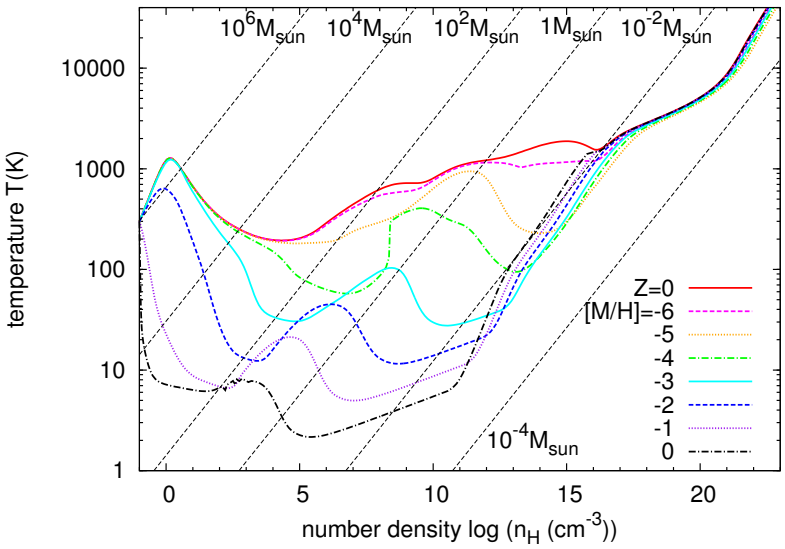

Figure 1.4. Temperature evolution of prestellar cloud cores with metallicities $\mathrm{Z/Z_\odot} = 0, 10^{-6}, 10^{-5}, 10^{-4}, 10^{-3}, 10^{-2}, 10^{-1}$ and 1 as a function of the central number density calculated by means of one-zone models [Omukai et al., 2010]. The dashed diagonal lines indicate values of constant Jeans masses. Adapted from Omukai et al. (2005).

of dust grains followed by dust thermal emission [Omukai, 2000, Schneider et al., 2002, Omukai et al., 2005, Schneider et al., 2006, 2012b].

The relative importance of molecular, metal and dust cooling depends on the density, the initial metallicity and the dust content of the collapsing core.

In Figure 1.4 we show the prestellar temperature evolution as a function of the core density computed with a one-zone model [Omukai et al., 2005]. The different lines represent different initial metallicities and the model also includes the effects of dust. Recalling that the minimum fragmentation mass scale is set by the Jeans mass (or Bonnor-Ebert mass) at the inflection point of the equation of state, the comparison between the minima achieved by clouds at different metallicities with the diagonal lines allows us to estimate the fragmentation mass as a function of metallicity.

In particular, the inspection of Figure 1.4 shows that there are different regimes of fragmentation: at low densities, in the primordial gas (that we have already discussed above) and when the metallicity is $\mathrm{Z} < 10^{-4}\ \mathrm{Z_\odot}$, molecular cooling dominates the evolution and high-mass fragments are formed, with $\mathrm{M_{BE}} \sim 10^2 - 10^3\,\mathrm{M_\odot}$. When $\mathrm{Z} \geq 10^{-4}\ \mathrm{Z_\odot}$, the

dominant coolants become OI and CII cooling but - being effective at relatively low densities - the corresponding fragment masses are still relatively large ($\mathrm{M_{BE}} \in 10-100\mathrm{M_{\odot}}$). At high densities, when $\mathrm{Z} \geq 10^{-5}\,\mathrm{Z_{\odot}}$, dust cooling becomes efficient and a new set of minima appears. Since the densities are much larger, the corresponding fragments masses are very small, between 10^{-2} and $1\,\mathrm{M_{\odot}}$. Hence, dust cooling enables the formation of low-mass and long-lived Pop II stars even at very low metallicities, when $\mathrm{Z} \geq 10^{-5}\mathrm{Z_{\odot}}$ [Schneider et al., 2002, 2004, 2006, 2012b,a].

Metal enrichment is highly inhomogeneous and cosmological simulations that have attempted to model the process and to estimate the rate of formation of Pop III stars as a function of redshift have shown that late Pop III star formation is still possible even at $\mathrm{z} \leq 6$ in pockets of pristine gas [Tornatore et al., 2007b, Wyithe and Cen, 2007, Ricotti et al., 2008, Maio et al., 2010, 2011, Muratov et al., 2013, Pallottini et al., 2014, Starkenburg et al., 2016, Xu et al., 2016c,a]. However, we expect that in Lyα cooling haloes whose progenitors are Pop III star forming mini-halos, metal enrichment has been very efficient. As a result of chemical feedback, most of these systems host metal-poor Pop II stars, with an initial mass function similar to the one observed in the Local Universe [de Bennassuti et al., 2014, Graziani et al., 2017, Marassi et al., 2014].

1.4 Observing the first galaxies

The detection of high redshift galaxies often relies on spectral properties of the hydrogen gas. In fact, hydrogen provides two important spectral features that are widely used to measure the redshift of the sources, either spectroscopically or by least expensive photometric techniques. Depending on the techinque adopted for their identification, high-z galaxies usually fall in two classes: Lyman-α emitters (hereafter LAE) and Lyman break galaxies (LBG).

LAE are galaxies that show a very prominent Lyman-α emission produced by hydrogen atoms in their ISM which have been excited by the UV radiation emitted by young stars. Lyman-α emission is a very narrow feature that can be easily detected with narrow band filters, giving a very precise identification of the redshift of the source. LBG are identified through the so called Lyman-break technique, via the distinctive “step” introduced into their

UV continuum emission by the effect of neutral hydrogen absorption, both in the ISM of the galaxy and in the IGM along the line-of-sight to the source. The great advantage of the Lyman-break selection method is that it can be applied using imaging with broad-band filters, such as Wide Field Camera 3 (WFC3) on board of the *Hubble Space Telescope* (HST). This allows the selection of large samples of potentially high-redshift galaxies, that are then spectroscopically followed-up to confirm their redshift. Very deep near infrared surveys, such as the Hubble Ultra Deep Survey (HUDF [Beckwith et al., 2006]) and Extremely Deep Survey (XDF Illingworth et al. [2013]) have been conducted using this technique.

It is important to stress that these two methods can efficiently select galaxies with young stellar populations that produce UV radiation, and with a small dust content in the ISM, to allow a fraction of this emitted radiation to escape. Indeed, observations done in the $[3–8]\mu$m range using the IRAC camera on board of the *Spitzer* space telescope have allowed to measure the Balmer spectral break in UV selected high-z galaxies (at $z > 5$ the rest-frame 3646Å break is observed at $> 2.2\mu$m). The strength of this break allows us to infer the age of the stellar population, with important implications for estimating the galaxy stellar mass.

In Fig 1.5 [taken from Dunlop et al., 2013] we show the redshifted spectral energy distribution (SED) of a young $z \sim 7$ galaxy (the adopted age and metallicity of this galaxy are 0.5 Gyr and 0.2 $Z_{\odot}$). The coloured shaded areas illustrate how the SED is sampled by the optical (i775, z850) and near infrared filters (Y105, J125, H160) in the HST ACS and WFC3 cameras, respectively, and by Spitzer IRAC at 3.6μm and 4.5μm. It is clear that the observations are able to probe both the Lyman and the Balmer breaks. The figure does not show nebular emission lines, that are expected to become particularly important for low-metallicity galaxies, and which can complicate the measurement of the strength of the Balmer break [Schaerer and de Barros, 2009]. With the advent of the *James Webb Space Telescope* it will be possible to observe the wavelength range between WFC3 and IRAC filters, that is currently observable only with ground-based K-imaging for the brightest objects. This will allow to have a better census of high-z galaxies, including systems with older ages and less prominent UV emission.

Finally, the advent of the *Atacama Large Millimetre Array* (ALMA) has opened the possibility to select galaxies via sub-mm/mm observations of their redshifted thermal dust

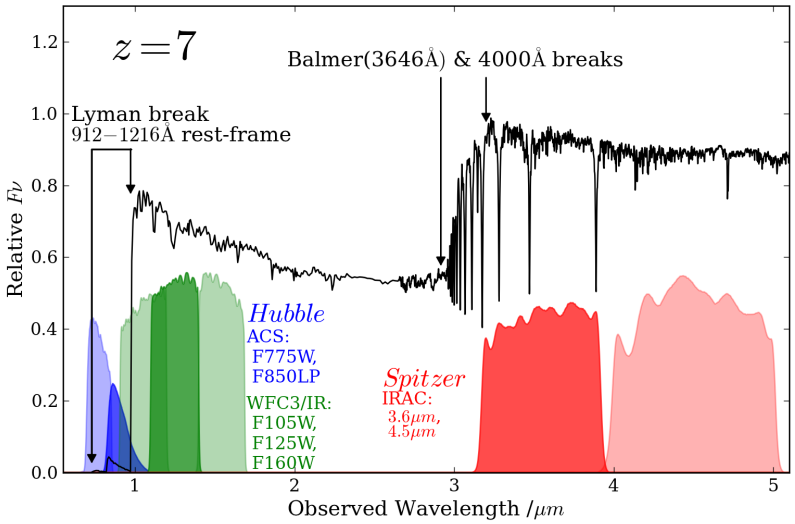

Figure 1.5. Typical spectrum of a LBG at redshift 7, where the Lyman and Balmer breaks have been identified by the arrows. The coloured shaded regions show HST and Spitzer filters. This figure illustrate the spectral coverage of current instruments on the restframe UV of high-z LBG. Adapted from Dunlop et al. 2013.

emission. Although the very first primeval galaxies will not be detectable by this approach, early chemical enrichment appears to be efficient and both dust and molecular emission have been detected in objects at z $>$ 6 [see the review of Carilli and Walter, 2013]. The first sources to be observed have been the host galaxies of bright quasars [e.g. Mortlock et al., 2011, Wu et al., 2015, Willott et al., 2010, Venemans et al., 2015, Bañados et al., 2016]. The rest-frame IR emission in these galaxies is powered by a strong starburst, with star formation rates of hundreds of solar masses per year, illuminating ISM dust masses that have been estimated to be as big as $\sim 10^8 M_\odot$ [e.g. Valiante et al., 2014]. As we will thoroughly discuss in the rest of the thesis, although we might expect dust to become less prevalent at extreme redshifts, dust enrichment can become very rapid and it is important to consider its effect on the UV properties of high-z galaxies.

Recently, using a mosaic of 45 ALMA pointings, Dunlop and collaborators have obtained a homogeneous image of the HUDF at 1.3 mm, the so-called ALMA Deep Field [Dunlop, 2016]. A picture showing some of the ALMA detections on top of the HUDF is presented in Figure 1.6. The analysis has led to the discovery of 16 sources, all with

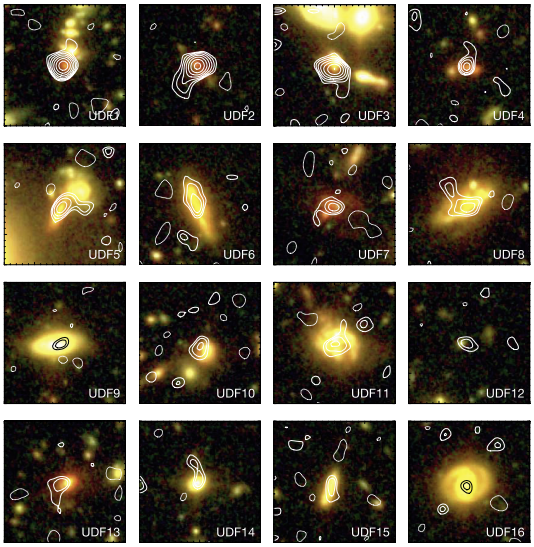

Figure 1.6. Colour (i 775 + Y105 + H160) HST postagestamp images of the 16 ALMA detected galaxies in the HUDF, with the contours from the ALMA 1.3-mm imaging overlaid. Each stamp is 6 × 6 arcseconds in size, with north to the top and east to the left. Adapted from Dunlop [2016].

a secure galaxy counterpart and redshift. Their physical processes are well constrained and all of these sources appear to be massive star forming galaxies, with a medium redshift of $< z >= 2.15$ [Dunlop, 2016]. Very likely, this is only the bright-end of dusty star forming galaxies, and uncertainties remain for fainter objects, which are responsible for the bulk of star formation at high redshift. One way to overcome their faintness is to exploit the sensitivity of ALMA and the power of gravitational lenses. For this reason, an observational campaign has been carried out to point ALMA on the Frontier Fields imaged by Hubble and Spitzer [Gonzalez-Lopez et al., 2016, González-López et al., 2017b,a, Laporte et al., 2017b,a]. These have been designed to exploit the lensing power (magnification $> 5-10$) of six massive clusters, and have enabled to detect high-z galaxies that are 10–50 times intrinsically fainter than any seen before. Indeed, the only two sources that have been detected in their thermal dust continuum at $z > 6$ are gravitationally lensed: the first one is the galaxy A1689-zD1 at $z = 7.5$ found by Watson et al. [2015] and recently re-observed with deeper ALMA data by Knudsen et al. [2017]. A1689-zD1 is strongly lensed by a factor of 9.3, it has an estimated stellar mass of $\sim 1.7 \times 10^9 M_\odot$, a total star formation rate (SFR) of $\sim 12 M_\odot/\mathrm{yr}$, and a dust mass comparable to that of the Milky Way,

$\mathrm{M_{dust}} \sim (3-6) \times 10^7 \mathrm{M_\odot}$ [Watson et al., 2015, Knudsen et al., 2017]. Given the relatively small Hubble time at $\mathrm{z} \sim 7.5$, explaining the origin of the dust mass in this galaxy is a challenge for theoretical models [Michałowski, 2015, Mancini et al., 2015]. In Chapter 2 we will discuss this issue in great details. The second source that has been recently identified in the ALMA Frontier Fields is the galaxy A2744 YD4 with $\mathrm{z} = 8.38$, despite the modest (~ 2) gravitational amplification [Laporte et al., 2017b]. Analysis of the available photometric data indicate that A2744 YD4 has a stellar mass of $2 \times 10^9 \mathrm{M_\odot}$, a star formation rate of $\sim 20 \mathrm{M_\odot/yr}$ and a dust mass of $6 \times 10^6 \mathrm{M_\odot}$. Although limited to only two sources, the above results show that ALMA has the potential to detect dust emission within the heart of the reionization era and thus further measures of this kind, in conjunction with JWST, offers the exciting prospect of tracing early star formation and onset of dust enrichment in the Universe.

1.4.1 The UV luminosity function at $\mathrm{z} > 5$

One of the most important quantities that characterize the high-z Universe is the UV luminosity function (hereafter LF) and its evolution with redshift. The LF is the number density of objects with a given observed magnitude or luminosity. LF are very important to estimate the total flux of ionizing photons at a given redshift, and they are also useful to understand from what class of objects the majority of the ionizing flux comes. Furthermore, LFs are also very important to estimate the cosmic star formation density, since the UV emission traces the ongoing star formation, and they also give insight on the hierarchical formation of the galaxies. A good description of the shape of the LF is given by the Schechter function:

$$\mathrm{n(M)dM} = 0.92\phi^* \left(10^{0.4(\mathrm{M^*-M})}\right)^{\alpha+1} \exp\left[-10^{0.4(\mathrm{M^*-M})}\right] \mathrm{dM}, \tag{1.26}$$

where $\mathrm{n(M)}$ is the number density of objects at a given $\mathrm{M_{UV}}$, ϕ^* is the normalization, $\mathrm{M^*}$ is the magnitude in which the number density of objects drops and α describes the LF dependence for $\mathrm{M_{UV}} < \mathrm{M^*}$. These parameters are derived from data fitting [e.g. McLure et al., 2009, Oesch et al., 2010, Bouwens et al., 2015, Finkelstein et al., 2015a, Castellano et al., 2010, McLure et al., 2010, 2013, Atek et al., 2015, Laporte et al., 2015, Bowler et al., 2014, 2015] and ϕ^*, n are usually expressed in units of $\mathrm{cMpc^{-3}}$.

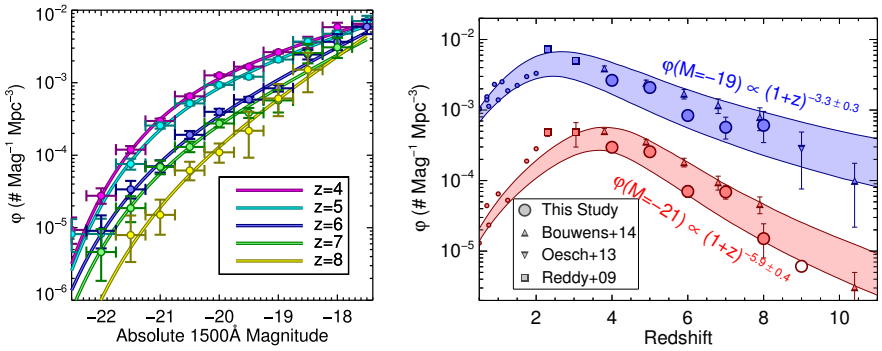

Figure 1.7. [left panel] Evolution of the luminosity function as a function of redshift. The points represent the observations while the curves represent the Schechter fit. [right panel] Comparison of the redshift evolution of the normalization of the Schechter function. The blue and red shaded areas represent the .68 percentile for the galaxies in the magnitude bin of $M_{UV} = -19$ and $M_{UV} = -21$ respectively. Although the Schechter fit captures the magnitude dependence of the LF, it is necessary to probe the faint end to better constrain its parameters. In particular, over/underestimating the values of the normalization ϕ might lead to over/underestimating the ionizing flux or the universal star formation rate density. Hence, it is crucial to have deep surveys in the UV and a careful modelling of the high redshift galaxies emitted flux. Both panels are taken from Finkelstein et al. [2015a].

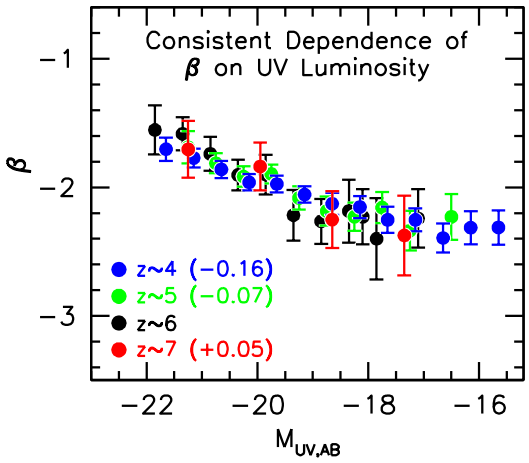

Figure 1.8. Redshift evolution of the CMR as in Bouwens et al. [2014]. The various colors represent data obtained at different redshifts. Note that to underline that a common trend is preserved with redshift, the β values have been rescaled by the factors reported in the legenda.

In Figure 1.7, we show the evolution with redshift of the LFs as reported by Finkelstein et al. [2015a]. The comparison of the different coloured lines shown in the right panel illustrates the redshift evolution of the bright-end of the LF, with fainter objects becoming progressively more common with respect to brighter ones with increasing z. The implication is that the most common sources of UV light at these redshifts have likely been small, UV faint galaxies. Hence, it is mandatory to correctly estimate the faint-end of the Schechter function in order to constrain the ionizing emissivity and to measure the star formation rate density at those redshift [Bromm and Yoshida, 2011]. In addition, the values of the Schechter parameter ϕ^*, which strongly impact the estimated number of faint galaxies, is very uncertain at redshift higher than 7, although a common trend is established among different authors (see the right panel of the Figure). Unfortunately, probing the faint end of the luminosity function is somehow limited by the sensibility of the HST, and new important constraints will be obtained by JWST.

1.4.2 The colour-magnitude relation of $z > 5$ galaxies

Another important observable that provides important information on the nature of the stellar populations of high-z galaxies and on the properties of their ISM is the Color Magnitude Relation (CMR). It correlates the spectral index β, used to describe the UV spectrum of a

star forming galaxy, with the UV magnitude $\mathrm{M_{UV}}$. Spectral synthesis models suggest that for a Pop II/I star forming galaxy the expected value of β is in the range $[-2.3, -2.5]$ [e.g. Meurer et al., 1999, Bouwens et al., 2014]. Hence, if lower values are observed, the corresponding stellar population is expected to be very metal poor [e.g. Bromm and Yoshida, 2011, Dunlop et al., 2012]. On the other hand, higher values of β imply that the ISM of the galaxy is likely to be already chemically enriched [e.g. Meurer et al., 1999, Bouwens et al., 2014, Mancini et al., 2015, Cullen et al., 2017] since the observed β values are influenced by dust extinction. In fact, Meurer et al. [1999] suggested to compare the observed value of β with that expected for the stellar population (the intrinisc one) as a technique to estimate the amount of extinction suffered by the stellar light. Although this method is very convenient to estimate the extinction using only UV data, its applicability is still debated both at low [Talia et al., 2015, Forrest et al., 2016] and high redshifts [Mancini et al., 2016, Cullen et al., 2017, Narayanan et al., 2017]. We will thoroughly discuss this point in Chapter 3 of this thesis.

Figure 1.8 illustrates the evolution of the CMR with redshift inferred by Bouwens et al. [2014]. The functional dependence of β from $\mathrm{M_{UV}}$ $\left(\frac{\partial\beta}{\partial \mathrm{M_{UV}}}\right)$ appears to be independent of redshift, although with we expect overall bluer colors with increasing redshift (the normalization is a function of the redshift z) [Bouwens et al., 2016]. The functional dependence of β with $\mathrm{M_{UV}}$ is mostly linear, and - although some authors have suggested a broken power-law [Bouwens et al., 2014] - the data is still not sufficient to rule out a simple linear dependence [Rogers et al., 2014].

Many attempts have been made to explain this trends using numerical simulations [e.g. Dayal et al., 2014, Khakhaleva-Li and Gnedin, 2016b], semi-analytical models [e.g. Wilkins et al., 2011] and semi-numerical techniques [Mancini et al., 2016, Cullen et al., 2017, Narayanan et al., 2017]. Chapter 4 will be devoted to a full discussion on the redshift evolution of high-z galaxy colours and the implication for the nature of dust in these galaxies, and its spatial distribution.

Chapter 2

The dust mass in $\mathrm{z} > 6$ normal star-forming galaxies

Observations at millimeter (mm) and sub-millimeter (sub-mm) wavelengths have provided convincing evidence of rapid dust enrichment at high redshift (for a recent review see [Carilli and Walter, 2013] and references therein). Dust masses as large as $\sim 10^8 \mathrm{M}_\odot$ have been inferred for $5 \leq \mathrm{z} \leq 7$ QSO host galaxies, requiring a very efficient dust formation channel that must operate in less than 1 Gyr of cosmic evolution. Theoretical studies have shown that although stellar sources of dust, including both Supernovae (SN) and Asymptotic Giant Branch (AGB) stars, can be fast enough to significantly contribute to high redshift dust enrichment [Valiante et al., 2009], the observed dust masses require efficient grain growth in the dense phase of the interstellar medium [ISM, Michałowski et al., 2010, Valiante et al., 2011, 2014]. Until very recently, sub-mm/mm continuum observations at $\mathrm{z} \sim 6-7$ have been limited to "extreme" galaxies, QSO hosts or strong starbursts, which are characterized by star formation rates ranging from several hundreds to thousands of solar masses per year. However, at these high redshifts we expect the bulk of the galaxy population to be characterized by "normal" galaxies, which form stars at rates from a few to a few tens of solar masses per year. Deep ALMA and Plateau de Bure Interferometer (PdBI) follow up observations have mostly provided upper limits on the dust mass of such galaxies[Kanekar et al., 2013, Ouchi et al., 2013, Ota et al., 2014, Schaerer et al., 2015, Maiolino et al., 2015], with the exception of the gravitationally lensed $\mathrm{z} = 7.5$ Lyman Break Galaxy (LBG) A1689-zD1, whose dust continuum emission has been recently detected with ALMA (Watson et

al. 2015). The estimated dust mass is $4^{+4}_{-2} \times 10^7 M_\odot$, showing that dusty galaxies have already formed at $z > 7$.

In this paper, we investigate early dust enrichment in "normal" star forming galaxies at $z \geq 6$. We use the output of a cosmological hydro-dynamical simulation which allows the prediction of the gas, stellar and metal content of galaxies along their hierarchical assembly [Maio et al., 2010]. We then post-process the simulation output with a semi-analytical chemical evolution model with dust [Valiante et al., 2009, 2011, 2014, de Bennassuti et al., 2014] to estimate their dust masses. A similar semi-numerical approach has been followed by [Dayal et al., 2010b], who considered the contribution to dust enrichment of SN and estimate the Far InfraRed (FIR) detectability of high-redshift galaxies classified as Lyman-α emitters (LAE). More recently, [Hirashita et al., 2014a] have been able to put constraints on the dust production rate by SN using the upper limit on the dust continuum emission of Himiko, one of the best-studied LAE at $z \sim 6.6$ [Ouchi et al., 2013]. Here we attempt to improve on these previous studies by considering dust enrichment from SN, AGB stars and grain growth in the ISM with the aim of assessing their relative contribution to the total mass of dust in the ISM of $z \geq 6$ galaxies. We compare the model predictions with currently available upper limits on the dust mass at $6 \leq z \leq 7.5$ and discuss the implications posed on the models by the newly discovered dusty galaxy at $z = 7.5$ [Watson et al., 2015].

The paper is organized as follows: in section 2.1 we give a brief presentation of the semi-numerical model; in section 2.2 we introduce the sample of observed galaxies that we have collected from literature papers, and in section 2.3 we discuss the main results. Finally, in section 2.3 we draw our main conclusions.

2.1 The model

In this Section is described the semi-numerical approach developed to compute the dust mass amount in high-z ($z \in [6, 7]$) galaxies' ISM. The approach is meant to combine reliable structure formation histories of galaxies, derived from the hydrodynamical simulation with cosmological scales already used in Maio et al. [2010], Campisi et al. [2011], Salvaterra et al. [2013], Dayal et al. [2013], with the theoretical prediction of the chemical enrichment of high-z galaxies, through the semi analytical code (hereafter SAM) used in

the works of Valiante et al. [2009, 2012, 2014], de Bennassuti et al. [2014]. This kind of approach is both flexible and reliable because it shrinks the number of free parameters used to model the structure formation, thanks to the numerical simulation, but still allows to explore the physical conditions of the ISM by varying the free parameters of the semi-numerical code. Therefore allowing the understanding of the various conditions that lead to the enrichment of dust in the ISM.

In particular selecting the galaxies in the redshift range $z \in [6, 7]$, we derived the star formation histories and the values of global quantities such as the total gas mass and the total metal mass for each galaxy along its merger tree. The description of the numerical simulation and the technique used to derive the above quantities is described in Section 2.1.1.

For each of the galaxies in the simulation sample we used the SFR, the metallicity and the total gas mass in its ISM to compute the input of the SAM an therefore compute for each galaxy's ISM the dust content. This second part of the procedure is described in Section 2.1.2.

2.1.1 The numerical simulation

We used a ΛCDM cosmological simulation already presented in Maio et al. [2010], here will be described only the relevant features and the simulation set-up, please consider referring to the Maio et al. [2010] paper for further details.

The simulation that has been used is performed with a custom version of GADGET2 code [Springel, 2005]. GADGET2 code uses a TreePM algorithm to compute the dynamical evolution of the dark matter while to solve the hydrodinamical equations related to the barionic component of the universe uses an SPH approach.

In the overdense regions on the domain, the code computes the star formation accounting for the stellar lifetimes using the lifetime function from Padovani and Matteucci [1993]. This allows to relax the instantaneous recycling approximation when the metal enrichment has to be computed. The metal yields assigned to each SNe are taken from Woosley and Weaver [1995] for core-collapse SNe, from Thielemann et al. [2003] for type-Ia SNe and from Heger and Woosley [2002] for pair instability SNe. Instead the AGBs' metal yields for each species of metal are taken from van den Hoek and Groenewe-

gen [1997]. At each given time the initial mass function (IMF) used to compute both the metals produced and the lifetime account for the metallicity (Z) of the starforming gas as described in Tornatore et al. [2007a]. In particular the stars that form in metal critical environment ($\mathrm{Z}_* < \mathrm{Z}_{\rm cr} = 10^{-4}\mathrm{Z}_\odot$) are chosen to have a Salpeter IMF with masses in range $\mathrm{M}_* \in [100, 500]\mathrm{M}_\odot$ and are labeled as population III stars (POPIII). For stars that form in an higher metallicity environment the IMF considered is a Sapeter with masses in range $[0.01, 100]\mathrm{M}_\odot$, these kind of stars are labeled POPII/I. Furthermore the SN explosions' feedback is taken into account by modelling the multi-phase interstellar medium (ISM) as in Springel and Hernquist [2003] with some additional development accounting for the diffusion of metals in the ISM to take into account of gas mixing presented in Maio et al. [2011].

To account for dust cooling the code takes into account of Hydrogen, Helium and Deuterium as shown in Yoshida et al. [2003], Maio et al. [2009] and is able to compute the cooling from resonant and fine structure lines of metals as in Maio et al. [2007].

The prescriptions above are very useful to track the POPIII POPII/I transition that occurs at very high redshifts. Indeed Tornatore et al. [2007b] using the same simulation suggest that the POPIII star formation peak at $\mathrm{z} \sim 6$ but continues up to redshift ~ 2.5 although with a very low efficiency (sSFR $= 10^{-5}$ $\mathrm{M}_\odot \mathrm{yr}^{-1}\mathrm{Mpc}^{-3}$).

Finally a uniform, redshift-dependent UV background produced by quasars and galaxies is also assumed [Haardt and Madau, 1996].

The cosmological parameters adopted for the simulations are:

$\Omega_{\rm M}$	Ω_Λ	$\Omega_{\rm b}$	h	n	σ_8
0.3	0.7	0.04	0.7	1	0.9

where $\Omega_{\rm M}, \Omega_\Lambda$ are the energy densities of the matter and the dark energy respectively, $\Omega_{\rm b}$ is the barionic fraction, h is the Hubble constant in unit of 100 km/s/Mpc, n and σ_8 are the index of the power law and the standard deviation[1] of the primordial linear density fluctuation power spectrum. The chosen box size is 30 h^{-1}cMpc containing 320^3 dark matter particles and the same amount of barionic (SPH) particles and the simulations started

[1] considering a top hat filter with a radius of $8\mathrm{h}^{-1}$ Mpc

at $z = 100$. This means that the mass of a dark matter particle is $6 \times 10^7\ h^{-1}M_\odot$ while for a SPH particle is $9 \times 10^6\ h^{-1}M_\odot$.

To derive the gravitational bound objects we used the friend of friend (FOF) algorithm embedded in the GADGET2 code together the SUBFIND algorithm. Galaxies are recognized to be bound objects that contain at least 32 total particles considering both barionic (SPH + stars) and dark matter ones.

Furthermore to avoid contamination of spurious sources we used for this study only galaxies that have at least 10 stellar particles. In our galaxy sample the above choice means that the galaxies have at least 145 total particles.

In this study we restrict the analysis to two redshift point: 6.14, 7.33. The number of galaxies at the redshift 6.14 is 1863 and drops to 1000 at redshift 7.33.

To better compare the simulated galaxies with the observed one we compute the intrinsic ultraviolet emission of each galaxy to neglect the galaxies that falls below the detectability. Under the hypothesis that dust extinction is not important for galaxies near the UV detection limit of Hubble space telescope (HST) (that is $M_{UV}^{AB} < -18$) we only considered intrinsic emission to perform the sample cut (we will relax this hypothesis in chapter 3).

To compute the intrinsic spectral energy distribution (SED) of each galaxy in the sample we sum up the spectrum of each stellar particle embedded. In doing so we assigned to each stellar particle a synthetic spectrum computed with StarBurst99 [Leitherer et al., 1999, Vázquez and Leitherer, 2005] choosing the population spectrum with the closest metallicity and age.

Finally we computed the M_{UV} using the formula:

$$M_{UV} = -2.5 \log_{10}\left[\frac{L(\lambda_{UV})}{4\pi D^2}\frac{\lambda^2}{c}\right] - 48.6 \tag{2.1}$$

where L is the luminosity for a given wavelength in units of $erg/s^{-1}/Å$, D is the source distance and is chosen to be 10 kpc since we are considering absolute magnitudes and finally $\lambda_{UV} = 1500Å$. We chose this wavelength because it is closer to the filters used from high redshift surveys and it is far from both the ionizing and Layman Werner (LW) radiation.

Considering now only the galaxies that have an intrinsic UV magnitude lower than

$\mathrm{M_{UV}} < -18$ (brighter that the detection limit of HST) we obtain a sample of 102 galaxies at redshift ~ 7 and 225 at redshift ~ 6.

The average ISM metallicities of these galaxies at both redshift are $5 \times 10^{-3}\mathrm{Z_\odot} \leq \mathrm{Z} \leq 0.1\mathrm{Z_\odot}$, the mass averaged age of their stellar populations is $40\mathrm{Myr} \leq \mathrm{t_{age}} \leq 200\mathrm{Myr}$ and finally their stellar mass is $7.5 \leq \log_{10}[\mathrm{M_{star}}] \leq 9.5$. Moreover their star formation rates are lower than $30\mathrm{M_\odot\,yr^{-1}}$, hence is legitimate to refer to them as "normal" galaxies

The dust content in a galaxy strongly depends on its star formation and metal enrichment and merging histories. Dust is also reprocessed in the ISM as, for instance, dust grains shuttering in the ISM thanks to SNe explosion[see for example Hirashita et al., 2016, and reference therein]. Unfortunately the approach used in this work doesn't allow to take into account of these processes, hence we will consider only star formation, metal enrichment and merging histories to compute the dust content of each galaxy taking into account of destruction processes re-scaling their efficiency with the star formation (see 2.1.2 for the description of the dust formation/evolution model). Please consider referring to Graziani [2017, in prep], Aoyama et al. [2017] for a better description of the dust formation/evolution in high redshift galaxies.

As I mentioned before to derive the input for the SAM code we need to track for each galaxy in the simulation its ancestors to reconstruct the merger tree. Hence I developed a code which is able to track all the galaxies' particles present at the considered end snapshot up the previous redshift tracking the id of the parents. This allows us to obtain a merger tree for each galaxy in the final snapshot. With the newly computed merger tree we were able to describe all the SAM required quantities for each galaxy in the simulated sample: the star formation histories $\mathrm{SFR(z)}$, the gas mass $\mathrm{M_{gas}(z)}$, and the metal mass $\mathrm{M_Z(z)}$.

2.1.2 The semi-analytical code

The SAM used in this work is the one developed in the work of Valiante et al. [2009] then applied to semi analytic merger tree models of high redshift QSOs by Valiante et al. [2011, 2012, 2014] and recently improved by de Bennassuti et al. [2014] to explain dust and metal content in the Milky Way and its progenitors. Please consider referring to this paper if you need a detailed explanation of the code, we will here refer only to the equation and processes regarding the dust formation since we used the metallicity and the hierarchical

scenario as computed from GADGET2 (see 2.1.1).

The equation describing the dust mass evolution is,

$$\dot{\mathrm{M}}_{\mathrm{d}}(\mathrm{t}) = -\mathrm{Z}_{\mathrm{d}}(\mathrm{t})\mathrm{SFR}(\mathrm{t}) + \dot{\mathrm{Y}}_{\mathrm{d}}(\mathrm{t}) - (1-\mathrm{X}_{\mathrm{c}})\frac{\mathrm{M}_{\mathrm{d}}(\mathrm{t})}{\tau_{\mathrm{d}}} + \mathrm{X}_{\mathrm{c}}\frac{\mathrm{M}_{\mathrm{d}}(\mathrm{t})}{\tau_{\mathrm{acc}}} \tag{2.2}$$

where $\mathrm{M_d}$ is the dust mass, $\mathrm{Z_d}$ is the dust to gas ratio in the ISM (i.e. $\mathrm{M_d/M_{gas}}$), $\mathrm{X_c}$ is the cold gas mass fraction chosen to be $1/2$[2] in this work and then further improved in chapter 3, τ_{d} and τ_{acc} are the dust destruction timescale and the dust accretion timescale and they will be discussed below.

The time dependent term $\dot{\mathrm{Y}}_{\mathrm{d}}(\mathrm{t})$ refers to the the dust production rate and it depends on the stellar IMF and on the adopted model of yields . We compute it as follows:

$$\dot{\mathrm{Y}}_{\mathrm{d}}(\mathrm{t}) = \int_{\mathrm{m(t)}}^{\mathrm{m_{up}}} \mathrm{m_d}(\mathrm{m},\mathrm{Z})\Phi(\mathrm{m})\mathrm{SFR}(\mathrm{t}-\tau_{\mathrm{m}})\mathrm{dm}, \tag{2.3}$$

where $\mathrm{m_d}$ is the dust mass yield (which is the dust mass per unit of star formation rate produced by a star with initial mass m and metallicity Z), $\Phi(\mathrm{m})$ is the stellar IMF, and $\mathrm{m(t)}$ is the mass of a star with a lifetime t.

To be consistent with the simulation used we chose a Salpeter IMF in the mass range $[0.01, 100]\mathrm{M_\odot}$ for POPII/I. We neglect the contribution of POPIII stars since their presence at the analysed redshifts is sub dominant as pointed out also in Dayal et al. [2010b].

The yields adopted are the following:

- van den Hoek and Groenewegen [1997], Zhukovska et al. [2008] for stars with masses $\mathrm{m} < 8\mathrm{M_\odot}$
- Woosley and Weaver [1995], Bianchi and Schneider [2007] for stars with masses $\mathrm{m} \in [12, 40]\mathrm{M_\odot}$, these yields take also into account of dust destruction in SNe reverse shock.
- we interpolate between the previous yields to compute the dust yields for stars with masses $\mathrm{m} \in [8, 12]\mathrm{M_\odot}$.
- we considered the stars with masses $\mathrm{m} > 40\mathrm{M_\odot}$ to end its life collapsing as black holes without polluting their environment.

[2]This is motivated by the fact that averaging over simulated galaxies with different masses this value range from 0.38 to 0.56 Vallini et al. [2012]

Finally the last two terms in the equation ($\tau_{\rm d}$, $\tau_{\rm acc}$) represent the dust destruction by interstellar shock waves and the dust accretion from gas metals in the cold and dense part of the ISM. We described these terms as in de Bennassuti et al. [2014] but we slightly modify the accretion term. In fact, given the gas phase metallicity Z, the temperature of the molecular phase of the ISM (note that we refer as molecular phase the dense and cold phase of the ISM despite its molecular content) $\rm T_{mol}$ and the density $\rm n_{mol}$, the accretion term is written as,

$$\tau_{\rm acc} = 20{\rm Myr} \times \left(\frac{\rm n_{mol}}{100{\rm cm^{-3}}}\right)^{-1} \left(\frac{\rm T_{mol}}{50{\rm K}}\right)^{-1/2} \left(\frac{\rm Z}{\rm Z_{\odot}}\right)^{-1} = \tau_{\rm acc,0} \left(\frac{\rm Z}{\rm Z_{\odot}}\right)^{-1} \tag{2.4}$$

where we have assumed that grains which experience grain growth have a typical size of $\sim 0.1\mu{\rm m}$ [Hirashita et al., 2014a]. It is important to stress that the gas phase metallicity Z is defined as the difference between the ISM metallicity $\rm Z_{ism}$ and the dust to gas ratio $\mathcal{D}$. Hence, the accretion saturates when $\rm Z_{ism} \sim \mathcal{D}$ and the gas-phase metal abundance is exhausted. For a gas at solar metallicity, with $\rm n_{mol} = 10^3 cm^{-3}$ and $\rm T_{mol} = 50K$, the accretion timescale is $\tau_{\rm acc,0} = 2{\rm Myr}$ [Asano et al., 2013]. Smaller grain sizes increase the grain surface area per unit of dust mass, thus shortening the accretion timescale [Kuo and Hirashita, 2012]. Since the simulation has not the resolution to trace the temperature nor the density of molecular of the ISM we chose to factor out a common average value of accretion timescale $\tau_{\rm acc,0}$ and explore the dependence of the results to its different values.

2.2 The observed sample

To compare our theoretical prediction with observations we collected a sample, which is summarized in Table 2.1, of the galaxies from the literature. For 8 out of the 9 galaxies, upper limits on the dust continuum emission have been obtained by means of deep ALMA and PdBI observations [Kanekar et al., 2013, Ouchi et al., 2013, Ota et al., 2014, Schaerer et al., 2015, Maiolino et al., 2015]. The $\rm z = 7.5$ LBG A1689-zD1 was the most distant UV-selected galaxy for which a dust continuum detection has been obtained with ALMA [Watson et al., 2015, Knudsen et al., 2017] before the recent discovery of Laporte et al. [2017b]. Unfortunately, galaxies with stellar masses comparable with A2744-YD4 [Laporte et al., 2017b] are not present in our relatively small simulated volume at $\rm z \sim 7.5$. Nevertheless, comparing the inferred dust mass and redshift of A2744-YD4 (Table 2.1)

Name	z	M_{UV} mag	Log M_{star} [$M_\odot$]	Log M_{dust} [$M_\odot$]
A1703-zD1[a]	6.800	-20.3	9.2 ± 0.3	< 7.36
z8-GND-5296[a]	7.508	-21.4	9.7 ± 0.3	< 8.28
HCM6A[b]	6.560	-20.8	9.5 ± 0.3	< 7.61
IOK-1[c]	6.960	-21.3	9.7 ± 0.3	< 7.43
Himiko[d]	6.595	-21.7	9.9 ± 0.3	< 7.30
BDF-3299[e]	7.109	-20.44	9.3 ± 0.3	< 7.02
BDF-512[e]	7.008	-20.49	9.3 ± 0.3	< 7.36
SDF-46975[e]	6.844	-21.49	9.8 ± 0.3	< 7.38
A1689-zD1[f]	7.500	-19.7	9.0 ± 0.3	7.51 ± 0.2
A2744-YD4[g]	8.38	–	$9.3^{+0.20}_{-0.19}$	$6.7^{+0.66}_{-0.16}$

Table 2.1. Physical properties of the galaxy sample collected from the literature. Lensed objects have been corrected using the appropriate magnification factor ($\mu = 4.5, 9$ and 9.3 for HCM6A, A1703-zD1 and A1689-zD1, respectively). All the quantities are computed assuming conversion factors, scaling relations and dust properties presented in the text. References: a: Schaerer et al. [2015]; b: Kanekar et al. [2013]; c: Ota et al. [2014]; d: Ouchi et al. [2013]; e: Maiolino et al. [2015]; f: Watson et al. [2015]; g Laporte et al. [2017b].

with Figure 2.2, it is clear that this observation requires efficient dust accretion.

For all these galaxies, the star formation rates estimated from the UV luminosity[3] range between 4.1 and 22.4 $M_\odot$/yr. Following Schaerer et al. [2015], we derived the stellar masses using the mean relation between the UV magnitude and the stellar mass obtained by the same authors from detailed fits of the spectral energy distribution of a sample of $z \sim 6.7$ LBGs, including nebular emission and dust attenuation:

$$\mathrm{Log}(M_{star}/M_\odot) = -0.45 \times (M_{UV} + 20) + 9.11. \quad (2.5)$$

Dayal et al. (2014) obtain a similar $M_{star}-M_{UV}$ relation on the basis of a theoretical model, which also accounts for the rapid decline of the UV luminosity with stellar ages.

Assuming that the dust is optically thin in the rest-frame FIR, the upper limits on the dust mass have been obtained taking into account the effect of the Cosmic Microwave Background (CMB) on the intrinsic dust emission [da Cunha et al., 2013]. In Table 2.1 we report dust masses adopting a dust temperature[4] $T_{dust,0} = 35$ K and a dust emissivity $k_{\nu_{res}} = k_0(\lambda_0/\lambda_{res})^\beta$ with $k_0 = 0.77\,cm^2/gr$, $\lambda_0 = 850\,\mu m$ and $\beta = 1.5$ [Ota et al., 2014]. The dust mass can increase/decrease by ~ 0.4 dex for variations in the dust temperature in the range $25K \leq T_{dust,0} \leq 45K$. In addition, the poorly constrained dust properties make the value of the emissivity coefficient to be adopted very uncertain [see Table 1 in Hirashita et al., 2014a]. At fixed dust temperature, we find that variations in k_ν among values adopted in the literature [Weingartner and Draine, 2001] or applied to submm observations of high-z galaxies [Michałowski et al., 2010, Valiante et al., 2014, Watson et al., 2015] introduce an additional ~ 0.3 dex uncertainty in the estimated dust mass.

2.3 Results

Figure 2.1 shows a comparison between the predicted dust masses of the simulated galaxies and the observations. We show the dust mass as a function of the stellar mass for all the simulated galaxies with intrinsic $M_{UV} \leq -18$ at $z = 6.33$ and $z = 7.14$. For each galaxy,

[3] We have adopted a conversion factor of $\mathcal{K}_{UV} = 1.15 \times 10^{-28}\,M_\odot\,yr^{-1}/erg\,s^{-1}Hz^{-1}$, as appropriate for a stellar population with metallicity $0.3\,Z_\odot < Z < Z_\odot$ formed at a constant SFR with a Salpeter IMF in the range $[0.1 - 100]\,M_\odot$ at age ~ 300 Myr [Madau and Dickinson, 2014].

[4] $T_{dust,0}$ is the dust temperature heated by a stellar radiation field at $z = 0$ [da Cunha et al., 2013].

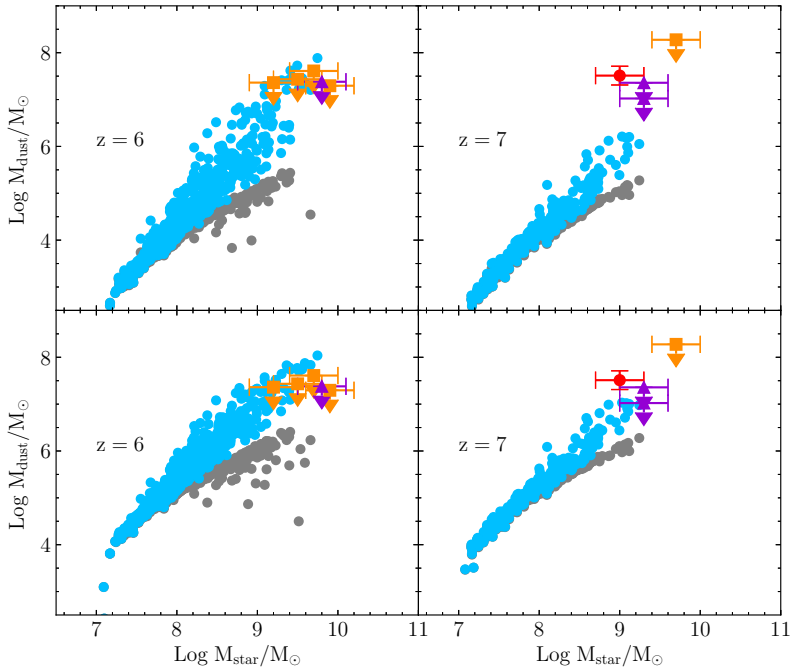

Figure 2.1. Predicted dust masses of the simulated galaxies as a function of the stellar mass. For each galaxy, the dust mass without (with) grain growth is shown by a square grey (circle blue) point (see text). The adopted grain growth timescale is $\tau_{acc,0} = 2$ Myr. In the lower panels, the reverse shock destruction of SN dust is neglected. For the sake of comparison, we have reported the same data points shown in Table 1 in the two panels: Schaerer et al. [2015] (squares), Maiolino et al. [2015](triangles) and Watson et al. [2015] (circle point).

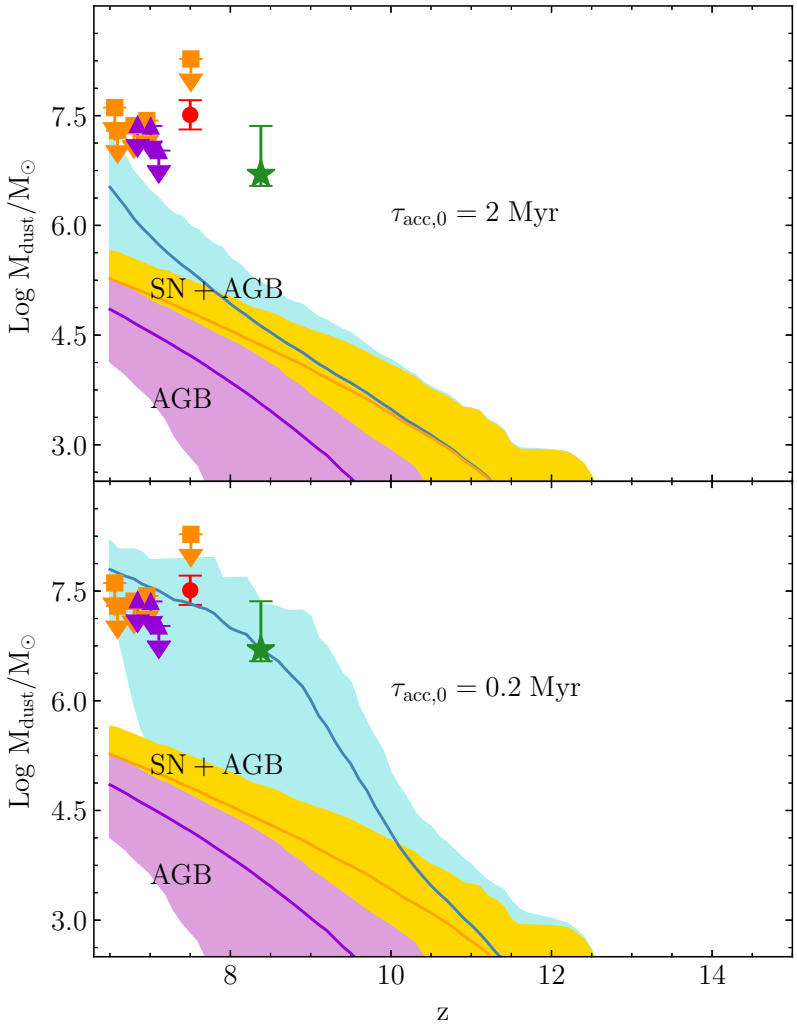

Figure 2.2. Redshift evolution of the dust mass for the simulated galaxies with stellar masses in the range $\mathrm{Log}\, M_{star}/M_\odot \geq 9$. Each line represents the average contribution of all the galaxies with the shaded area indicating the dispersion among different evolutionary histories. The lower, intermediate and upper lines show the contribution to the total mass of dust of AGB stars, stellar sources and grain growth with an accretion timescale of $\tau_{acc,0} = 2$ Myr (upper panel) and 0.2 Myr (lower panel). The galaxy A1689-zD1 and A2744-YD4 are shown respectively as a red dot and green star [Watson et al., 2015, Laporte et al., 2017b].

the light grey point represents the mass of dust that is produced by stellar sources (AGB stars and SNe) after grain destruction and astration (eq. 2.2 without grain growth), and the blue point is the total dust mass, including the effect of grain growth in the ISM. Here we have assumed a grain growth timescale $\tau_{\rm acc,0} = 2\,$Myr. Due to the lower metallicities, grain growth is not efficient at stellar masses $\rm M_{star} < 10^8 M_\odot$. In these small galaxies, we predict that all the existing dust mass is entirely contributed by stellar sources. Galaxies with larger stellar masses have experienced a larger degree of chemical enrichment and the gas metallicities are high enough to activate efficient grain growth, although with a large scatter. Yet, due to the time required to enrich the ISM with metals, the bulk of the dust mass in the most massive galaxies is grown between $\rm z \sim 7$ and $\rm z \sim 6$. In fact, while at $\rm z \sim 7$ all the simulated galaxies have $\rm M_{dust} < 2 \times 10^6\,M_\odot$, at $\rm z \sim 6$ there are several galaxies with dust masses $\rm 10^7 M_\odot \leq M_{dust} \leq 10^8\,M_\odot$. Note that the observational data points, that we have reported in both panels for the sake of comparison, refer to galaxies which span a redshift range $6.5 \leq \rm z \leq 7.5$ (see Table 1).

These results depend on the adopted stellar dust yield and grain growth timescale. In the lower panel of Figure 2.1 we show the effect of reducing the efficiency of grain destruction by the SN reverse shock: if all the grains survive the passage of the reverse shock, the effective SN dust yields is ~ 20 times larger and the resulting dust masses contributed by stellar sources increase by a comparable factor. These SN yields bracket the observations of dust masses in SN and SN remnants obtained with the *Herschel* satellite (see Fig. 6 in Schneider et al. [2014]). The figure shows that although the total dust mass is larger, even with maximally efficient SN dust enrichment the predicted dust masses at $\rm z \sim 7$ are $\rm M_{dust} < 10^7 M_\odot$, too small to account for the observed dust mass in A1689-zD1. We conclude that in order to account for the existing dust mass in this galaxy, a shorter grain growth timescale is required.

It is interesting to analyse the relative contribution of AGB stars, SN and grain growth as a function of redshift. Figure 2.2 shows the redshift evolution of the dust mass for galaxies with $\rm M_{star} > 10^9\,M_\odot$ at redshift 6.14. We separate the contribution from AGB stars, stellar sources, and the total mass of dust, including grain growth with an accretion timescale $\tau_{\rm acc,0} = 2\,$Myr (upper panel) and 0.2 Myr (lower panel). As expected from Figure 2.1, grain growth provides the dominant contribution, exceeding the dust produced by stellar

sources already at $z < 10 - 12$. Among the stellar sources, SN appear always dominant, but the average contribution of AGB stars can be as large as $\sim 40\%$. This confirms that the contribution of AGB stars to high redshift dust formation can not be neglected, especially for the galaxies currently targeted by observational searches [Valiante et al., 2009]. Finally, in the lower panel we show that the dust mass detected in A1689-zD1 requires very efficient grain growth, with a timescale $\tau_{\rm acc,0} = 0.2\,{\rm Myr}$, one order of magnitude shorter than required to reproduce the observed dust-to-gas ratio in the Milky Way and in most local dwarf galaxies [de Bennassuti et al., 2014]. This, in turn, implies that the cold atomic and molecular phases of the ISM, where grain growth is more efficient, must have an average density of $\sim 10^4 {\rm cm}^{-3}$ (see eq. 2.4). Such a value is comparable to the molecular gas density inferred from CO excitation analyses of starburst galaxies at comparable (although slightly smaller) redshifts [see Carilli and Walter, 2013]. Moreover, the molecular phase in these high-redshift star-forming galaxies may also be warmer, leading to somewhat lower $\tau_{\rm acc,0}$. Although plausible, our study suggests that these conditions must be exceptional, as if they were to apply to all galaxies a $z > 6.5$, current upper limits on the dust continuum emission for normal star forming galaxies at $6.5 < z < 7.5$ would be exceeded.

Chapter 3

Interpreting the evolution of galaxy colours from z = 8 to 5

3.1 Introduction

In the last decade, data from the *Hubble Space Telescope*[1] (HST), especially after the advent of the Wide Field Camera (WFC3), allowed us to collect large samples of galaxies at $z \sim 7-8$, with smaller samples extending up to $z \sim 9-11$ [McLure et al., 2013, Bouwens et al., 2014, Oesch et al., 2014, Bouwens et al., 2015, McLeod et al., 2015, Finkelstein et al., 2015a], among which the two most distant spectroscopically confirmed galaxies at $z = 8.68$ [Zitrin et al., 2015] and $z = 11.1$ [Oesch et al., 2016]. Since spectroscopic observations of galaxies at $z > 6$ with ground-based telescopes are very challenging, observers have developed alternative, photometry-based techniques to both select high-z candidates and estimate their physical properties. For example, the total stellar mass, the stellar age and the ongoing star formation rate (SFR) can be estimated from spectral energy distribution (SED) fitting and colour index analyses.

Two key quantities are generally used to characterize the properties of the first galaxies and of their dominant stellar populations: the UV luminosity function (LF) and the observed UV spectral slope, β ($f_\lambda \propto \lambda^\beta$, Meurer et al. 1999). The LF, defined as the number density of galaxies per unit magnitude, provides important constraints on star formation efficiencies at different redshifts and on their evolutionary status, especially at early times

[1] http://www.stsci.edu

[Bouwens et al., 2011]. As the first structures collapse and assemble their stellar content, the inter-stellar medium (ISM) is progressively enriched with metals and dust. Dust extinction affects the UV luminosity and should leave a signature in the galaxy LF. While for low-redshift galaxies dust extinction can be corrected by measuring the far infrared emission (FIR), observations of high-z galaxies with millimeter (mm) telescopes, such as the *Atacama Large Millimeter Array* (ALMA) and the *Plateau de Bure Interferometer* (PdBI), have mostly provided upper limits on the rest-frame FIR emission of $z > 6$ UV-selected galaxies [Kanekar et al., 2013, Ouchi et al., 2013, Ota et al., 2014, Schaerer et al., 2015, Maiolino et al., 2015, Zavala et al., 2015], with two notable exception [Watson et al., 2015, Knudsen et al., 2017, Laporte et al., 2017b]. For this reason, it has become a common practice to estimate the effects of dust extinction using the observed β slope, or UV colour.

Despite a vigorous debate in the past ten years, recent observational results appear to converge on a common trend for the shape and the evolution of the UV LF in the redshift range $4 < z < 8$ [Bouwens et al., 2015], down to an AB magnitude of –16 at $z = 4, 5$ and of $\sim$ –17 at $z = 6, 7$ and 8. At even higher redshifts, even the deepest observations in blank fields can only probe the bright-end of the LF, providing important constraints on the volume density of the most luminous galaxies with $M_{UV} < -20$ at $z = 9$ and 10 [Bouwens et al., 2015]. An efficient way to push the observations to fainter luminosities is to exploit the gravitational lensing magnification of massive galaxy clusters. Results from the HST programs CLASH and Hubble Frontier Fields (HFF) have increased the statistics of candidate galaxies at the highest redshifts, providing better constraints on the evolution of the faint-end slope of the LF and placing the first limits on the LF at $z \sim 10$ [Atek et al., 2015, McLeod et al., 2015, 2016, Livermore et al., 2016] .

It is custumary to fit the LF with a Schechter function, which has a power-law behaviour with slope α at the faint-end, an exponential cut-off brighter than a characteristic luminosity (magnitude) L_* (M_*) and a volume density of ϕ_* at this characteristic luminosity,

$$\frac{dn}{dL} = \phi(L) = \left(\frac{\phi_*}{L_*}\right)\left(\frac{L}{L_*}\right)^{\alpha} e^{-L/L_*}. \tag{3.1}$$

In general, the evolution of the LF with redshift is characterized by means of variations of these Schechter parameters and is consistent with a steady growth in the volume density and luminosity of galaxies with time. In particular, there is a significant evidence for a steepening of the faint-end slope with z, in agreement with the predicted steepening of the

halo mass function, a modest evolution of M_* and a decrease of ϕ_* from $\mathrm{z} \sim 4$ to $\mathrm{z} \sim 7$ [Bouwens et al., 2015]. Some observations at $\mathrm{z} = 9$ and 10 suggest a faster evolution, and that the luminosity densities inferred from current samples are ~ 2 times lower than the values extrapolated from the trends at $4 < \mathrm{z} < 8$ [Bouwens et al., 2015]. Other studies support a smoother evolution from $\mathrm{z} = 8$ to 9 [McLeod et al., 2015, 2016, Finkelstein et al., 2015a]. Indeed, the recent discovery of GN-z11, a luminous galaxy with $\mathrm{M_{UV}} = -22.1$ at $\mathrm{z} = 11$ [Oesch et al., 2016] may indicate that the LF at the very bright end does not follow a Schechter functional form, possibly due to less efficient feedback at very high redshifts [Bowler et al., 2014, Dayal et al., 2014, Finkelstein et al., 2015b, Waters et al., 2016].

To convert the observed UV luminosity to a SFR and compare the above findings to theoretical predictions, dust extinction is usually estimated using the observed β slopes and the so-called IRX-β relationship by Meurer et al. [1999], who proved that, at $\mathrm{z} < 3$, the amount of SED reddening directly correlates with the β value, as also confirmed by independent theoretical predictions (e.g. Wilkins et al. 2012). Although this relation has been calibrated on starburst galaxies at low redshifts, and assumes a constant mean intrinsic slope of $\beta = -2.23$, this procedure has been widely adopted in high-z galaxy surveys [see Bouwens et al., 2012]. However, the value of β is also a function of important properties of the stellar populations, such as their ages, metallicity and initial mass function (IMF). Although with large uncertainties, observational trends have been reported which quantify the dependence of β on the UV luminosity and redshift [Stanway et al., 2005, Wilkins et al., 2011, Finkelstein et al., 2012, Bouwens et al., 2012, Castellano et al., 2012, Dunlop et al., 2013]. In general, the observations are consistent with a decreasing reddening towards lower luminosities and higher redshift. A coherent analysis of the observed β for galaxies in a wide redshift range, from $\mathrm{z} \sim 4$ to $\mathrm{z} \sim 7$, has been recently made by Bouwens et al. [2014], who confirm a strong evidence for a dependence of the average β on the UV luminosity, the so-called Colour-Magnitude-Relation (CMR, Rogers et al. 2014), with brighter galaxies being redder and fainter galaxies being bluer, and a flattening of the relation at luminosities faintward of $\mathrm{M_{UV}} \sim -19$. They also report a small but clear evolution with time, with galaxies at fixed luminosity becoming bluer with z. For the faint galaxies with $-19 < \mathrm{M_{UV}} < -17$, the mean β at $\mathrm{z} \sim 4, 5$ and 6 is -2.03, -2.14 and -2.24 respectively. Extrapolation of this trend to $\mathrm{z} \sim 7$ and 8 suggests mean values of -2.35 and

-2.45, consistent - within the errors - with the observed ones.

Theoretical studies have attempted to interpret the data by means of numerical simulations or semi-analytical models. Wilkins et al. [2012] explored the sensitivity of the intrinsic β slopes to the IMF and to the recent star formation and metal enrichment histories of low-z galaxies. They find a distribution of β values with a scatter of 0.3, which introduces an uncertainty in the inferred dust attenuation when a constant intrinsic slope is assumed. This scatter is significantly reduced for galaxies at $z \sim 6$, but the mean intrinsic β decreases with z. If this is not properly taken into account and the locally calibrated relation is applied, dust attenuation is systematically underestimated [Wilkins et al., 2013]. Gonzalez-Perez et al. [2013] have demonstrated the dependence of the galaxy UV colours on the adopted dust properties and, in particular, on the dust extinction curve. With the aim of intepreting high-z Lyman-α emitters (LAEs) and Lyman Break Galaxies (LBGs) observations, Dayal et al. [2010a] and Dayal and Ferrara [2012] used a numerical simulation to derive intrinsic galaxy properties and a semi-analytical model to estimate dust attenuation. They explored the resulting UV LF and the dependence of β on the galaxy UV luminosity with and without dust attenuation. They found that dust attenuation improves the agreement with the observations, but the observed CMR was not reproduced by the model results. More recently, Khakhaleva-Li and Gnedin [2016b] post-processed the results of cosmological simulations with a simple dust model that assumes a constant dust-to-metal mass ratio in the neutral gas and that dust is instantaneously sublimated in hot ionized regions. They used a Monte Carlo radiative transfer code to predict UV attenuation and IR re-emission of their model galaxies. By means of a detailed comparison with observations at $5 \leq z \leq 10$, they concluded that, in order to assess the effects of dust in the ISM of high-z galaxies, the complex interplay of dust creation and destruction processes should be fully incorporated into numerical simulations.

With this aim, in Chapter 2 we have presented a semi-numerical model which includes a physically motivated description of dust evolution, accounting for dust enrichment by Supernovae (SNe) and Asymptotic Giant Branch (AGB) stars, the effects of dust destruction by SN shocks and grain growth in the dense cold phase of the ISM (see also Valiante et al. 2009, 2011, de Bennassuti et al. 2014). We then compared the model predictions with the limits on the dust mass inferred from mm-observations of $z > 6$ galaxies, deriving interest-

ing constraints on the properties of their ISM and on the nature of dust at high-z. Here we extend this previous investigation with the goal of intepreting the observed UV luminosities and colours of galaxies at $5 < z < 8$.

This Chapter is organized as follows. In Section 3.2 we describe our method and the assumptions made to compute the dust content and luminous properties of the simulated galaxies. In Section 3.3 we first discuss the predicted physical properties of the galaxies at $5 \leq z \leq 8$. Then we derive the UV LFs and β slopes assuming no dust extinction, and discussing the dependence of the results on the extinction model. In Section 3.4 we introduce the model that better reproduce the observed UV LFs and CMR. We analyze the origin of the scatter around the mean values at different z, both in the CMR and in the stellar mass - UV luminosity relation. We compute the IR excess and dust attenuation factors, comparing with observationally inferred correlations. Finally, in Section **??** we summarize the results and draw the main conclusions.

3.2 Method

In this section we describe the semi-numerical model that we have developed. First, we infer the intrinsic galaxy properties using the output of a hydro-dynamical simulation of structure formation described in Section 3.2.1. To compute the *intrinsic* UV luminosity of each galaxy, we calculate the spectral energy distribution (SED) as described in Section 3.2.2. We then couple the simulated output, in particular the star formation rate (SFR), metallicity (Z) and mass of gas (M_g) of each simulated galaxy, with a semi-analytical model to estimate the dust mass (M_d) as in Chapter 2 [Mancini et al., 2015]. To accomplish this goal, we have used a more advanced version of the semianalytical model used in Chapter 2 to trace the dust enrichment of both the dense and diffuse part of the ISM (see below for additional details). A brief summary of this method is provided in Section 3.2.3. Finally, in Section 3.2.4, we present the method adopted to compute dust extinction.

3.2.1 Cosmological simulation

The simulation used is the same as in Chapter 2 and [Mancini et al., 2015]. We will briefly summarize here the main characteristics and the particle resolutions. The simulation box

has a size of 30 h^{-1} Mpc (comoving), with periodic boundary conditions. The total number of dark matter and gas particles is $\mathrm{N_p} = 2 \times 320^3$ and the dark matter (gas) particle mass is $\mathrm{M^p_{DM}} = 6 \times 10^7\,\mathrm{h}^{-1}\mathrm{M}_\odot$ ($\mathrm{M^p_g} = 9 \times 10^6 \mathrm{h}^{-1}\mathrm{M}_\odot$). In Sec. 3.3.1 we discuss the impact of the simulation volume and mass resolution on this study. Dark matter halos are identified by means of an FOF algorithm as a group of at least 32 gravitationally bound particles.

By tracking the star particles along the redshift evolution we also reconstruct the merger tree of each simulated galaxy. This is needed to compute the evolution in redshift of the star formation rate, the gas mass and metallicity, which have been used to initialize the dust evolution model, as detailed in Section 3.2.3.

3.2.2 Intrinsic galaxy spectra

The *intrinsic* SED of a galaxy depends on the IMF, age and metallicity of each stellar population that contributes to the emission. Since the mass fraction of active Pop III stars is negligible[2] at $5 < \mathrm{z} < 8$ (see also Salvaterra et al. 2011), we consider the UV luminosity contributed by Pop II/I stars using the spectral synthesis model StarBurst99 (hereafter SB99, Leitherer et al. 1999, Vázquez and Leitherer 2005). We assume that each star particle, which represents a single stellar population, is formed in an istantaneous burst. The routines of SB99 responsible for computing dust extinction have been disabled and only the stellar and nebular emission is accounted for. In this way, we compute a database of intrinsic spectra in the metallicity range $0.02\,\mathrm{Z}_\odot \leq \mathrm{Z}_* \leq 1\,\mathrm{Z}_\odot$ for stellar ages $2\,\mathrm{Myr} \leq \mathrm{t}_\star \leq 1\,\mathrm{Gyr}$. The database is used to assign an intrinsic luminosity $\mathrm{l}^{\mathrm{i}}_\lambda(\mathrm{Z}_*, \mathrm{t}_*)$ to each star particle i and the cumulative *intrinsic* SED of the j-th galaxy to which the star particle belongs is computed as,

$$\mathrm{L}^{\mathrm{j}}_\lambda = \sum_{\mathrm{i}} \mathrm{l}^{\mathrm{i}}_\lambda(\mathrm{Z}_*, \mathrm{t}_*)\,\mathrm{M}_{*,\mathrm{i}}, \tag{3.2}$$

where $\mathrm{M}_{*,\mathrm{i}}$ is the mass of the i-th star particle.

[2]We find that the mass fraction of Pop III stars decreases with the UV luminosity ranging from ~ 0.1 at $\mathrm{M_{UV}} = -18$ to $\sim 10^{-3}$ at $\mathrm{M_{UV}} = -22$. However, in all but 2 galaxies at $\mathrm{z} \sim 6$, Pop III stars have already disappeared due to their short lifetimes, and their contribution to the UV emission at $\mathrm{z} < 8$ can be safely neglected.

3.2.3 Dust evolution model

Dust grains can form by condensation of gas-phase metals in the ejecta of SNe [Todini and Ferrara, 2001, Nozawa et al., 2003, Schneider et al., 2004, Bianchi and Schneider, 2007, Cherchneff and Lilly, 2008, Cherchneff and Dwek, 2009, Sarangi and Cherchneff, 2013, Marassi et al., 2014, 2015] and in the atmosphere of AGB stars [Ferrarotti and Gail, 2006, Zhukovska et al., 2008, Ventura et al., 2012b,a, Di Criscienzo et al., 2013, Nanni et al., 2013, Ventura et al., 2014, Schneider et al., 2014]. Once created by stars and dispersed in the interstellar medium of a galaxy, dust grains evolve depending on the environmental conditions. In the dense cold phase of the ISM, dust grains can grow by accretion of gas-phase elements [Asano et al., 2013, Hirashita et al., 2014b] while in the hot diffuse phase the grains can be efficiently destroyed by interstellar shocks [Bocchio et al., 2014]. All these processes are reviewed in Draine [2011] and have been implemented in chemical evolution models with dust [Valiante et al., 2009, 2011, de Bennassuti et al., 2014]. Since the cosmological simulation does not have the resolution to describe the different phases of the ISM which are relevant to dust evolution, the values it provides are only indicative of the average physical conditions of their ISM. To circumvent this limitation, we follow the same approach adopted in Chapter 2, where dust enrichment in each galaxy can be described self-consistently within the average properties predicted by the simulation.

Following de Bennassuti et al. [2014], we adopt a 2-phase ISM model with a diffuse component (warm/hot low-density gas), where dust can be destroyed by SN shocks, and a dense or molecular cloud component (cold and dense gas), where star formation and grain growth occur. The time evolution of the ISM mass (gas and dust, $\mathrm{M_{ISM}}$), the mass in heavy elements (gas-phase metals and dust, $\mathrm{M_Z}$) and the dust mass ($\mathrm{M_d}$) in the diffuse (diff) and molecular cloud (MC) phase is described by the following system of equations:

$$\dot{\mathrm{M}}^{\mathrm{mc}}_{\mathrm{ISM}}(\mathrm{t}) = \dot{\mathrm{M}}_{\mathrm{cond}}(\mathrm{t}) - \mathrm{SFR}(\mathrm{t}) \tag{3.3}$$

$$\dot{\mathrm{M}}^{\mathrm{diff}}_{\mathrm{ISM}}(\mathrm{t}) = -\dot{\mathrm{M}}_{\mathrm{cond}}(\mathrm{t}) + \dot{\mathrm{R}}(\mathrm{t}) + \dot{\mathrm{M}}_{\mathrm{inf}}(\mathrm{t}) - \dot{\mathrm{M}}_{\mathrm{ej}}(\mathrm{t}) \tag{3.4}$$

$$\dot{\mathrm{M}}^{\mathrm{mc}}_{\mathrm{Z}} = \dot{\mathrm{M}}^{\mathrm{Z}}_{\mathrm{cond}}(\mathrm{t}) - \mathrm{SFR}(\mathrm{t})\,\mathrm{Z_{mc}} \tag{3.5}$$

$$\dot{\mathrm{M}}^{\mathrm{diff}}_{\mathrm{Z}} = -\dot{\mathrm{M}}^{\mathrm{Z}}_{\mathrm{cond}}(\mathrm{t}) + \dot{\mathrm{Y}}_{\mathrm{Z}}(\mathrm{t}) \tag{3.6}$$

$$\dot{\mathrm{M}}^{\mathrm{mc}}_{\mathrm{d}} = \dot{\mathrm{M}}^{\mathcal{D}}_{\mathrm{cond}}(\mathrm{t}) - \mathrm{SFR}(\mathrm{t})\,\mathcal{D}_{\mathrm{mc}} + \frac{\mathrm{M}^{\mathrm{mc}}_{\mathrm{d}}(\mathrm{t})}{\tau_{\mathrm{acc}}} \tag{3.7}$$

$$\dot{\mathrm{M}}_{\mathrm{d}}^{\mathrm{diff}} = -\dot{\mathrm{M}}_{\mathrm{cond}}^{\mathcal{D}}(\mathrm{t}) + \dot{\mathrm{Y}}_{\mathrm{d}}(\mathrm{t}) - \frac{\mathrm{M}_{\mathrm{d}}^{\mathrm{diff}}(\mathrm{t})}{\tau_{\mathrm{d}}}, \tag{3.8}$$

where the time-dependent star formation rate (SFR) and the infall and outflow rates ($\dot{\mathrm{M}}_{\mathrm{inf}}$ and $\dot{\mathrm{M}}_{\mathrm{ej}}$) are computed from the simulation outputs, $\mathrm{Z} = \mathrm{M_Z}/\mathrm{M_{ISM}}$ and $\mathcal{D} = \mathrm{M_d}/\mathrm{M_{ISM}}$ are the ISM mass fractions in heavy elements and dust, τ_{d} and τ_{acc} are the dust destruction and accretion timescales and will be defined below. The terms $\dot{\mathrm{M}}_{\mathrm{cond}}, \dot{\mathrm{M}}_{\mathrm{cond}}^{\mathrm{Z}}$, and $\dot{\mathrm{M}}_{\mathrm{cond}}^{\mathcal{D}}$ describe the ISM, heavy elements and dust mass exchange between the diffuse phase and the molecular phase. Since these terms can not be directly inferred from the simulation, we must resort to indirect constraints. By assuming that the SFR can be represented by the Kennicutt-Schmidt relation, the mass of molecular gas can be estimated as,

$$\mathrm{M}_{\mathrm{ISM}}^{\mathrm{mc}} = \mathrm{SFR}(\mathrm{t})\frac{\tau_{\mathrm{ff}}}{\epsilon_*}, \tag{3.9}$$

where $\epsilon_* = 0.01$ is the star formation efficiency [Krumholz et al., 2012] and

$$\tau_{\mathrm{ff}} = \sqrt{\frac{3\pi}{64\,\mathrm{G}\,\mathrm{m_H}\,\mathrm{n_{mol}}}} \tag{3.10}$$

is the free-fall timescale at the mean density of molecular clouds $\rho_{\mathrm{mol}} \sim 2\,\mathrm{m_H}\,\mathrm{n_{mol}}$ [Schneider et al., 2016], and we assume $\mathrm{n_{mol}} = 10^3$ cm^{-3} to be consistent with the value adopted for the grain growth timescale (see below). We use the above condition to compute $\dot{\mathrm{M}}_{\mathrm{cond}}$. The mass exchange of heavy elements and dust depends on the degree of enrichment of each phase. Hence, we compute $\dot{\mathrm{M}}_{\mathrm{cond}}^{\mathrm{Z}}$ by requiring the heavy elements abundance in the molecular clouds, $\mathrm{Z_{mc}}$, to be equal to the metallicity of newly formed stars predicted by the simulation, $\mathrm{Z_*}$, and we assume that $\dot{\mathrm{M}}_{\mathrm{cond}}^{\mathcal{D}} = \mathcal{D}/\mathrm{Z}\,\dot{\mathrm{M}}_{\mathrm{cond}}^{\mathrm{Z}}$. Finally, $\dot{\mathrm{R}}$, $\dot{\mathrm{Y}}_{\mathrm{Z}}$ and $\dot{\mathrm{Y}}_{\mathrm{d}}$ are, respectively, the return mass fraction, the yields of heavy elements and the dust yields produced by stellar sources and depend on the SFR, the IMF, and on the adopted metal and dust stellar yields. Following Valiante et al. [2009] we compute them as:

$$\dot{\mathrm{R}}(\mathrm{t}) = \int_{\mathrm{m(t)}}^{\mathrm{m_{up}}} (\mathrm{m} - \mathrm{w_m}(\mathrm{m},\mathrm{Z}))\,\Phi(\mathrm{m})\,\mathrm{SFR}(\mathrm{t}-\tau_{\mathrm{m}})\,\mathrm{dm}, \tag{3.11}$$

$$\dot{\mathrm{Y}}_{\mathrm{Z}}(\mathrm{t}) = \int_{\mathrm{m(t)}}^{\mathrm{m_{up}}} \mathrm{m_Z}(\mathrm{m},\mathrm{Z})\,\Phi(\mathrm{m})\,\mathrm{SFR}(\mathrm{t}-\tau_{\mathrm{m}})\,\mathrm{dm}, \tag{3.12}$$

and

$$\dot{\mathrm{Y}}_{\mathrm{d}}(\mathrm{t}) = \int_{\mathrm{m(t)}}^{\mathrm{m_{up}}} \mathrm{m_d}(\mathrm{m},\mathrm{Z})\,\Phi(\mathrm{m})\,\mathrm{SFR}(\mathrm{t}-\tau_{\mathrm{m}})\,\mathrm{dm}, \tag{3.13}$$

where $\tau_{\rm m}$ is the lifetime of a star with mass $\rm m$, $\Phi(\rm m)$ is the IMF, $\rm w_m, m_Z$, and $\rm m_d$ are, respectively, the mass of the stellar remnant, of heavy elements and dust produced by a star with mass $\rm m$ and metallicity Z, and the integral is computed from the upper mass limit of the IMF down to the mass that has a lifetime $\tau_{\rm m} = \rm t$. For stars with mass $\rm m < 8 M_\odot$ we adopt dust yields from Zhukovska et al. [2008], while for stars in the mass range $12\ \rm M_\odot$ to $40\ \rm M_\odot$ dust yields are taken from Bianchi and Schneider [2007], including the effect of dust destruction by the SN reverse shock [Bocchio et al., 2016]. For stars in the intermediate mass range $8\,\rm M_\odot < m < 12\,M_\odot$ the dust yields are computed interpolating from the values corresponding to the most massive AGB progenitor and the least massive SN progenitor. Finally, stars with $\rm m > 40\,M_\odot$ are assumed to collapse to a black hole, without enriching the surrounding ISM. The other terms in the right-hand side of equations (3.3)-(3.8) account for the effects of astration and dust reprocessing in the ISM. The dust destruction timescale is modelled as in Valiante et al. [2011] and de Bennassuti et al. [2014],

$$\tau_{\rm d} = \frac{\rm M_{ISM}^{diff}}{\rm R'_{SN} \epsilon_d M_s(v_s)}, \tag{3.14}$$

where $\rm M_s(v_s) = 6800 M_\odot \langle E_{51}\rangle / (v_s/100 km/s)^2$ is the mass shocked to a velocity of at least $\rm v_s$ by a SN in the Sedov-Taylor phase, $\rm R'_{SN}$ is the *effective* SN rate, since not all SNe are equally efficient at destroying dust [McKee, 1989], $\epsilon_{\rm d}$ is the dust destruction efficiency, and $\langle \rm E_{51}\rangle$ is the average SN energy in units of 10^{51} erg. In what follows, we assume $\rm R'_{SN} = 0.15 R_{SN}$, where $\rm R_{SN}$ is the core-collapse SN rate, $\langle \rm E_{51}\rangle = 1.2$, $\rm v_s = 200$ km/s, and $\epsilon_{\rm d} = 0.48$ [Nozawa et al., 2006].

The grain growth timescale is parametrized as in Chapter 2. As stated in Chapter 2, the numerical simulation resolution is not enough to track the cold ISM (at the scales where the grain growth is efficient). Hence, we estimate the accretion timescale as:

$$\tau_{\rm acc} = \tau_{\rm acc,0} \left(\frac{\rm Z}{\rm Z_\odot} \right)^{-1}. \tag{3.15}$$

In particular we take $\tau_{\rm acc,0} = 2$ Myr that corresponds to a molecular number density $\rm n_{mol} = 10^{-3}$ and a temperature of the molecular gas of $\rm T_{mol} = 50$ K. These conditions have been shown to reproduce the observed dust-to-gas ration of local galaxies over a wide range of metallicities [de Bennassuti et al., 2014]. In addition, we have shown in Chapter 2 [Mancini et al., 2015] that, with these parameters, the model predictions are consistent

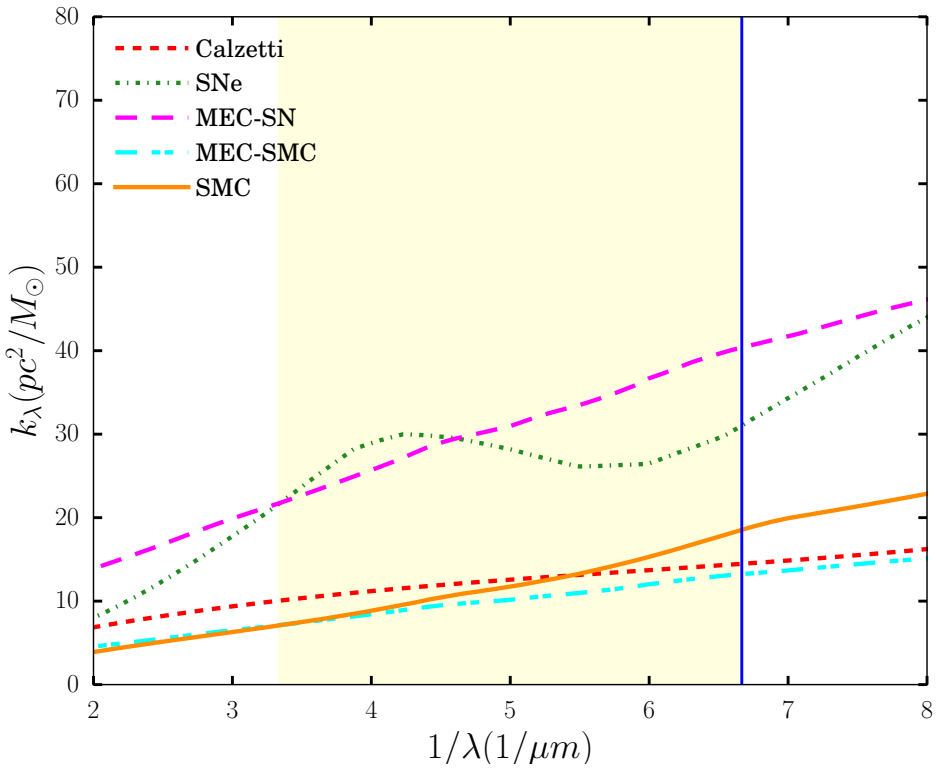

Figure 3.1. Extinction coefficient per unit dust mass as a function of $1/\lambda$. The lines represent different grain models: SMC (orange solid), Calzetti (red dashed, normalized at $\lambda = 3000$ Å to the Milky Way extinction curve), SN (dark green dot-dashed) and MEC normalized at $\lambda = 3000$ Å to the SN extinction curve (magenta long-dashed) and to the SMC curve (cyan dot-dashed). The vertical solid blue line corresponds to the wavelength $\lambda = 1500$ Å at which we compute the galaxy rest-frame luminosity, and the shaded region is the rest-frame UV wavelength range 1500 Å $\leq \lambda \leq 3000$ Å used to compute the β slopes (see text).

with the upper limits on the dust mass inferred from deep ALMA and PdB observations of galaxies at z > 6 (see the observations shown in Fig. 3.4). As pointed out earlier, the observed dust mass in the galaxies A1689-zD1 at z $= 7.5$ and A2744-YD4 at z $= 8.38$ can only be explained using a value of $\tau_{\rm acc,0} = 0.2$ Myr (see also Section 3.1).

3.2.4 Modeling the extinction

The radiation flux escaping a galaxy can be derived from its intrinsic emission, given by eq. (3.2), and accounting for the wavelength dependent extinction of the galactic ISM. In our computational scheme, stellar populations are represented by stellar particles which

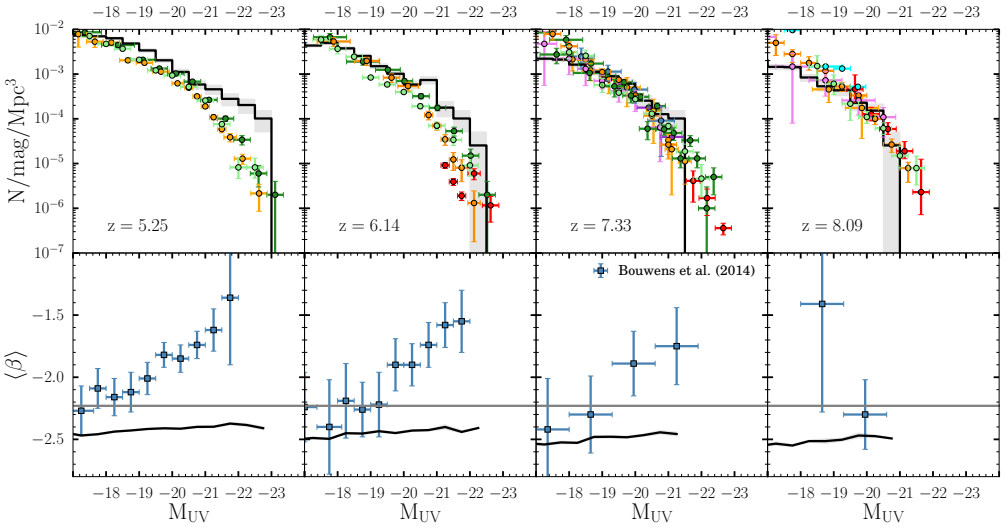

Figure 3.2. *Top Panel:* comparison between the *intrinsic* UV LF of the simulated galaxies (black lines) and the observations at redshift $z \sim 5, 6, 7$ and 8 (from left to right). The data are taken from McLure et al. [2009] (orange), Oesch et al. [2010] (dark blue), Bouwens et al. [2015] (dark green), Finkelstein et al. [2015a] (light green), Castellano et al. [2010] (dark violet), McLure et al. [2010] (light orange), McLure et al. [2013] (dark orange), Atek et al. [2015] (cyan), Laporte et al. [2015] (light violet), and Bowler et al. [2014, 2015] (red). The shaded regions indicate Poissonian errors. *Bottom Panel*: mean spectral index $\langle\beta\rangle$ as function of the *intrinsic* magnitude M_{UV} at the same redshifts. The model prediction for the intrinsic colours are shown as solid black lines with shaded regions indicating the standard errors on the mean. Blue squares indicate the observations by Bouwens et al. [2014]. The horizontal solid grey line shows the value $\beta = -2.23$ that is adopted in the Meurer et al. [1999] relation (see text). A coloured version of this figure is available online.

can experience different absorptions/obscurations depending on the columns of dust in their surroundings. For this reason, we compute the flux emerging from the j-th galaxy by applying a different extinction to each stellar particles i, and then summing up their contribution to obtain the total escaping luminosity:

$$\bar{\mathrm{L}}^{\mathrm{j}}_{\lambda} = \sum_{\mathrm{i}} \mathcal{K}^{\mathrm{i}}(\tau_{\lambda})\, \mathrm{l}^{\mathrm{i}}_{\lambda}\, \mathrm{M}_{*,\mathrm{i}}, \tag{3.16}$$

where $\mathcal{K}^{\mathrm{i}}(\tau_{\lambda})$ is the extinction factor per stellar particle, as a function of the optical depth τ_{λ} at a specific wavelength λ. Note that the modeling of $\mathcal{K}^{\mathrm{i}}(\tau_{\lambda})$ is a complicated task because of the multi-phase nature of the ISM: both the medium surrounding each stellar particle and the diffuse ISM contribute to the extinction. Hence, $\mathcal{K}^{\mathrm{i}}(\tau_{\lambda})$ depends on the dust content and on its spatial distribution relative to the stars. During their lifetime, stars evolve, changing their intrinsic SED, and interact with their environment through mechanical, chemical and radiative feedback effects. For these reasons, the values of $\mathcal{K}^{\mathrm{i}}(\tau_{\lambda})$ experienced by stellar populations change with time.

In our reference model, we assume that all stars form in molecular clouds, from which they escape in a typical timescale $\mathrm{t_{esc}}$[3], moving into the diffuse phase. Hence, if the age of the stellar population is $\mathrm{t}_{\star} < \mathrm{t_{esc}}$, the emitted radiation is extinguished by the additional column of dust of the parent molecular cloud, namely:

$$\begin{aligned} \tau_{\lambda} &= \tau^{\mathrm{mc}}_{\lambda} + \tau^{\mathrm{diff}}_{\lambda} \quad \textit{if} \quad \mathrm{t}_{\star} < \mathrm{t_{esc}} \\ \tau_{\lambda} &= \tau^{\mathrm{diff}}_{\lambda} \quad \textit{if} \quad \mathrm{t}_{\star} \geq \mathrm{t_{esc}}. \end{aligned} \tag{3.17}$$

A similar model was originally proposed by Charlot and Fall [2000] as an idealised description of the ISM to compute the effects of dust on the integrated spectral properties of galaxies, and it has been applied by Forero-Romero et al. [2010] to describe the clumpy structure of the ISM in high-z galaxies. The observed flux is finally computed solving the radiative transfer equation in both phases, by assuming a homogeneous, one-dimensional and isotropic gas/dust distribution, i.e. :

[3]This value can be also interpreted as the molecular cloud dissipation timescale.

$$\mathcal{K}^{\rm i}(\tau_\lambda) = {\rm e}^{-(\tau_\lambda^{\rm mc}+\tau_\lambda^{\rm diff})} \quad if \;\; {\rm t}_\star < {\rm t}_{\rm esc}$$
$$\mathcal{K}^{\rm i}(\tau_\lambda) = {\rm e}^{-\tau_\lambda^{\rm diff}} \quad if \;\; {\rm t}_\star \geq {\rm t}_{\rm esc}. \tag{3.18}$$

More details on the calculation of τ_λ for both phases can be found in the next section.

3.2.5 Dust optical depth

The optical depth at a fixed λ depends both on the type of absorbers present in the medium and on their column density. Observations of high-z galaxies probe the restframe UV range, where the radiation is mostly extinguished by dust and the optical depth can be computed as,

$$\tau_\lambda = \Sigma_{\rm d}\, {\rm k}_\lambda, \tag{3.19}$$

where $\Sigma_{\rm d}$ is the dust column density and ${\rm k}_\lambda$ is the extinction coefficient per unit dust mass. We assume that molecular clouds can be approximated as spheres of constant mass ${\rm M}_{\rm cloud}$ and volume density ${\rm n}_{\rm mol}$, and that their surface density can be expressed as,

$$\Sigma_{\rm ISM}^{\rm mc} = 9.9\times10^2\,\frac{{\rm M}_\odot}{{\rm pc}^2}\,\left(\frac{{\rm M}_{\rm cloud}}{10^{6.5}\;{\rm M}_\odot}\right)^{1/3}\left(\frac{{\rm n}_{\rm mol}}{1000\;{\rm cm}^{-3}}\right)^{2/3}, \tag{3.20}$$

where we adopt ${\rm n}_{\rm mol} = 1000\,{\rm cm}^{-3}$ (see Section 3.2.3) and a cloud mass of ${\rm M}_{\rm cloud} = 10^{6.5}\,{\rm M}_\odot$, which corresponds to the typical mass of the largest giant molecular clouds observed in the Milky Way [Murray, 2011]. Following Hutter et al. [2014], we compute the diffuse gas column density as,

$$\Sigma_{\rm ISM}^{\rm diff} = \frac{{\rm M}_{\rm ISM}^{\rm diff}}{\pi {\rm r}_{\rm d}^2} \tag{3.21}$$

and the radius of the gas distribution as ${\rm r}_{\rm d} = 4.5\,\lambda\,{\rm r}_{\rm vir}$ [Ferrara et al., 2000], where ${\rm r}_{\rm vir}$ is the dark matter halo virial radius and $\lambda = 0.04$ is the mean value of the dark matter halo spin distribution. Finally, under the assumption that dust is uniformly mixed with the gas, the dust surface densities in the two phases can be derived as $\Sigma_{\rm d}^{\rm mc} = \mathcal{D}_{\rm mc}\,\Sigma_{\rm ISM}^{\rm mc}$ and $\Sigma_{\rm d}^{\rm diff} = \mathcal{D}_{\rm diff}\,\Sigma_{\rm ISM}^{\rm diff}$.

The dust extinction coefficient, ${\rm k}_\lambda$, depends on the grain size distribution and on the optical properties of the grain species. Unfortunately, we still lack a model that is able to

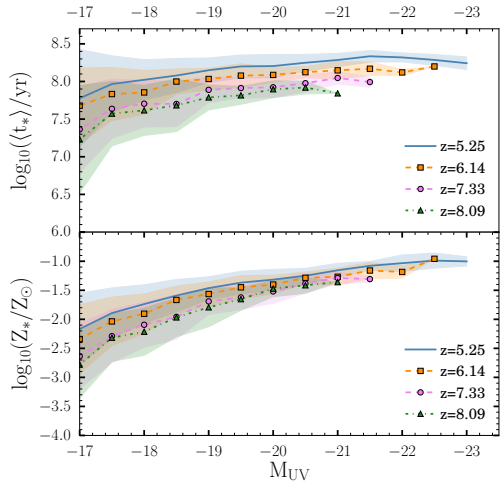

Figure 3.3. Mass-averaged stellar age (top panel) and metallicity (bottom panel) of the simulated galaxies as a function of their intrinsic UV magnitude ($\lambda = 1500$Å). The different lines indicate the mean values at redshift ~ 5 (blue solid), 6 (orange dashed with squares), 7 (magenta dashed with dots) and 8 (green dotted with triangles). The shaded regions indicate the 1-σ deviation. A coloured version of the figure is available online.

self-consistently predict the evolution of the dust mass and extinction properties. In the local Universe, the average dust extinction properties of the Milky Way, the Large and Small Magellanic Clouds are different, probably as a result of their different star formation and chemical evolution histories [Cardelli et al., 1989, Pei, 1992, Weingartner and Draine, 2001]. At high redshifts, the SED of star forming galaxies is generally modeled with the Calzetti et al. [1994] attenuation law, although a steeper extinction curve, such as the SMC, often provides a better description [Reddy et al., 2010]. Using a sample of quasars at $3.9 \leq z \leq 6.4$, Gallerani et al. [2010] inferred a mean extinction curve that is flatter than the SMC curve which is generally applied to quasar at $z < 4$. They discussed the possibility that this difference may indicate either a different dust production mechanism at high redshift, or a different mechanism for processing dust into the ISM and suggested that the same transitions may also apply to normal, star-forming galaxies at $z > 4$. Indeed, at $z \sim 6$ evidence of an extinction law very similar to the one predicted by theoretical models for dust formed in SN ejecta has been found in the spectra of the reddened quasar SDSSJ1048+46 at $z = 6.2$ [Maiolino et al., 2004], the GRB050904 afterglow at $z = 6.3$ [Stratta et al., 2007] and the GRB071025 at $z \sim 5$ (Perley et al. 2010, see however Zafar et al. 2010 for a different conclusion).

Since we do not know how the dust extinction properties change with redshift, here we consider four different extinction curves, that we show in Fig. 3.1: the SMC extinction curve [Weingartner and Draine, 2001, Pei, 1992], the Calzetti model [Calzetti et al., 2000],

the extinction curve derived for grains formed in SN ejecta [Bianchi and Schneider, 2007], and the mean extinction curve (MEC) inferred by [Gallerani et al., 2010][4] The vertical solid line indicates the value $\lambda = 1500\,\text{Å}$ at which we compute the galaxy restframe UV luminosity, and the shaded region identifies the wavelength range where we compute the β slopes. In this range, the Calzetti, SMC and MEC models show a smooth increase with λ^{-1}, although with a different slope. Conversely, the SN extinction curve shows a spectral bump due to amorphous carbon grains [Bianchi and Schneider, 2007]. Overall, we expect the MEC curve normalized to the SN extinction coefficient at $\lambda = 3000\,\text{Å}$ to have the largest effect on the restframe UV colours. In fact, the extinction coefficient per unit dust mass for this model at $1500\,\text{Å}$ is a factor ≈ 2.7 larger than the one predicted by the Calzetti extinction curve.

3.3 Results

In this section, we first present the physical properties of the simulated galaxies at $5 \leq \text{z} \leq 8$, and we compute their *intrinsic* UV luminosities and β slopes. We then explore the effects of dust extinction as predicted by different extinction models.

3.3.1 Physical properties of early galaxies

For each simulated galaxy, we first compute the absolute UV magnitude at $1500\,\text{Å}$, M_{UV}, and the β slope in the wavelength range $[1500-3000]\,\text{Å}$, from the SED presented in Section 3.2.2. Hence, we assume that the UV emission produced by the stellar populations does not suffer any extinction from interstellar dust. At each redshift, we distribute galaxies in different magnitude bins and compute the resulting UV LF and the average colour, $\langle\beta\rangle$.

Fig. 3.2 shows a comparison between the model predictions and a collection of observational data taken from the literature (see the caption for details). At $\text{z} \sim 7-8$, the *intrinsic* LFs underpredict the number of galaxies at the bright-end (with $\text{M}_{\text{UV}} \leq -21$) and at the faint-end (with $\text{M}_{\text{UV}} \geq -18$). This is an effect of the limited volume size and mass resolution of the simulation (see also Salvaterra et al. 2013). At lower z, the effect of numerical

[4]The MEC and Calzetti attenuation models have been normalized at $\lambda = 3000\,\text{Å}$ to the values predicted by the SN and SMC and by the Milky Way extinction curves, respectively.

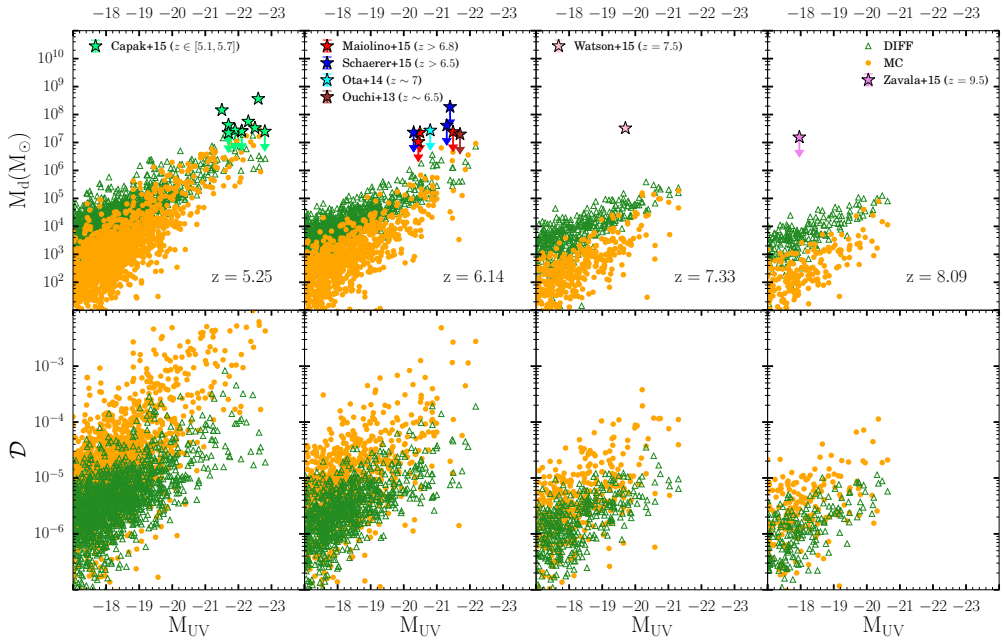

Figure 3.4. The dust mass (*top panels*) and dust-to-gas mass ratio (*bottom panels*) as a function of the intrinsic UV magnitude of the simulated galaxies at z $\sim 5, 6, 7$, and 8 (from left to right). In each panel, we show the dust mass and dust-to-gas mass ratio in molecular clouds (orange dots) and in the diffuse phase (green triangles). In the upper panel we also show data and upper limits from Kanekar et al. [2013], Ouchi et al. [2013], Ota et al. [2014], Capak et al. [2015], Schaerer et al. [2015], Maiolino et al. [2015], Watson et al. [2015], and Zavala et al. [2015], see text.

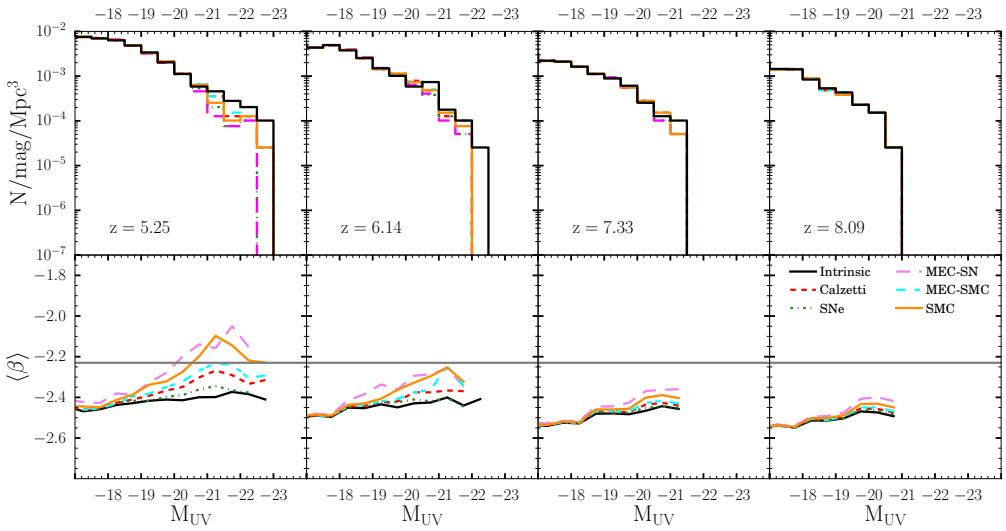

Figure 3.5. Predicted UV LF (*top panels*) and β slopes (*bottom panels*) at z $= 5, 6, 7$, and 8 (from left to right) assuming $t_{esc} = 0$ and different dust extinction curves, colour-coded as in Fig. 3.1. In each panel, we also report the *intrinsic* LFs and β shown in Fig. 3.2 (black solid lines). The horizontal grey lines in the bottom panels show the value $\beta = -2.23$ adopted in the Meurer et al. [1999] relation. A coloured version of this figure is available online.

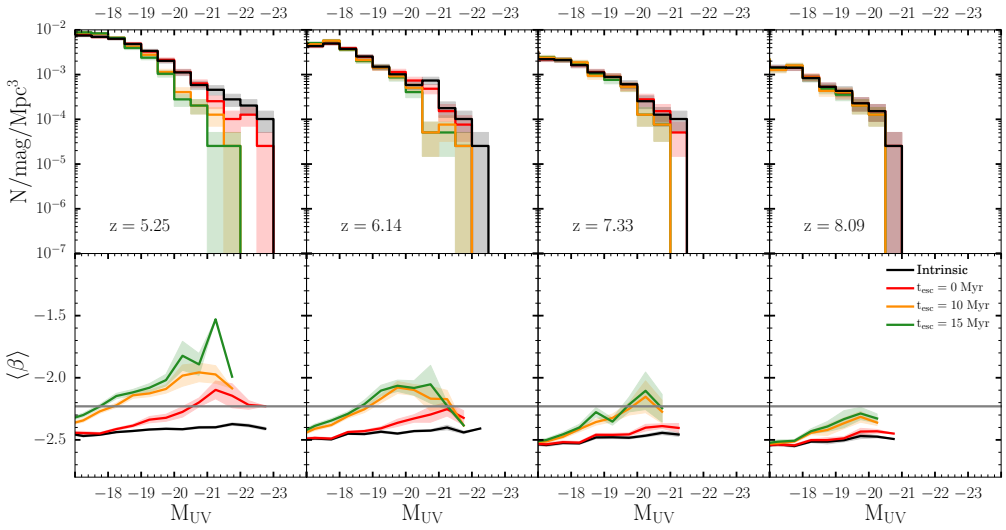

Figure 3.6. Same as in Fig.3.5, but assuming an SMC extinction curve and varying the parameter t_{esc} from 0 to 15 Myr. The shaded regions represent Poissonian errors (top panels) and standard errors on the mean (bottom panels).

resolution is smaller, but we do not find any galaxy with *intrinsic* $\mathrm{M_{UV}} \leq -23$ in the simulated volume. In a future study, we plan to apply this analysis to a new simulation with a larger box size and a comparable mass resolution. In fact, our main interest is to increase the statistics at the high-mass end, where we expect the effects of dust extinction to be more prominent. Within these limitations, at $\mathrm{z} < 7$ the number of galaxies at the bright-end is larger than observed, as already discussed by Salvaterra et al. [2013], Dayal et al. [2013], Finkelstein et al. [2015a] and Khakhaleva-Li and Gnedin [2016b]. We find that, *while the observed LF at* $\mathrm{z} \sim 8$ *is consistent with negligible dust extinction, at* $\mathrm{z} \sim 5$ *observations seem to require significant dust extinction at all luminosities brighter than* $\mathrm{M_{UV}} \sim -18$.

At all redshifts, the predicted *intrinsic* $\langle\beta\rangle$ slopes are much bluer than observed, particularly at the bright end (bottom panels). The simulated galaxies show similar colours at all luminosities, with $\langle\beta\rangle \sim -2.5$, and only a very modest increase with cosmic time. These colours are bluer than the $\beta = -2.23$ adopted in the Meurer et al. [1999] relation (shown by the horizontal grey line), as already noticed by Wilkins et al. [2012].

The above trends can be easily understood by looking at the mean physical properties of the stellar populations in the simulated galaxy samples. Fig. 3.3 shows the mass-averaged stellar age (upper panel) and metallicity (bottom panel) of the simulated galaxies at $5 \leq \mathrm{z} \leq 8$ as a function of their *intrinsic* UV magnitudes. We find that galaxies with a given luminosity tend to be slightly younger and less metal-enriched at higher redshift ($80\,\mathrm{Myr} \leq \langle \mathrm{t_*} \rangle \leq 160\,\mathrm{Myr}$ and $0.03\,\mathrm{Z_\odot} \leq \langle \mathrm{Z_*} \rangle \leq 0.06\,\mathrm{Z_\odot}$ for galaxies with $\mathrm{M_{UV}} = -20$ and $5 \leq \mathrm{z} \leq 8$), and that the average stellar age and metallicity increases with the *intrinsic* UV luminosity, showing a larger dispersion of values for fainter galaxies with $\mathrm{M_{UV}} \geq -18$. However, their overall properties do not show a significant evolution with UV magnitude and redshift, consistent with their relatively constant *intrinsic* UV colours.

Over the same UV luminosity and redshift range, the dust mass in their ISM varies significantly. This is shown in Fig. 3.4, where we plot the dust mass, $\mathrm{M_d}$, derived as explained in Section 3.2.3, and the dust-to-gas mass ratio, $\mathcal{D}$, as a function of the *intrinsic* UV magnitudes. The dust mass increases with UV luminosity and - for a given luminosity - galaxies become more dust-enriched with cosmic time. As already discussed in Chapter 2, the dust mass increases with stellar mass, hence with the *intrinsic* UV luminosity. In low-mass galaxies, the dust mass has mostly a stellar origin (SNe and AGB stars). In mas-

sive and chemically evolved galaxies, grain growth becomes progressively more efficient, providing the dominant contribution to the total dust mass. Hence, the dust mass in the molecular phase increases with galaxy luminosity and becomes as large as the dust mass in the diffuse phase for galaxies with *intrinsic* $\mathrm{M_{UV}} < -20$.

In Fig. 3.4 we also show the data and upper limits on the dust mass inferred from observations at $\mathrm{z} \sim 5.1 - 5.7$ [Capak et al., 2015], $\mathrm{z} \sim 6.5 - 7$ [Kanekar et al., 2013, Ouchi et al., 2013, Ota et al., 2014, Schaerer et al., 2015, Maiolino et al., 2015], $\mathrm{z} \sim 7.5$ [Watson et al., 2015] and $\mathrm{z} \sim 9.6$ (Zavala et al. 2015, that we arbitrarily report in the $\mathrm{z} \sim 8$ panel). As in Chapter 2 [Mancini et al., 2015], we have estimated the dust mass from the observed mm flux assuming optically thin emission, a dust emissivity $\mathrm{k}_{\nu_{\mathrm{res}}} = \mathrm{k}_0(\lambda_0/\lambda_{\mathrm{res}})^{\beta}$ (with $\mathrm{k}_0 = 0.77\,\mathrm{cm}^2/\mathrm{gr}$, $\lambda_0 = 850\,\mu\mathrm{m}$ and $\beta = 1.5$, Ota et al. 2014), and a dust temperature of 35 K. The resuting dust masses (shown as starred data points) have been reported only for indicative purposes, as a more meaningful comparison between model predictions and observations is given in Section 3.4. While the predicted dust masses are consistent with observations at $\mathrm{z} \sim 5.1 - 5.7$ and with the upper limits inferred at $\mathrm{z} > 6$, the data reported by Watson et al. [2015], and recently confirmed with deeper observations by Knudsen et al. [2017], on the $\mathrm{z} = 7.5$ galaxy A1689-zD1, requires more efficient grain growth, as if the galaxy were characterized by a denser ISM [Mancini et al., 2015, Michałowski, 2015].

Due to their different gas content, the average dust-to-gas mass ratio is smaller in the diffuse phase than in molecular clouds and, in both phases, $\mathcal{D}$ grows with UV luminosity. Hence, we expect the most massive galaxies, with the largest *intrinsic* UV luminosity, to experience a larger degree of dust extinction. Yet, $\mathcal{D}$ shows a large dispersion, particularly in the molecular phase, and galaxies with the same *intrinsic* UV luminosity can be characterized by values of $\mathcal{D}$ which differs by 2 - 3 orders of magnitudes, particularly at lower z. At $\mathrm{z} \lesssim 6$, galaxies with $\mathrm{M_{UV}} \leq -21$ have dust masses which range between $10^6\,\mathrm{M}_\odot$ and $\approx 5 \times 10^7\,\mathrm{M}_\odot$ and dust-to-gas mass ratios in the molecular phase that can reach values of $\mathcal{D} \geq 10^{-3}$. Conversely, at $\mathrm{z} \gtrsim 7$, most of the simulated galaxies have $\mathrm{M_d} < 10^6\mathrm{M}_\odot$ and $\mathcal{D} < 10^{-4}$. On the basis of these results we expect dust extinction to be more relevant for bright galaxies, particularly at $\mathrm{z} \lesssim 6$, where the deviations between the *intrinsic* UV LF and the data, shown in Figure 3.2, are more significant.

3.3.2 The effects of dust extinction on the UV luminosities and colours

We first consider the simplest model of dust extinction from the diffuse phase only, computing the optical depth using Eqs. (3.17)-(3.18) with $t_{esc} = 0$. In Fig. 3.5, we show the UV LF and CMR assuming the SMC, the Calzetti, the SN and the MEC extinction curves. For reference, we also show the *intrinsic* UV LF and $\langle\beta\rangle$ colours discussed in the previous section, assuming no dust extinction. It is clear that dust extinction decreases the number of galaxies at the bright end, particularly at $z \leq 6$. The strongest effect is achieved using the MEC-SN and SN curves, as these models predict the largest k_λ at $\lambda = 1500$ Å, followed by the SMC, the Calzetti and the MEC-SMC curves (see Fig. 3.1). These different models have an even larger effect on the CMR, as this is sensitive to the shape of the extinction curve over the wavelength range $1500\,\text{Å} \leq \lambda \leq 3000\,\text{Å}$. In fact, while the SN, the Calzetti, and the MEC-SMC models introduce only a mild reddening in the predicted colours, the SMC and MEC-SN models increase the $\langle\beta\rangle$ creating a dependence on the UV magnitude, with the brightest galaxies being redder than the fainter ones. Hence, this analysis shows that *estimating dust attenuation from the observed β can lead to very different results depending on the adopted extinction curve. A flat extinction curve in the UV can hide a significant mass of dust under relatively blue colours*. Overall, we find that - due to the low $\mathcal{D}$ of the diffuse phase (see Fig. 3.4), when $t_{esc} = 0$ dust extinction introduces only a modest reddening to the UV colours and it has a negligible effet on the LFs at $z \gtrsim 6$.

We finally discuss the effects of dust extinction on young stellar populations that are still embedded in their parent molecular clouds, assuming $t_{esc} = 10$ and 15 Myr in Eqs. (3.17)-(3.18). The results are shown in Fig. 3.6, where we have adopted the SMC extinction curve. For reference, we also report in the same figure the *intrinsic* UV LF and colours as well as the results discussed above, when $t_{esc} = 0$. Not surprisingly, *the longer the time young stellar populations spend in their natal molecular clouds, the largest is the effect of dust extinction, both on the bright-end of the luminosity function and on the β slopes* (see also Forero-Romero et al. 2010). Due to the larger values of $\mathcal{D}$ in the molecular phase, the predicted $\langle\beta\rangle$ for $M_{UV} = -20$ galaxies at $z \sim 8$ increases from ~ -2.5 when $t_{esc} = 0$ (essentially the *intrinsic β* value) to ~ -2.3 when $t_{esc} = 10 - 15$ Myr. The increasing efficiency of grain growth causes $M_{UV} = -20$ galaxies at $z \sim 5$ to have $\langle\beta\rangle = -2.3$ when $t_{esc} = 0$ and as large as -2 (-1.8) when $t_{esc} = 10$ (15) Myr.

3.4 Comparison with observations

In this section, we first compare the model predictions with the observed UV LFs and CMR. Then, we analyze the origin of the scatter around the CMR and the stellar mass - UV luminosity relation at different z. Finally, we compute the IRX and dust attenuation factors as a function of β.

3.4.1 UV luminosity function and Colour-Magnitude-Relation

To compare the predicted LFs and CMR with the observed ones we follow Bouwens et al. [2014, 2015] and adopt the same procedure to compute the LFs and $\langle\beta\rangle$ from the synthetic galaxies SEDs.

At each redshift, filters sample different ranges of the rest-frame galaxy SED. To be consistent with Bouwens et al. [2014], we use the z850, Y105 and H160 filters for galaxies at $\mathrm{z} \sim 5$, Y105 and H160 filters for $\mathrm{z} \sim 6$, H160 and J125 filters for $\mathrm{z} \sim 7$ and H160 and JH140 filters for $\mathrm{z} \sim 8$[5]. To compute the AB magnitude at each filter, we first define the pivot wavelength of a given filter a with transmission T_λ as,

$$\lambda_{\mathrm{p}}^{\mathrm{a}} = \sqrt{\frac{\int_{-\infty}^{+\infty} \lambda\, \mathrm{T}_\lambda(\lambda)\, \mathrm{d}\lambda}{\int_{-\infty}^{+\infty} \mathrm{T}_\lambda(\lambda)/\lambda\, \mathrm{d}\lambda}}. \tag{3.22}$$

Then, we compute the weighted filter flux $\mathrm{F_a}$ for a source at redshift z with a given flux f_λ as,

$$\mathrm{F_a} = \frac{\int_{-\infty}^{+\infty} \lambda\, \mathrm{f}(\lambda/(1+\mathrm{z}))\, \mathrm{T}(\lambda)\, \mathrm{d}\lambda}{\int_{-\infty}^{+\infty} \lambda\, \mathrm{T}(\lambda)\, \mathrm{d}\lambda}. \tag{3.23}$$

Finally, we define the absolute AB magnitude as,

$$\mathrm{M}_{\mathrm{AB}}^{\mathrm{a}} = -2.5 \log_{10}\left[\frac{\mathrm{F_a}}{\mathrm{erg\,s^{-1}\,\text{Å}^{-1}}}\left(\frac{\lambda_{\mathrm{p}}^{\mathrm{a}}}{\text{Å}}\right)^2 (1+\mathrm{z})^{-2}\right] - 97.78. \tag{3.24}$$

The β slopes at $\mathrm{z} \sim 5$ are computed as a least-square linear fit on the three filters, wheras at

[5]With z850, Y105, J125, JH140 and H160 we refer to HST filters F850LP, F105W, F125W, F140W and F160W, respectively.

higher z we use the relation[6],

$$\beta = \frac{\log_{10}(F_a/F_b)}{\log_{10}(\lambda_p^a/\lambda_p^b)}. \quad (3.25)$$

The first step is slightly different from the method adopted by Bouwens et al. [2014], where they use the effective wavelength assuming a power spectrum of $\propto \lambda^{-2}$ instead of the pivot wavelength. Finally, to compare with the LFs computed by Bouwens et al. [2015], we evaluate the AB magnitude at 1600 Å assuming a spectral slope given by the corresponding photometric β.

The results are plotted in Fig. 3.7. Model predictions at $5 \leq z \leq 8$ are obtained assuming the SMC extinction curve and $t_{esc} = 10$ (orange curve) and 15 Myr (green curve). The shaded regions represent Poissonian errors associated to each magnitude bin. In the bottom panels we show the results of the systematic analysis by Bouwens et al. (2014, blue data points) and the corresponding best-fit relation (black dot-dashed lines). For comparison, we also report data from Wilkins et al. [2011], Finkelstein et al. [2012], Bouwens et al. [2012], Dunlop et al. [2012, 2013], and Duncan et al. [2014], all shown with grey data points. At $z \sim 8$, current observations of the β slopes are highly uncertain, due to the small sizes of galaxy samples and photometric uncertainties introduced by the limited filter separation. The grey shaded region in the $z \sim 8$ bottom panel shows the CMR relation obtained extrapolating the lower-z slope and the best-fit intercept at $z \sim 8$ [Bouwens et al., 2014].

Although both models appear to well reproduce the trend of an increasing reddening with luminosity observed by Bouwens et al. (2014) at $5 \leq z \leq 7$, at the brightest luminosities the statistics is too poor for a meaningful comparison. At each redshift, we identify a limiting luminosity above which the number of sources per magnitude bin is < 10, and we illustrate the corresponding magnitude range with dashed lines. To better populate this luminosity range, a larger simulation volume would be required. In fact, at $5 \lesssim z \lesssim 6$ the number of simulated galaxies with *intrinsic* $-23 \leq M_{UV} \leq -20.5$ ranges between 40 and 65. These are the galaxies which suffer the largest dust extinction, with $\langle A_{UV} \rangle \sim 1.7\,(1.1)$ at $z \sim 5$ (6), and are observed at $-21.3 \leq M_{UV} \leq -18.8$ ($-21.9 \leq M_{UV} \leq -19.4$). Extrapolating these trends, we predict the brightest galaxies observed at $z \leq 6$ with $M_{UV} \lesssim -22$

[6]To estimate the error introduced by this procedure, we compute the photometric β for synthetic spectra with known β in the range -3 and 0 and we find that the difference between the photometric determination and the input value is always less than 2%.

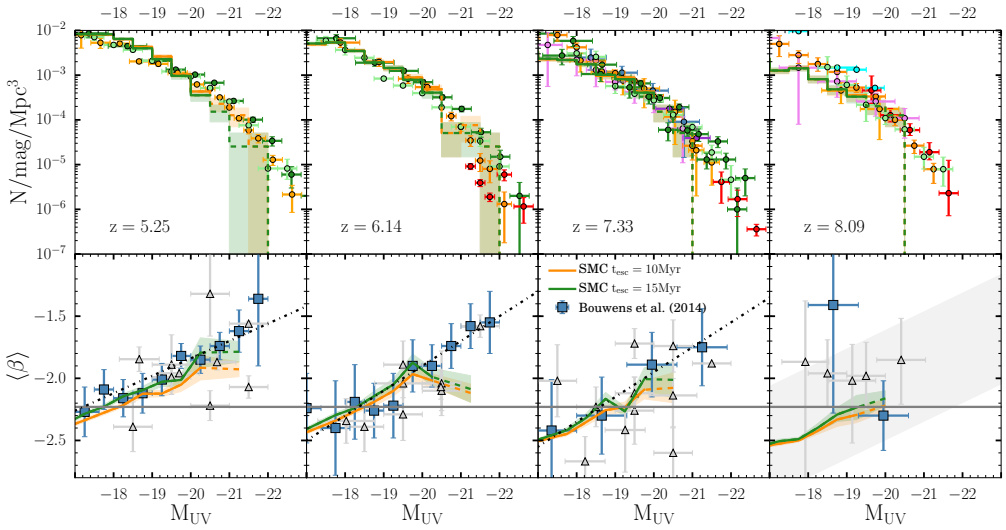

Figure 3.7. Comparison between the predicted UV luminosity functions (*top panels*) and $\langle\beta\rangle$ slopes (*bottom panels*) with observations. Data are the same as in Fig. 3.2. In the bottom panels we have added observations from Wilkins et al. [2011], Finkelstein et al. [2012], Bouwens et al. [2012], Dunlop et al. [2012, 2013], and Duncan et al. (2014, all shown with grey data points). The black dot-dashed lines represent the best-fit to the observations of Bouwens et al. (2014, blue data points) at $z \sim 5, 6$, and 7 and the shaded grey region is obtained extrapolating the lower-z slope and the best-fit intercept at $z \sim 8$. The theoretical models adopt a SMC extinction curve and $t_{esc} = 10$ (solid orange) and 15 Myr (solid green) with shaded regions representing the Poissonian errors in each magnitude bin (*top panels*) and the standard errors on the mean values (*bottom panels*). Dashed lines indicate the luminosity range where less than 10 model galaxies are found in each magnitude bin (see text). The horizontal grey lines show the value $\beta = -2.23$ adopted in the Meurer et al. [1999] relation. A coloured version of this Figure is available online.

to be massive ($M_{star} > 5 \times 10^{10} M_{\odot}$) and dust-enriched ($M_{dust} > 10^{8} M_{\odot}$), with typical $A_{UV} > 1.7$, consistent with their relatively red observed colours, $\langle\beta\rangle \sim -1.5$ (see Fig. 3.10).

We conclude that while the ISM dust has a negligible effect on the galaxy UV LFs at $z \sim 7$ and 8, it reduces the number of galaxies with $M_{UV} \geq -18$ and ≥ -19 at $z \sim 5$ and 6 to values in very good agreement with observations. The CMR and its dependence on z is sensitive to the extinction properties of the grains and to the dust distribution in the ISM. In particular, *the observed trends suggest a steep extinction curve in the wavelength range* $1500\,\text{Å} \leq \lambda \leq 3000\,\text{Å}$*, and that stars with age* ≤ 15 *Myr are embedded in their dense molecular natal clouds and their UV luminosity suffers a larger dust extinction.*

When the grains are assumed to follow the MEC normalized to the SN extinction coefficient at $\lambda = 3000$Å (see the curve shown in Fig.3.1), the number of galaxies with $M_{UV} \leq -19$ at $z \sim 5$ is too small compared to the observed LF. Conversely, if the MEC is normalized to the SMC extinction coefficient at $\lambda = 3000$Å, the flatter slope at shorter wavelenghts reduces the predicted $\langle\beta\rangle$, at odds with observations. A better agreement is found if, following Gallerani et al. [2010], the MEC is assumed to reflect a population of grains with intermediate properties between SN and SMC dust, and we adopt a normalization factor equal to $k_{MEC} = (1-p)\,k_{SMC} + p\,k_{SN}$ at 3000 Å. *Current observations do not allow to discriminate between the SMC and MEC models if* $p \leq 40\%$. It is interesting to note that evidence for an SMC-like extinction curve being preferred for galaxies at high-z has been reported in many recent observational studies [Tilvi et al., 2013, Oesch et al., 2013, Capak et al., 2015, Bouwens et al., 2016].

Independently of the grain properties, the observed CMR requires dust evolution models in a 2-phase ISM, where SNe and AGB stars contribute to dust enrichment, dust grains grow their mass in dense molecular clouds, and are destroyed by SN shocks in the diffuse phase.

This conclusion is further strengthened by comparing our results with the recent studies by Shimizu et al. [2014], Finkelstein et al. (2015, see in particular their Section 7), and Khakhaleva-Li and Gnedin [2016b]. In these studies, the dust-to-gas mass ratio has been assumed to simply scale with the gas metallicity. In Shimizu et al. [2014], they reproduce the observed UV-luminosity function and β evolution with redshift at $z \geq 7$ by adjusting the dust-to-metal mass ratio, the effective radius of the dust distribution, and a parameter which

controls the relative dust/star geometry. In the semi-analytical models that Finkelstein et al. [2015a] compare with observations, a dust slab model is adopted and the normalization of the dust optical depth is assumed to be $\propto \exp(-z/2)$ to obtain a reasonably good fit to the observed UV-LFs at $z \geq 5$. They suggest that this scaling may be physically interpreted as due to an evolution of the dust-to-metal ratio or of the dust geometry. Our model allows to predict the redshift and luminosity dependence of the dust optical depth, with the only free parameter being the residence time of young stars in molecular clouds. Finally, using a dust radiative transfer model, Khakhaleva-Li and Gnedin [2016b] reproduce the observed UV-LFs at $z \sim 6$ and 7, but their predictions are inconsistent with the data at $z \sim 8$ and lead to colour-magnitude relations that are shallower than observed. In their model dust is assumed to scale with metallicity and to be instantaneously sublimated in ionized regions. While the latter is certainly a reasonable assumption, it is not enough to capture the complex dynamical interplay between dust formation and destruction in the different phases of the ISM, which is ultimately responsible for the observed evolution with redshift of the luminosity and the dust extinction.

3.4.2 Scatter in the $\beta - M_{UV}$ and $M_{star} - M_{UV}$ relations

High-z galaxy samples show a considerable scatter in the measured β slopes, even after accounting for observational effects [Castellano et al., 2012, Bouwens et al., 2014, Rogers et al., 2014]. Studying the distribution of galaxy colours at different redshifts can provide interesting indications on the origin and evolution of the CMR.

Fig. 3.8 shows the predicted distribution of galaxy colours at $z \sim 5, 6, 7$, and 8 as a function of the UV magnitude, assuming the SMC extinction curve and $t_{esc} = 15$ Myr. Each data point represents an individual galaxy, colour-coded depending on the mass of dust present in its ISM. The shaded regions show the $1-\sigma$ scatter around the CMR shown in Fig. 3.7 (green line) using the same UV magnitude bins. The amount of scatter in the colour distribution increases with cosmic time, as a result of the progressively larger degree of dust enrichment. At each z, the scatter in the colour distribution increases with luminosity, as the brightest galaxies are also more massive and dust enriched. This is consistent with the analysis of Rogers et al. [2014] of a galaxy sample at $z \sim 5$, where they find an increasing width of the colour distribution towards brighter galaxies. We find that there is a minimum

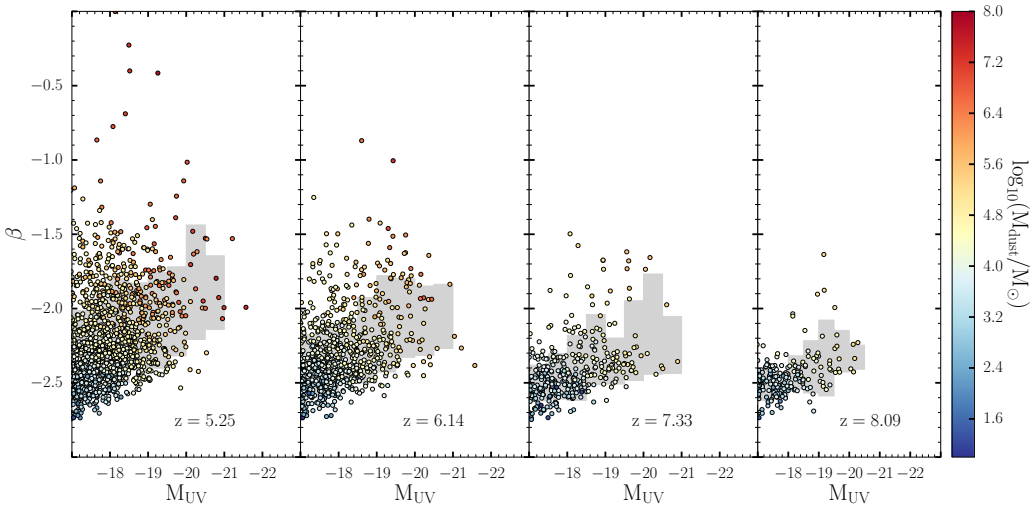

Figure 3.8. Predicted β slopes as a function of the UV magnitude at $z \sim 5, 6, 7$ and 8 (from left to right). Each data point represents a galaxy and it is colour-coded according to the mass of dust in the ISM (colour scale on the right). We have assumed the SMC extinction curve and $t_{esc} = 15$ Myr. The grey shaded regions show the 1-σ scatter around the CMR shown in Fig. 3.7. A coloured version of this Figure is available online.

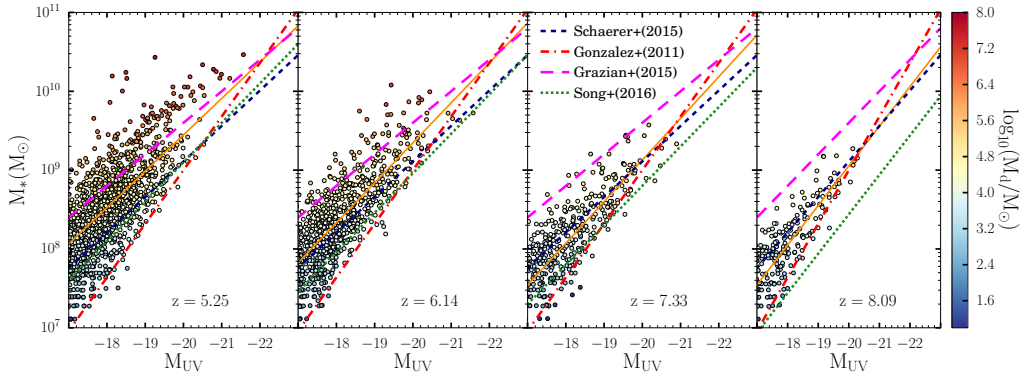

Figure 3.9. Same as Fig. 3.8 but for the stellar mass. In each panel, the solid line is the best-fit relation for the simulated galaxies and the other lines show the relations inferred from observational data by González et al. [2011], Grazian et al. [2015], Schaerer et al. [2015] and Song et al. [2016]. A coloured version of this Figure is available online.

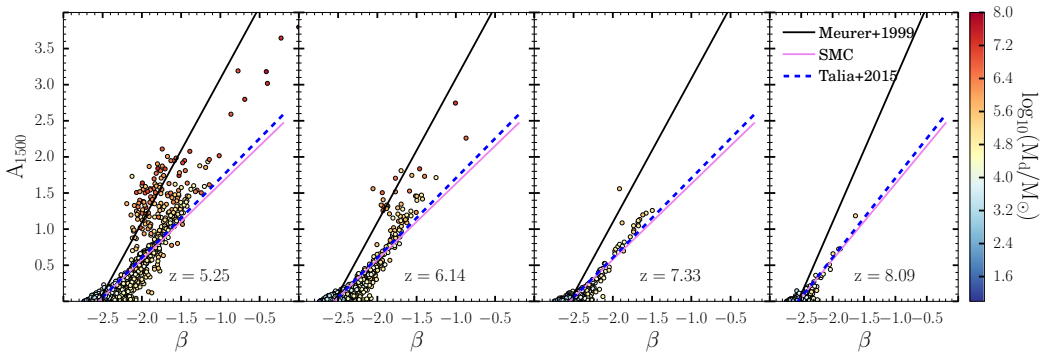

Figure 3.10. Same as Fig. 3.11 but for the dust attenuation factor at 1500 Å. A coloured version of this Figure is available online.

value of β that grows with UV luminosity as a consequence of a minimum level of dust enrichment produced by stellar sources. This effect is independent of z but the number of galaxies at the bright end grows with time. At each z, galaxies with the reddest colours can have largely different luminosities: for a given β slope, the brightest galaxies are generally dustier. *At* $z \lesssim 6$*, sources with luminosities in the range* $-18 \leq M_{UV} \leq -19$*, where we have adequate statistics, appear to be a mix of intrinsically faint blue galaxies and of red objects which have suffered strong dust extinction. The latter population grows with cosmic time as a result of progressively more efficient grain-growth in their ISM.*

Fig. 3.9 shows that the population of dusty, UV-faint galaxies at $z \sim 5$ and 6 lie off the mean $M_{star} - M_{UV}$ relations inferred from observations at comparable and higher-z [González et al., 2011, Duncan et al., 2014, Grazian et al., 2015, Schaerer et al., 2015, Song et al., 2016][7] Using deep optical and infrared imaging provided by HST, Spitzer and the VLT in the CANDELS-UDS, GOODS-South and HUDF, Grazian et al. [2015] show that the data at $3.5 < z < 4.5$ are consistent with a constant mass-to-light ratio but with a considerable scatter. In particular, they find a population of relatively faint

[7]Systematic uncertainties associated with sample selection and stellar mass estimation lead to large discrepancies between different observational studies, even when using the same data set [Song et al., 2016]. At higher redshift, the scatter is reduced and the simulated galaxies follow a tighter $M_{star} - M_{UV}$ relation. This may be an evolutionary effect, as $z \sim 7$ and 8 galaxies have experienced limited dust enrichment. However, due to the limited volume of our simulation, we can not exclude that massive, dusty, UV faint galaxies may have formed at these redshifts. Interestingly, there are observational evidences for massive, red galaxies at $z \sim 4-5$ [Grazian et al., 2015, Song et al., 2016].

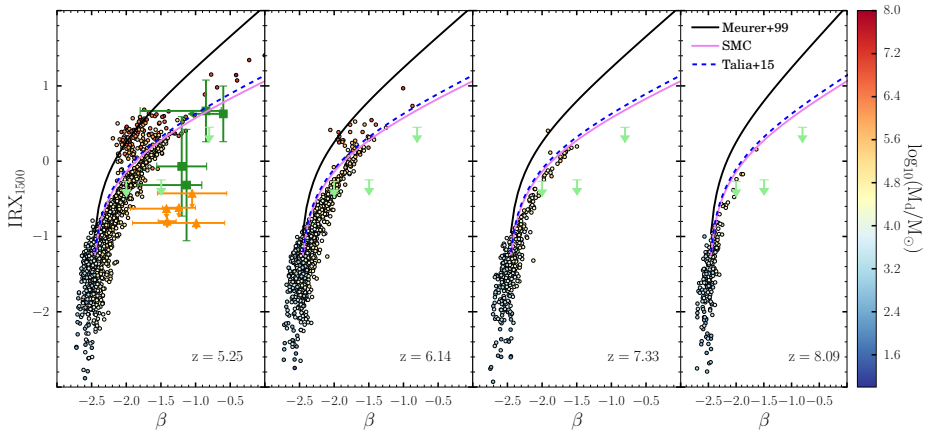

Figure 3.11. The IR excess as a function of UV slope β for the simulated galaxies at z $\sim 5, 6, 7$ and 8 (from left to right). Each data point represents a galaxy and it is colour-coded according to the mass of dust in the ISM (colour scale on the right). We have assumed the SMC extinction curve and $t_{esc} = 15$ Myr. The black solid lines show the Meurer et al. [1999] correlation with $\beta_0 = -2.5$, the blue dashed lines show the relation inferred by Talia et al. [2015], and the magenta solid lines the relation predicted for the SMC extinction curve. The data points at z ~ 5 represent the ALMA detected (green squares) and ALMA non detected (orange triangles) sources reported by Capak et al. [2015]. The upper limits shown in all panels with light green triangles are the results recently reported by Bouwens et al. [2016] for galaxies at z $\sim 4-10$ (see text). A coloured version of this Figure is available online.

galaxies (with $M_{UV} \sim -18$) with masses $M_{star} \sim 10^{11} M_{\odot}$, which can be comparable in number to UV bright galaxies with the same stellar mass. Because of their red colours, these galaxies can not be selected by standard LBG criteria based on UV rest-frame colours. The difference between the galaxy stellar mass function inferred from UV-selected star forming galaxies by González et al. [2011] and the mass function derived by Duncan et al. [2014] and Grazian et al. [2015] has been interpreted as due to a growing contribution of massive dusty galaxies at z $\lesssim 5.5$. While at higher redshifts there is better agreement, this may be due to a selection effect and the epoch of appearance of massive dusty galaxies may require future deep infrared surveys [Grazian et al., 2015].

3.4.3 The IR excess

Dust attenuation of star forming galaxies at high redshift is commonly evaluated using methods based on the observed correlation between the spectral slope β and the infrared

excess, IRX [Meurer et al., 1999]. The latter is defined as the ratio between the IR to UV fluxes (at $\lambda = 1600\,\text{Å}$), IRX $= \text{Log}\,\text{F}_{\text{IR}}/\text{F}_{1600}$ and it is a measure of dust absorption. Hence the IRX-β relation shows that dust absorption is correlated to UV reddening and provides a powerful tool to reconstruct the unattenuated UV flux when only UV rest-frame data is available. The original idea was proposed by Meurer et al. [1999] using a sample of local starbursts from which the following relations were derived:

$$\text{IRX} = \text{Log}(10^{0.4\text{A}_{1600}} - 1) + 0.076 \pm 0.044, \tag{3.26}$$

and

$$\text{A}_{1600} = 4.43 + 1.99\beta, \tag{3.27}$$

where $\text{A}_{1600} = 1.086\,\tau_{1600}$ is the dust attenuation at $1600\,\text{Å}$ and the dispersion on the fit was 0.55 mag in A_{1600} and 0.28 on β [Meurer et al., 1999]. The relation obviously depends on the intrinsic spectrum of the sources and on the extinction curve. The zero point of the relation implies that the intrinsic spectral slope of the sources is assumed to be $\beta_0 = -2.23$. This value has been reported as a grey solid line in Figs. 3.5 - 3.7 to show that all the simulated galaxies at $5 \leq \text{z} \leq 8$ have bluer intrinsic colours. Indeed, modifications of the original relation to account for the lower metallicities and younger ages of galaxies at high redshift have been proposed in the literature. Using a small sample of galaxies at $\text{z} \sim 2.8$–3 with deep IR observations and measured spectroscopic metallicities from the CANDELS+HUGS survey, Castellano et al. [2014] derived the relation $\text{A}_{1600} = 5.32 + 1.99\beta$. This implies a value of the intrinsic slope $\beta_0 = -2.67$, consistent with the sub-solar metallicities and young ages inferred for their sample galaxies. In Figs. 3.11 and 3.10 we show the Meurer et al. [1999] relation modified assuming a value of $\beta_0 = -2.5$, the mean intrinsic colours of the simulated galaxies (solid black lines). In the same figures, we also show the much flatter relations derived by Talia et al. [2015] using the UV spectra of a sample of 62 IR-selected galaxies at $1 < \text{z} < 3$ (blue dashed lines), which is more consistent with the relation inferred by Pettini et al. [1998] for the SMC extinction curve (solid magenta lines). The inferred IRX - β is known to depend on the galaxy sample selection method. While UV and optically selected samples distribute systematically lower than starbursts on the IRX - β plane [Cortese et al., 2006, Boissier et al., 2007], two different distributions are found in IR-selected samples. Luminous and Ultraluminous IR galaxies

distribute above the Meurer et al. [1999] relation [Goldader et al., 2002, Takeuchi et al., 2010, Howell et al., 2010, Reddy et al., 2010, Overzier et al., 2011, Casey et al., 2014, Forrest et al., 2016], quiescent star forming galaxies distribute below it [Takeuchi et al., 2010, Buat et al., 2012, Talia et al., 2015].

The figures also show the simulated galaxies at $5 \leq z \leq 8$, colour-coded depending on the level of dust enrichment. We have assumed the SMC extinction curve and $t_{esc} = 15$ Myr. For each galaxy, we compute the IRX at 1500 Å assuming that all the absorbed UV radiation is re-emitted in the IR. We account also for the contribution of resonantly scattered Lyman-α photons, which is estimated to be 7% of the UV radiation [Khakhaleva-Li and Gnedin, 2016b].

At $z \sim 7$ and 8, we find that all the simulated galaxies are characterized by an IRX considerably smaller than that predicted by the Meurer et al. [1999] relation, and are consistent with that predicted for the SMC and the one derived by Talia et al. [2015]. However, a second population of dusty galaxies appears at $z \lesssim 6$, which progressively shifts towards the Meurer et al. [1999] relation, although with a large scatter. This is the same population that lies off the stellar mass - UV luminosity relation shown in Fig. 3.9 and that dominates the scatter in the colour distribution shown in Fig. 3.8. *Our analysis suggests that lower stellar mass and less chemically mature galaxies at high-z are characterized by smaller IRX and A_{1500} than implied by the Meurer et al. [1999] relation for galaxies with the same colours.* Their ISM dust is mostly contributed by stellar sources and their dust attenuation is smaller, consistent with what has been found for young (< 100 Myr) LBGs at $z \sim 3$ by Siana et al. [2009] and Reddy et al. [2010], and more recently by [Bouwens et al., 2016] using ALMA 1.22 mm-continuum observations of a 1 arcmin^2 region in the Hubble Ultra Deep Field. However, we find that *massive and more chemically evolved galaxies, where grain growth in dense gas increases the mass of ISM dust, introduce a considerable scatter in the IRX at a given UV continuum slope*. At $z \sim 5.25$, galaxies with $-2 < \beta < -1.5$ can have IRX in the range 0.3 - 4 and it is very hard to infer the proper dust attenuation factor from the UV slope alone (see Fig.3.10).

In Fig. 3.11 we also show the IR excess of $z \sim 5.1-5.7$ galaxies inferred by Capak et al. [2015], which have been argued to be significantly more dust-poor and less IR-luminous than lower z galaxies with similar UV colours. To be consistent with the data points shown

in Fig.3.4, we have computed the IRX values of the Capak et al. [2015] sources, from their measured (or upper limits) 158 μm flux, adopting a modified black body spectrum with emissivity index $\beta = 1.5$ [Ota et al., 2014] and a dust temperature $\mathrm{T_d} = 35$ K, as described in Section 3.1. This yields values of the FIR emissivities that are 25% larger, but consistent within the errors, with the ones reported by (Capak et al. 2015, see their Table 5). We find that simulated galaxies which follow the SMC and the Talia et al. [2015] correlations at the same z are marginally compatible with the IRX of the ALMA detected sources (green squares), given the large uncertainties on their β slopes. However, the simulated galaxies with IRX compatible with the upper limits inferred for the ALMA undetected sources (orange triangles) have significantly bluer colours, consistent with their low dust content. Our study confirms that it is difficult to explain the low IRX of the Capak et al. [2015] sources, unless their β slopes have been overestimated or the dust temperature (hence the FIR flux) has been underestimated. A similar conclusion applies to the recent results reported by Bouwens et al. [2016] using stacked constraints on the IRX for a sample of $\mathrm{z} \sim 4-10$ galaxies of the HUDF obtained with deep 1.2 mm-continuum observations (see the upper limits in Fig. 3.11). A more detailed analysis of these latest findings is deferred to a future study.

Chapter 4

Conclusions

Dust plays a very important role in the star formation cycle. It promotes the formation of molecular hydrogen [Krumholz et al., 2012, Gnedin and Kravtsov, 2010], hence affecting the rate of star formation [Bigiel et al., 2008, Krumholz et al., 2011]. At very low metallicities, collisional excitation of dust grains followed by thermal emission provides an important cooling channel in star forming regions, possibly allowing the formation of the first low-mass and long-lived stars [Schneider et al., 2002, 2006, 2012b]. However, the origin of dust at high redshift and the level of dust enrichment expected in the first low-metallicity galaxies are still debated issues.

Due to the short evolutionary timescales of their stellar progenitors, SNe have been proposed to be the major sources of dust at high redshift. Indeed, theoretical models have shown that a few hundreds days after the explosions, gas-phase metals can condense in the expanding SN ejecta, forming a large variety of grain species [Todini and Ferrara, 2001, Nozawa et al., 2003, Bianchi and Schneider, 2007, Cherchneff and Lilly, 2008, Sarangi and Cherchneff, 2013, Marassi et al., 2014, 2015]. When compared to observations of SN remnants done with Herschel and - more recently - with ALMA [Gomez and Matsuura, 2012, Dunne et al., 2009, Barlow et al., 2010, Matsuura et al., 2011, Otsuka et al., 2010, De Looze et al., 2017], that are sensitive to the dynamically dominant cold dust component, the predicted masses of freshly formed dust are in broad agreement [Schneider et al., 2014]. Yet, a large uncertainty remains on the fraction of freshly formed dust that will survive the passage of the reverse shock [Bianchi and Schneider, 2007, Bocchio et al., 2016]. For example, following the predicted time evolution of the dust mass in the ejecta of SN 1987A

and CasA, Bocchio et al. [2016] find that SN 1987A is too young for the reverse shock to have affected the dust mass. Hence the observed dust mass of $[0.7 - 0.9]$ $\mathrm{M}_{\odot}$ in this source is indicative of the mass of freshly formed dust in SN ejecta. In Cas A, the reverse shock has already destroyed $\sim$ 10% of the initial dust mass. However, the largest dust mass destruction is predicted to occur between 10^3 and 10^5 yr after the explosions. Hence, current observations can only provide an upper limit to the effective SN dust yields, and can not be used to quantify the contribution of SNe to dust enrichment, as often done in the literature [Watson et al., 2015, Laporte et al., 2017a].

The contribution of AGB to high-z dust enrichment has often been neglected, based on the assumption that their longer evolutionary timescales prevent them from reaching their dust production phase at $\mathrm{z} > 6$. However, this is rather a misconception as the evolutionary timescales of intermediate mass stars with masses between ~ 2 to $\sim 8\,\mathrm{M}_{\odot}$ range between 40 Myr and 1 Gyr, and hence these stars have enough time to reach their dust production phase even at $\mathrm{z} \geq 6$ [Valiante et al., 2009]. Rather, their contribution to early dust enrichment depends on the mass- and metallicity-dependent dust yields. Using AGB dust yields from Ferrarotti and Gail [2006], Zhukovska et al. [2008], Valiante et al. [2009] have shown that AGB stars can contribute up to $\sim$ 50% of the total dust mass produced by a burst of stars in less than 300 Myr. These figures have been recently revised in light of new AGB dust yields that are computed following the time-dependent chemical composition of the stellar atmospheres as predicted by numerical stellar models [Ventura et al., 2012b,a, Di Criscienzo et al., 2013, Ventura et al., 2014]. These new models predict a larger metallicity dependence of dust production rates of massive AGB stars. As a result, it is found that at $\mathrm{Z} < 0.2\,\mathrm{Z}_{\odot}$ AGB contribution to the total dust mass is always sub-dominant with respect to that of SNe, and at higher metallicities it becomes dominant on longer timescales, $\sim$ 500 Myr [Schneider et al., 2015].

Clearly, the relative importance of SNe and AGB stars as sources of dust at high-z is still debated and it depends on persisting modelling uncertainties of dust production, and on the star formation history and chemical evolution of individual galaxies. In addition, once injected in the ISM, dust grains will be exposed to a large variety of physical conditions that will affect their physical properties [Hirashita et al., 2014a, 2016]. Among these, shocked gas fronts propagating in the ISM as result of SN explosions are believed to be the principal

environments where grain destruction can occur [McKee et al., 1987, Jones et al., 1994, Bocchio et al., 2014]. In the environments where dust survives, the grains can grow in mass by accreting gas phase metals (Draine 2011, Hirashita 2012, Hirashita and Li 2013, Köhler et al. 2015, but see however Ferrara et al. 2016).

Many successful progresses have been made in implementing dust enrichment in galaxies by both semi-analytic [Valiante et al., 2012, 2014, de Bennassuti et al., 2014, 2017, Popping et al., 2017], semi-numerical [Dayal et al., 2010b, Dayal and Ferrara, 2012, Wilkins et al., 2013, 2016, Khakhaleva-Li and Gnedin, 2016a, Cullen et al., 2017, Narayanan et al., 2017], and numerical models [Bekki, 2015, McKinnon et al., 2017, Zhukovska et al., 2016, Aoyama et al., 2017]. In this Ph.D. thesis, I have presented our original contribution to these advancements [Mancini et al., 2015, 2016], where we have developed a new semi-numerical model to investigate the earliest phases of dust enrichment in the Universe and how these affect the properties of the first galaxies. In particular, the questions we have tried to answer are the following.

What is the dominant stellar source of dust in $\mathrm{z} > 6$ galaxies?
With our semi-numerical model, we have reconstructed individual star formation histories of galaxies with masses $\mathrm{M_{star}} > 10^9\,\mathrm{M_\odot}$. For each of these, we have estimated the mass of dust produced by SNe and AGB stars. On average, we find that stellar sources of dust dominate the ISM enrichment at $\mathrm{z} > 10$, below which grain growth in dense ISM clouds provides the dominant contribution. Among stellar sources of dust, SNe appear always dominant, but the average contribution of AGB stars can be as large as $\sim 40\%$. This confirms that the contribution of AGB stars to high-redshift dust formation cannot be neglected, especially for the galaxies currently targeted by observational searches [Valiante et al., 2009, Mancini et al., 2015].

What are the physical conditions that allow rapid dust enrichment at high redshifts?
Observational data targeting normal star forming galaxies at $\mathrm{z} > 6$ have so far provided conflicting evidence for the presence of dust in their ISM. In most cases, ALMA data have been able to provide only upper limits on their dust thermal emission [Kanekar et al., 2013, Ouchi et al., 2013, Ota et al., 2014, Schaerer et al., 2015, Maiolino et al., 2015, Zavala

et al., 2015]. On the other hand, the detection of large dust masses in two gravitationally lensed galaxies, A1689-zD1 at $z = 7.5$ [Watson et al., 2015] and A2744 YD4 at $z = 8.38$ have challenged the idea that dust enrichment can be neglected for these high-z systems [Michałowski, 2015, Mancini et al., 2015]. Indeed, A1689-zD1 has been able to accumulate a dust mass comparable to that of the Milky Way, $M_{dust} \sim (3-6) \times 10^7 M_{\odot}$ in less than 600 Myr of cosmic evolution (assuming star formation to have started at $z \sim 25$). The analysis that we have carried out suggests that very efficient grain growth must have occurred in the ISM of this galaxy, with a grain growth time-scale $\tau_{acc,0} = 0.2$ Myr, one order of magnitude shorter than required to reproduce the observed dust-to-gas ratio in the Milky-Way and in most local dwarf galaxies [de Bennassuti et al., 2014, Zhukovska, 2014]. Most notably, the same grain growth time-scale would be able to explain the $6 \times 10^6 M_{\odot}$ dust mass inferred for A2744 YD4 [Laporte et al., 2017a] $z = 8.38$, only 600 Myr after the Big Bang. Conversely, a similarly small grain growth time-scale - if applied to all the galaxies at these high redshifts - would largely exceed the upper limits obtained from ALMA observations of $6 \leq z \leq 7$ galaxies [Kanekar et al., 2013, Ouchi et al., 2013, Ota et al., 2014, Schaerer et al., 2015, Maiolino et al., 2015]. Our study suggests that in these high redshift faint dusty star forming galaxies the cold atomic and molecular phases of the ISM, where grain growth is more efficient, must have had an average density of $\sim 10^4\,cm^{-3}$, comparable to the molecular gas density inferred from CO excitation analyses of starburst galaxies at comparable (although slightly smaller) redshifts [Carilli and Walter, 2013]. Interestingly, a recent follow-up study of A2744 YD4 suggests that the galaxy could be an interacting system of two proto-galaxies or an early disk in formation with a clumpy structure arising from dynamical instabilities [Knudsen et al., 2017]. In either case, the average density of the gas is increased and these conditions seem to make A1689-zD1 suitable for accelerated grain growth.

How does dust enrichment affect the UV properties of $5 \leq z \leq 8$ galaxies?

To explore how dust extinction could affect the UV luminosities and colours of high-z galaxies, as a first step we have computed the UV LF and CMR for all the simulated galaxies, using the metallicity and age-dependent stellar emission spectra, but assuming no dust extinction. The comparison with existing observational data shows that while the observed

LF at $z \sim 8$ is consistent with negligible dust extinction, at $z \sim 5$ observations seem to require significant dust extinction at all luminosities brighter than $M_{UV} = -18$, in agreement with independent studies [Salvaterra et al., 2013, Dayal et al., 2013, Khakhaleva-Li and Gnedin, 2016a]. At all redshifts, the predicted intrinsic β slopes are much bluer than observed, particularly at the bright end. Hence, our study suggests that even a modest level of dust enrichment can significantly affect the UV colours of high redshift galaxies, particularly at the bright end [Mancini et al., 2016].

What can we learn from existing data on the properties of dust at $5 \leq z \leq 8$?
Using our semi-numerical approach, we have explored different dust extinction models, varying the dust extinction law and time interval during which stars are still embedded in their natal clouds, thus experiencing a larger dust extinction. We find that current data on the UV LF and CMR at $5 \leq z \leq 8$ seem to favour a steep, SMC-like extinction law and a cloud residence time of ≤ 15 Myr. Using this simple model, we analyze the scatter in the colour distribution, and we find that this increases with cosmic time, as a result of the progressively larger degree of dust enrichment. At each z, the scatter in the colour distribution increases with luminosity, as the brightest galaxies are also more massive and dust enriched. Hence, our analysis suggests that $z \geq 5$ galaxies are a mix of intrinsically faint blue galaxies and of red objects which have suffered strong dust extinction, and that the latter population grows with time, as a result of more efficient grain-growth in their ISM [Mancini et al., 2016].

These findings indicate that physical properties derived only from rest-frame UV data should be taken with care. Indeed, lower stellar mass and less chemically mature galaxies at high-z are characterized by smaller IRX and A_{1500} than implied by the Meurer et al. (1999) relation for galaxies with the same colours. As a result, their star formation rate may be overestimated if dust attenuation factors are derived using the Meurer et al. (1999) relation, and that more realistic dust correction for young galaxies, which have not yet experienced major dust enrichment, can be derived from their UV colours using a flatter IRX - relation, such as the one implied by the SMC curve. On the other hand, we also predict a population of dusty, UV-faint galaxies at $z \sim 5$ and 6 that lies off the mean $M_{star} - M_{UV}$ relations inferred from observations at comparable and higher-z [González

et al., 2011, Duncan et al., 2014, Grazian et al., 2015, Schaerer et al., 2015]. Indeed, the difference between the galaxy stellar mass function inferred from UV-selected star forming galaxies by González et al. [2011] and the mass function derived by Duncan et al. [2014], Grazian et al. [2015] using deep optical and infrared data has been interpreted as due to a growing contribution of massive dusty galaxies at $z \leqslant 5.5$.

Finally, our model predictions are in tension with the IR excess of $z \sim 5.1-5.7$ galaxies inferred by [Capak et al., 2015], which have been argued to be significantly more dust-poor and less IR-luminous than lower redshift galaxies with similar UV colours. We suggest that the β slopes of these galaxies may have been overestimated or that their IR luminosities (that are derived from a single data point) may have been underestimated due to a poor assumption on the dust temperature or on the dust emissivity [Mancini et al., 2016]. These suggestions have proved to be correct by new analyses of the same sample [Barišić et al., 2017, Faisst et al., 2017] and the new observations are in much better agreement with the theoretical predictions.

What is the best strategy to improve our understanding of early dust formation?
The progresses made in the past few years have demonstrated that ALMA has the potential to detect dust emission from galaxies up to $z \sim 7.5$ and beyond, and the upcoming James Webb Space Telescope will be able to extend rest-frame UV observations up to very high redshifts, allowing to probe the first phases of metal and dust enrichment in the Universe. In order to fully exploit the physical information encoded in these extraordinary data, theoretical models must be able to predict the properties of the interstellar medium of these galaxies, including their dust content. Recent attempts have been made to include dust formation and its reprocessing in the ISM directly in numerical simulations [Bekki, 2015, McKinnon et al., 2017, Zhukovska et al., 2016, Aoyama et al., 2017, Graziani, 2017, in prep]. Ultimately, this is were we have to convey our theoretical efforts and the work presented in this Ph.D. thesis represents an important step in this direction.

Bibliography

T. Abel, G. L. Bryan, and M. L. Norman. The Formation of the First Star in the Universe. *Science*, 295:93–98, January 2002. doi: 10.1126/science.295.5552.93.

P. Anninos and M. L. Norman. The Role of Hydrogen Molecules in the Radiative Cooling and Fragmentation of Cosmological Sheets. ApJ, 460:556, April 1996. doi: 10.1086/176992.

S. Aoyama, K.-C. Hou, I. Shimizu, H. Hirashita, K. Todoroki, J.-H. Choi, and K. Nagamine. Galaxy simulation with dust formation and destruction. MNRAS, 466: 105–121, April 2017. doi: 10.1093/mnras/stw3061.

R. S. Asano, T. T. Takeuchi, H. Hirashita, and A. K. Inoue. Dust formation history of galaxies: A critical role of metallicity for the dust mass growth by accreting materials in the interstellar medium. *Earth, Planets, and Space*, 65:213–222, March 2013. doi: 10.5047/eps.2012.04.014.

H. Atek, J. Richard, J.-P. Kneib, M. Jauzac, D. Schaerer, B. Clement, M. Limousin, E. Jullo, P. Natarajan, E. Egami, and H. Ebeling. New Constraints on the Faint End of the UV Luminosity Function at z $\sim$ 7-8 Using the Gravitational Lensing of the Hubble Frontier Fields Cluster A2744. ApJ, 800:18, February 2015. doi: 10.1088/0004-637X/800/1/18.

E. Bañados, B. P. Venemans, R. Decarli, E. P. Farina, C. Mazzucchelli, F. Walter, X. Fan, D. Stern, E. Schlafly, K. C. Chambers, H.-W. Rix, L. Jiang, I. McGreer, R. Simcoe, F. Wang, J. Yang, E. Morganson, G. De Rosa, J. Greiner, M. Baloković, W. S. Burgett, T. Cooper, P. W. Draper, H. Flewelling, K. W. Hodapp, H. D. Jun, N. Kaiser, R.-P. Kudritzki, E. A. Magnier, N. Metcalfe, D. Miller, J.-T. Schindler, J. L. Tonry, R. J. Wainscoat, C. Waters, and Q. Yang. The Pan-STARRS1 Distant z > 5.6 Quasar Survey:

More than 100 Quasars within the First Gyr of the Universe. ApJS, 227:11, November 2016. doi: 10.3847/0067-0049/227/1/11.

N. A. Bahcall and X. Fan. The Most Massive Distant Clusters: Determining Ω and σ_8. ApJ, 504:1–6, September 1998. doi: 10.1086/306088.

J. M. Bardeen, J. R. Bond, N. Kaiser, and A. S. Szalay. The statistics of peaks of Gaussian random fields. ApJ, 304:15–61, May 1986. doi: 10.1086/164143.

I. Barišić, A. L. Faisst, P. L. Capak, R. Pavesi, D. A. Riechers, N. Z. Scoville, K. C. Cooke, J. S. Kartaltepe, C. M. Casey, and V. Smolčić. Dust Properties of [CII] Detected z $\sim$ 5.5 Galaxies: New HST/WFC3 Near-IR Observations. *ArXiv e-prints*, July 2017.

R. Barkana and A. Loeb. In the beginning: the first sources of light and the reionization of the universe. Phys. Rep., 349:125–238, July 2001. doi: 10.1016/S0370-1573(01)00019-9.

R. Barkana and A. Loeb. Concentrating the dark matter in galaxy clusters through tidal stripping of baryonically compressed galactic halos. MNRAS, 405:1969–1975, July 2010. doi: 10.1111/j.1365-2966.2010.16587.x.

M. J. Barlow, O. Krause, B. M. Swinyard, B. Sibthorpe, M.-A. Besel, R. Wesson, R. J. Ivison, L. Dunne, W. K. Gear, H. L. Gomez, P. C. Hargrave, T. Henning, S. J. Leeks, T. L. Lim, G. Olofsson, and E. T. Polehampton. A Herschel PACS and SPIRE study of the dust content of the Cassiopeia A supernova remnant. A&A, 518:L138, July 2010. doi: 10.1051/0004-6361/201014585.

G. D. Becker, M. Rauch, and W. L. W. Sargent. High-Redshift Metals. I. The Decline of C IV at z > 5.3. ApJ, 698:1010–1019, June 2009. doi: 10.1088/0004-637X/698/2/1010.

S. V. W. Beckwith, M. Stiavelli, A. M. Koekemoer, J. A. R. Caldwell, H. C. Ferguson, R. Hook, R. A. Lucas, L. E. Bergeron, M. Corbin, S. Jogee, N. Panagia, M. Robberto, P. Royle, R. S. Somerville, and M. Sosey. The Hubble Ultra Deep Field. AJ, 132:1729–1755, November 2006. doi: 10.1086/507302.

K. Bekki. Cosmic Evolution of Dust in Galaxies: Methods and Preliminary Results. ApJ, 799:166, February 2015. doi: 10.1088/0004-637X/799/2/166.

J. Benjamin, C. Heymans, E. Semboloni, L. van Waerbeke, H. Hoekstra, T. Erben, M. D. Gladders, M. Hetterscheidt, Y. Mellier, and H. K. C. Yee. Cosmological constraints from the 100-deg^2 weak-lensing survey. MNRAS, 381:702–712, October 2007. doi: 10.1111/j.1365-2966.2007.12202.x.

S. Bertone and F. Stoehr, Whit. D. M.. M. Galactic winds and transport of metals into the IGM in semi-analytic simulations. In R. de Grijs and R. M. González Delgado, editors, *Starbursts: From 30 Doradus to Lyman Break Galaxies*, volume 329 of *Astrophysics and Space Science Library*, page P6, May 2005.

S. Bianchi and R. Schneider. Dust formation and survival in supernova ejecta. MNRAS, 378:973–982, July 2007. doi: 10.1111/j.1365-2966.2007.11829.x.

F. Bigiel, A. Leroy, F. Walter, E. Brinks, W. J. G. de Blok, B. Madore, and M. D. Thornley. The Star Formation Law in Nearby Galaxies on Sub-Kpc Scales. AJ, 136:2846–2871, December 2008. doi: 10.1088/0004-6256/136/6/2846.

M. Bocchio, A. P. Jones, and J. D. Slavin. A re-evaluation of dust processing in supernova shock waves. A&A, 570:A32, October 2014. doi: 10.1051/0004-6361/201424368.

M. Bocchio, S. Marassi, R. Schneider, S. Bianchi, M. Limongi, and A. Chieffi. Dust grains from the heart of supernovae. A&A, 587:A157, 2016.

S. Boissier, A. Gil de Paz, A. Boselli, B. F. Madore, V. Buat, L. Cortese, D. Burgarella, J. C. Muñoz-Mateos, T. A. Barlow, K. Forster, P. G. Friedman, D. C. Martin, P. Morrissey, S. G. Neff, D. Schiminovich, M. Seibert, T. Small, T. K. Wyder, L. Bianchi, J. Donas, T. M. Heckman, Y.-W. Lee, B. Milliard, R. M. Rich, A. S. Szalay, B. Y. Welsh, and S. K. Yi. Radial variation of attenuation and star formation in the largest late-type disks observed with galex. ApJS, 173:524, 2007.

W. B. Bonnor. The Formation of the Nebulae. With 3 Figures. ZAp, 39:143, 1956.

R. Bouwens, M. Aravena, R. Decarli, F. Walter, E. da Cunha, I. Labbe, F. Bauer, F. Bertoldi, C. Carilli, S. Chapman, E. Daddi, J. Hodge, R. Ivison, A. Karim, O. Le Fevre, B. Magnelli, K. Ota, D. Riechers, I. Smail, P. van der Werf, A. Weiss, P. Cox, D. Elbaz, J. Gonzalez-Lopez, L. Infante, P. Oesch, J. Wagg, and S. Wilkins. ALMA Spectroscopic

Survey in the Hubble Ultra Deep Field: The Infrared Excess of UV-selected z=2-10 galaxies as a function of UV-continuum Slope and Stellar Mass. *ArXiv e-prints*, June 2016.

R. J. Bouwens, G. D. Illingworth, P. A. Oesch, I. Labbé, M. Trenti, P. van Dokkum, M. Franx, M. Stiavelli, C. M. Carollo, D. Magee, and V. Gonzalez. Ultraviolet Luminosity Functions from 132 z ∼ 7 and z ∼ 8 Lyman-break Galaxies in the Ultra-deep HUDF09 and Wide-area Early Release Science WFC3/IR Observations. ApJ, 737:90, August 2011. doi: 10.1088/0004-637X/737/2/90.

R. J. Bouwens, G. D. Illingworth, P. A. Oesch, M. Franx, I. Labbé, M. Trenti, P. van Dokkum, C. M. Carollo, V. González, R. Smit, and D. Magee. UV-continuum Slopes at z ∼ 4-7 from the HUDF09+ERS+CANDELS Observations: Discovery of a Well-defined UV Color-Magnitude Relationship for z ≥ 4 Star-forming Galaxies. ApJ, 754:83, August 2012. doi: 10.1088/0004-637X/754/2/83.

R. J. Bouwens, G. D. Illingworth, P. A. Oesch, I. Labbé, P. G. van Dokkum, M. Trenti, M. Franx, R. Smit, V. Gonzalez, and D. Magee. UV-continuum Slopes of > 4000 z ∼ 4-8 Galaxies from the HUDF/XDF, HUDF09, ERS, CANDELS-South, and CANDELS-North Fields. ApJ, 793:115, October 2014. doi: 10.1088/0004-637X/793/2/115.

R. J. Bouwens, G. D. Illingworth, P. A. Oesch, M. Trenti, I. Labbé, L. Bradley, M. Carollo, P. G. van Dokkum, V. Gonzalez, B. Holwerda, M. Franx, L. Spitler, R. Smit, and D. Magee. UV Luminosity Functions at Redshifts z ∼ 4 to z ∼ 10: 10,000 Galaxies from HST Legacy Fields. ApJ, 803:34, April 2015. doi: 10.1088/0004-637X/803/1/34.

R. A. A. Bowler, J. S. Dunlop, R. J. McLure, A. B. Rogers, H. J. McCracken, B. Milvang-Jensen, H. Furusawa, J. P. U. Fynbo, Y. Taniguchi, J. Afonso, M. N. Bremer, and O. Le Fèvre. The bright end of the galaxy luminosity function at z≃7: before the onset of mass quenching? MNRAS, 440:2810–2842, May 2014. doi: 10.1093/mnras/stu449.

R. A. A. Bowler, J. S. Dunlop, R. J. McLure, H. J. McCracken, B. Milvang-Jensen, H. Furusawa, Y. Taniguchi, O. Le Fèvre, J. P. U. Fynbo, M. J. Jarvis, and B. Häußler. The galaxy luminosity function at z ≃ 6 and evidence for rapid evolution in the bright end from z ≃ 7 to 5. MNRAS, 452:1817–1840, September 2015. doi: 10.1093/mnras/stv1403.

V. Bromm. Formation of the first stars. *Reports on Progress in Physics*, 76(11):112901, November 2013. doi: 10.1088/0034-4885/76/11/112901.

V. Bromm and A. Loeb. The formation of the first low-mass stars from gas with low carbon and oxygen abundances. Nature, 425:812–814, October 2003. doi: 10.1038/nature02071.

V. Bromm and N. Yoshida. The First Galaxies. ARA&A, 49:373–407, September 2011. doi: 10.1146/annurev-astro-081710-102608.

V. Bromm, A. Ferrara, P. S. Coppi, and R. B. Larson. The fragmentation of pre-enriched primordial objects. MNRAS, 328:969–976, December 2001. doi: 10.1046/j.1365-8711.2001.04915.x.

V. Bromm, P. S. Coppi, and R. B. Larson. The Formation of the First Stars. I. The Primordial Star-forming Cloud. ApJ, 564:23–51, January 2002. doi: 10.1086/323947.

V. Buat, S. Noll, D. Burgarella, E. Giovannoli, V. Charmandaris, M. Pannella, H. S. Hwang, D. Elbaz, M. Dickinson, G. Magdis, N. Reddy, and E. J. Murphy. Goods-herschel: dust attenuation properties of uv selected high redshift galaxies. A&A, 545:A141, 2012.

D. Calzetti, A. L. Kinney, and T. Storchi-Bergmann. Dust extinction of the stellar continua in starburst galaxies: The ultraviolet and optical extinction law. ApJ, 429:582–601, July 1994. doi: 10.1086/174346.

D. Calzetti, L. Armus, R. C. Bohlin, A. L. Kinney, J. Koornneef, and T. Storchi-Bergmann. The Dust Content and Opacity of Actively Star-forming Galaxies. ApJ, 533:682–695, April 2000. doi: 10.1086/308692.

M. A. Campisi, U. Maio, R. Salvaterra, and B. Ciardi. Population III stars and the long gamma-ray burst rate. MNRAS, 416:2760–2767, October 2011. doi: 10.1111/j.1365-2966.2011.19238.x.

P. L. Capak, C. Carilli, G. Jones, C. M. Casey, D. Riechers, K. Sheth, C. M. Carollo, O. Ilbert, A. Karim, O. Lefevre, S. Lilly, N. Scoville, V. Smolcic, and L. Yan. Galaxies at redshifts 5 to 6 with systematically low dust content and high [c ii] emission. Nature, 522(422), 2015.

J. A. Cardelli, G. C. Clayton, and J. S. Mathis. The relationship between infrared, optical, and ultraviolet extinction. ApJ, 345:245, 1989.

C. L. Carilli and F. Walter. Cool Gas in High-Redshift Galaxies. ARA&A, 51:105–161, August 2013. doi: 10.1146/annurev-astro-082812-140953.

C. M. Casey, N. Z. Scoville, D. B. Sanders, N. Lee, A. Cooray, S. L. Finkelstein, P. Capak, A. Conley, G. De Zotti, D. Farrah, H. Fu, E. Le Floc'h, O. Ilbert, R. J. Ivison, and T. T. Takeuchi. Are dusty galaxies blue? insights on uv attenuation from dust-selected galaxies. ApJ, 796:95, 2014.

M. Castellano, A. Fontana, D. Paris, A. Grazian, L. Pentericci, K. Boutsia, P. Santini, V. Testa, M. Dickinson, M. Giavalisco, R. Bouwens, J.-G. Cuby, F. Mannucci, B. Clément, S. Cristiani, F. Fiore, S. Gallozzi, E. Giallongo, R. Maiolino, N. Menci, A. Moorwood, M. Nonino, A. Renzini, P. Rosati, S. Salimbeni, and E. Vanzella. The bright end of the z $\sim$ 7 UV luminosity function from a wide and deep HAWK-I survey. A&A, 524: A28, December 2010. doi: 10.1051/0004-6361/201015195.

M. Castellano, A. Fontana, A. Grazian, L. Pentericci, P. Santini, A. Koekemoer, S. Cristiani, A. Galametz, S. Gallerani, E. Vanzella, K. Boutsia, S. Gallozzi, E. Giallongo, R. Maiolino, N. Menci, and D. Paris. The blue UV slopes of z $\sim$ 4 Lyman break galaxies: implications for the corrected star formation rate density. A&A, 540:A39, April 2012. doi: 10.1051/0004-6361/201118050.

M. Castellano, V. Sommariva, A. Fontana, L. Pentericci, P. Santini, A. Grazian, R. Amorin, J. L. Donley, J. S. Dunlop, H. C. Ferguson, F. Fiore, A. Galametz, E. Giallongo, Y. Guo, K.-H. Huang, A. Koekemoer, R. Maiolino, R. J. McLure, D. Paris, D. Schaerer, P. Troncoso, and E. Vanzella. Constraints on the star-formation rate of z $\sim$ 3 lbgs with measured metallicity in the candels goods-south field. A&A, 566:A19, 2014.

S. Charlot and S. M. Fall. A simple model for the absorption of starlight by dust in galaxies. ApJ, 539:718, 2000.

I. Cherchneff and E. Dwek. The Chemistry of Population III Supernova Ejecta. I. Formation of Molecules in the Early Universe. ApJ, 703:642–661, September 2009. doi: 10.1088/0004-637X/703/1/642.

I. Cherchneff and S. Lilly. Primordial Massive Supernovae as the First Molecular Factories in the Early Universe. ApJ, 683:L123–L126, August 2008. doi: 10.1086/591906.

B. Ciardi and A. Ferrara. The First Cosmic Structures and Their Effects. Space Sci. Rev., 116:625–705, February 2005. doi: 10.1007/s11214-005-3592-0.

P. C. Clark, S. C. O. Glover, R. S. Klessen, and V. Bromm. Gravitational Fragmentation in Turbulent Primordial Gas and the Initial Mass Function of Population III Stars. ApJ, 727:110, February 2011. doi: 10.1088/0004-637X/727/2/110.

S. Cole, W. J. Percival, J. A. Peacock, P. Norberg, C. M. Baugh, C. S. Frenk, I. Baldry, J. Bland-Hawthorn, T. Bridges, R. Cannon, M. Colless, C. Collins, W. Couch, N. J. G. Cross, G. Dalton, V. R. Eke, R. De Propris, S. P. Driver, G. Efstathiou, R. S. Ellis, K. Glazebrook, C. Jackson, A. Jenkins, O. Lahav, I. Lewis, S. Lumsden, S. Maddox, D. Madgwick, B. A. Peterson, W. Sutherland, and K. Taylor. The 2dF Galaxy Redshift Survey: power-spectrum analysis of the final data set and cosmological implications. MNRAS, 362:505–534, September 2005. doi: 10.1111/j.1365-2966.2005.09318.x.

L. Cortese, A. Boselli, V. Buat, G. Gavazzi, S. Boissier, A. Gil de Paz, M. Seibert, B. F. Madore, and D. C. Martin. Uv dust attenuation in normal star-forming galaxies. i. estimating the $l_{\rm TIR}/l_{\rm FUV}$ ratio. ApJ, 637:242, 2006.

F. Cullen, R. J. McLure, S. Khochfar, J. S. Dunlop, and C. Dalla Vecchia. The First Billion Years project: constraining the dust attenuation law of star-forming galaxies at $z \simeq 5$. MNRAS, 470:3006–3026, September 2017. doi: 10.1093/mnras/stx1451.

E. da Cunha, B. Groves, F. Walter, R. Decarli, A. Weiss, F. Bertoldi, C. Carilli, E. Daddi, D. Elbaz, R. Ivison, R. Maiolino, D. Riechers, H.-W. Rix, M. Sargent, and I. Smail. On the Effect of the Cosmic Microwave Background in High-redshift (Sub-)millimeter Observations. ApJ, 766:13, March 2013. doi: 10.1088/0004-637X/766/1/13.

P. Dayal and A. Ferrara. Lyα emitters and Lyman-break galaxies: dichotomous twins. MNRAS, 421:2568–2579, April 2012. doi: 10.1111/j.1365-2966.2012.20486.x.

P. Dayal, A. Ferrara, and A. Saro. The cool side of Lyman alpha emitters. MNRAS, 402: 1449, 2010a.

P. Dayal, H. Hirashita, and A. Ferrara. Detecting Lyman alpha emitters in the submillimetre. MNRAS, 403:620–624, April 2010b. doi: 10.1111/j.1365-2966.2009.16164.x.

P. Dayal, J. S. Dunlop, U. Maio, and B. Ciardi. Simulating the assembly of galaxies at redshifts z = 6-12. MNRAS, 434:1486–1504, September 2013. doi: 10.1093/mnras/stt1108.

P. Dayal, A. Ferrara, J. S. Dunlop, and F. Pacucci. Essential physics of early galaxy formation. MNRAS, 445:2545–2557, December 2014. doi: 10.1093/mnras/stu1848.

M. de Bennassuti, R. Schneider, R. Valiante, and S. Salvadori. Decoding the stellar fossils of the dusty Milky Way progenitors. MNRAS, 445:3039–3054, December 2014. doi: 10.1093/mnras/stu1962.

M. de Bennassuti, S. Salvadori, R. Schneider, R. Valiante, and K. Omukai. Limits on Population III star formation with the most iron-poor stars. MNRAS, 465:926–940, February 2017. doi: 10.1093/mnras/stw2687.

I. De Looze, M. J. Barlow, B. M. Swinyard, J. Rho, H. L. Gomez, M. Matsuura, and R. Wesson. The dust mass in Cassiopeia A from a spatially resolved Herschel analysis. MNRAS, 465:3309–3342, March 2017. doi: 10.1093/mnras/stw2837.

A. L. DeSouza and S. Basu. The luminosity of Population III star clusters. MNRAS, 450: 295–304, June 2015. doi: 10.1093/mnras/stv523.

M. Di Criscienzo, F. Dell'Agli, P. Ventura, R. Schneider, R. Valiante, F. La Franca, C. Rossi, S. Gallerani, and R. Maiolino. Dust formation in the winds of AGBs: the contribution at low metallicities. MNRAS, 433:313–323, July 2013. doi: 10.1093/mnras/stt732.

Bruce T. Draine. *Physics of the Interstellar and Intergalactic Medium*. Princeton Univ. Press, 2011.

K. Duncan, C. J. Conselice, A. Mortlock, W. G. Hartley, Y. Guo, H. C. Ferguson, R. Davé, Y. Lu, J. Ownsworth, M. L. N. Ashby, A. Dekel, M. Dickinson, S. Faber, M. Giavalisco, N. Grogin, D. Kocevski, A. Koekemoer, R. S. Somerville, and C. E. White. The mass evolution of the first galaxies: stellar mass functions and star formation rates at $4 < z < 7$ in the CANDELS GOODS-South field. MNRAS, 444:2960, 2014.

J. S. Dunlop. A Deep ALMA Image of the Hubble Ultra Deep Field. *The Messenger*, 166: 48–52, December 2016.

J. S. Dunlop, R. J. McLure, B. E. Robertson, R. S. Ellis, D. P. Stark, M. Cirasuolo, and L. de Ravel. A critical analysis of the ultraviolet continuum slopes (β) of high-redshift galaxies: no evidence (yet) for extreme stellar populations at z > 6. MNRAS, 420:901, 2012.

J. S. Dunlop, A. B. Rogers, R. J. McLure, R. S. Ellis, B. E. Robertson, A. Koekemoer, P. Dayal, E. Curtis-Lake, V. Wild, S. Charlot, R. A. A. Bowler, M. A. Schenker, M. Ouchi, Y. Ono, M. Cirasuolo, S. R. Furlanetto, D. P. Stark, T. A. Targett, and E. Schneider. The uv continua and inferred stellar populations of galaxies at z $\simeq$ 7-9 revealed by the hubble ultra-deep field 2012 campaign. MNRAS, 432:3520, 2013.

L. Dunne, S. J. Maddox, R. J. Ivison, L. Rudnick, T. A. Delaney, B. C. Matthews, C. M. Crowe, H. L. Gomez, S. A. Eales, and S. Dye. Cassiopeia A: dust factory revealed via submillimetre polarimetry. MNRAS, 394:1307–1316, April 2009. doi: 10.1111/j.1365-2966.2009.14453.x.

R. Ebert. Über die Verdichtung von H I-Gebieten. Mit 5 Textabbildungen. ZAp, 37:217, 1955.

A. L. Faisst, P. L. Capak, L. Yan, R. Pavesi, D. A. Riechers, I. Barisic, K. C. Cooke, J. S. Kartaltepe, and D. C. Masters. Are high redshift Galaxies hot? - Temperature of z > 5 Galaxies and Implications on their Dust Properties. *ArXiv e-prints*, August 2017.

H. Feldman, R. Juszkiewicz, P. Ferreira, M. Davis, E. Gaztañaga, J. Fry, A. Jaffe, S. Chambers, L. da Costa, M. Bernardi, R. Giovanelli, M. Haynes, and G. Wegner. An Estimate of $\Omega_{\rm m}$ without Conventional Priors. ApJ, 596:L131–L134, October 2003. doi: 10.1086/379221.

A. Ferrara, M. Pettini, and Y. Shchekinov. Mixing metals in the early Universe. MNRAS, 319:539–548, December 2000. doi: 10.1046/j.1365-8711.2000.03857.x.

A. Ferrara, S. Viti, and C. Ceccarelli. The problematic growth of dust in high-redshift galaxies. MNRAS, 463:L112–L116, November 2016. doi: 10.1093/mnrasl/slw165.

A. S. Ferrarotti and H.-P. Gail. Composition and quantities of dust produced by AGB-stars and returned to the interstellar medium. A&A, 447:553–576, February 2006. doi: 10.1051/0004-6361:20041198.

S. L. Finkelstein, C. Papovich, B. Salmon, K. Finlator, M. Dickinson, H. C. Ferguson, M. Giavalisco, A. M. Koekemoer, N. A. Reddy, R. Bassett, C. J. Conselice, J. S. Dunlop, S. M. Faber, N. A. Grogin, N. P. Hathi, D. D. Kocevski, K. Lai, K.-S. Lee, R. J. McLure, B. Mobasher, and J. A. Newman. Candels: The Evolution of Galaxy Rest-frame Ultraviolet Colors from z = 8 to 4. ApJ, 756:164, September 2012. doi: 10.1088/0004-637X/756/2/164.

S. L. Finkelstein, R. E. Ryan, Jr., C. Papovich, M. Dickinson, M. Song, R. S. Somerville, H. C. Ferguson, B. Salmon, M. Giavalisco, A. M. Koekemoer, M. L. N. Ashby, P. Behroozi, M. Castellano, J. S. Dunlop, S. M. Faber, G. G. Fazio, A. Fontana, N. A. Grogin, N. Hathi, J. Jaacks, D. D. Kocevski, R. Livermore, R. J. McLure, E. Merlin, B. Mobasher, J. A. Newman, M. Rafelski, V. Tilvi, and S. P. Willner. The evolution of the galaxy rest-frame ultraviolet luminosity function over the first two billion years. ApJ, 810:71, 2015a.

S. L. Finkelstein, M. Song, P. Behroozi, R. S. Somerville, C. Papovich, M. Milosavljević, A. Dekel, D. Narayanan, M. L. N. Ashby, A. Cooray, G. G. Fazio, H. C. Ferguson, A. M. Koekemoer, B. Salmon, and S. P. Willner. An Increasing Stellar Baryon Fraction in Bright Galaxies at High Redshift. ApJ, 814:95, December 2015b. doi: 10.1088/0004-637X/814/2/95.

K. Finlator. Gas Accretion and Galactic Chemical Evolution: Theory and Observations. In A. Fox and R. Davé, editors, *Astrophysics and Space Science Library*, volume 430 of *Astrophysics and Space Science Library*, page 221, 2017. doi: 10.1007/978-3-319-52512-9_10.

J. E. Forero-Romero, G. Yepes, S. Gottlöber, S. R. Knollmann, A. Khalatyan, A. J. Cuesta, and F. Prada. Simulated versus observed uv emission at high redshift: a hint for a clumpy interstellar medium? MNRAS, 403:L31, 2010.

B. Forrest, K.-V. H. Tran, A. R. Tomczak, A. Broussard, I. Labbé, C. Papovich, M. Kriek,

R. J. Allen, M. Cowley, M. Dickinson, K. Glazebrook, J. van Houdt, H. Inami, G. G. Kacprzak, L. Kawinwanichakij, D. Kelson, P. J. McCarthy, A. Monson, G. Morrison, T. Nanayakkara, S. E. Persson, R. F. Quadri, L. R. Spitler, C. Straatman, and V. Tilvi. Uv to ir luminosities and dust attenuation determined from ~4000 k-selected galaxies at $1 < z < 3$ in the zfourge survey. ApJ, 818:L26, 2016.

S. Gallerani, R. Maiolino, Y. Juarez, T. Nagao, A. Marconi, S. Bianchi, R. Schneider, F. Mannucci, T. Oliva, C. J. Willott, L. Jiang, and X. Fan. The extinction law at high redshift and its implications. A&A, 523:A85, 2010.

L. Gao, N. Yoshida, T. Abel, C. S. Frenk, A. Jenkins, and V. Springel. The first generation of stars in the Λ cold dark matter cosmology. MNRAS, 378:449–468, June 2007. doi: 10.1111/j.1365-2966.2007.11814.x.

N. Y. Gnedin and A. V. Kravtsov. On the Kennicutt-Schmidt Relation of Low-Metallicity High-Redshift Galaxies. ApJ, 714:287–295, May 2010. doi: 10.1088/0004-637X/714/1/287.

N. Y. Gnedin, G. D. Becker, and X. Fan. Cosmic Reionization on Computers: Properties of the Post-reionization IGM. ApJ, 841:26, May 2017. doi: 10.3847/1538-4357/aa6c24.

J. D. Goldader, G. Meurer, T. M. Heckman, M. Seibert, D. B. Sanders, D. Calzetti, and C. C. Steidel. Far-infrared galaxies in the far-ultraviolet. ApJ, 568:651, 2002.

H. Gomez and M. Matsuura. The origin of dust in galaxies in the Herschel and ALMA era. *Astronomy and Geophysics*, 53(6):6.19–6.23, December 2012. doi: 10.1111/j.1468-4004.2012.53619.x.

V. González, I. Labbé, R. J. Bouwens, G. Illingworth, M. Franx, and M. Kriek. Evolution of galaxy stellar mass functions, mass densities, and mass-to-light ratios from $z \sim 7$ to $z \sim 4$. ApJ, 735:L34, 2011.

J. Gonzalez-Lopez, F. E. Bauer, C. Romero-Canizales, R. Kneissl, E. Villard, R. Carvajal, S. Kim, N. Laporte, T. Anguita, M. Aravena, R. J. Bouwens, L. Bradley, M. Carrasco, R. Demarco, H. Ford, E. Ibar, L. Infante, H. Messias, A. M. Munoz Arancibia, N. Nagar, N. Padilla, E. Treister, P. Troncoso, and A. Zitrin. VizieR Online Data Catalog: ALMA

Frontier Fields Survey. I. (Gonzalez-Lopez+, 2017). *VizieR Online Data Catalog*, 359, October 2016.

J. González-López, F. E. Bauer, M. Aravena, N. Laporte, L. Bradley, M. Carrasco, R. Carvajal, R. Demarco, L. Infante, R. Kneissl, A. M. Koekemoer, A. M. Muñoz Arancibia, P. Troncoso, E. Villard, and A. Zitrin. The ALMA Frontier Fields Survey III: 1.1 mm Emission Line Identifications in Abell 2744, MACSJ0416.1-2403, MACSJ1149.5+2223, Abell 370, and Abell S1063. *ArXiv e-prints*, April 2017a.

J. González-López, F. E. Bauer, C. Romero-Cañizales, R. Kneissl, E. Villard, R. Carvajal, S. Kim, N. Laporte, T. Anguita, M. Aravena, R. J. Bouwens, L. Bradley, M. Carrasco, R. Demarco, H. Ford, E. Ibar, L. Infante, H. Messias, A. M. Muñoz Arancibia, N. Nagar, N. Padilla, E. Treister, P. Troncoso, and A. Zitrin. The ALMA Frontier Fields Survey. I. 1.1 mm continuum detections in Abell 2744, MACS J0416.1-2403 and MACS J1149.5+2223. A&A, 597:A41, January 2017b. doi: 10.1051/0004-6361/201628806.

V. Gonzalez-Perez, C. G. Lacey, C. M. Baugh, C. S. Frenk, and S. M. Wilkins. The ultraviolet colours and dust attenuation of Lyman-break galaxies. MNRAS, 429:1609–1625, February 2013. doi: 10.1093/mnras/sts446.

A. Grazian, A. Fontana, P. Santini, J. S. Dunlop, H. C. Ferguson, M. Castellano, R. Amorin, M. L. N. Ashby, G. Barro, P. Behroozi, K. Boutsia, K. I. Caputi, R. R. Chary, A. Dekel, M. E. Dickinson, S. M. Faber, G. G. Fazio, S. L. Finkelstein, A. Galametz, E. Giallongo, M. Giavalisco, N. A. Grogin, Y. Guo, D. Kocevski, A. M. Koekemoer, D. C. Koo, K.-S. Lee, Y. Lu, E. Merlin, B. Mobasher, M. Nonino, C. Papovich, D. Paris, L. Pentericci, N. Reddy, A. Renzini, B. Salmon, M. Salvato, V. Sommariva, M. Song, and E. Vanzella. The galaxy stellar mass function at 3.5 $\leq$z $\leq$ 7.5 in the candels/uds, goods-south, and hudf fields. A&A, 575:A96, 2015.

L. Graziani. MNRAS, 2017, in prep.

L. Graziani, M. de Bennassuti, R. Schneider, D. Kawata, and S. Salvadori. The history of the dark and luminous side of Milky Way-like progenitors. MNRAS, 469:1101–1116, July 2017. doi: 10.1093/mnras/stx900.

T. H. Greif, J. L. Johnson, V. Bromm, and R. S. Klessen. The First Supernova Explosions: Energetics, Feedback, and Chemical Enrichment. ApJ, 670:1–14, November 2007. doi: 10.1086/522028.

T. H. Greif, S. C. O. Glover, V. Bromm, and R. S. Klessen. The First Galaxies: Chemical Enrichment, Mixing, and Star Formation. ApJ, 716:510–520, June 2010. doi: 10.1088/0004-637X/716/1/510.

T. H. Greif, S. D. M. White, R. S. Klessen, and V. Springel. The Delay of Population III Star Formation by Supersonic Streaming Velocities. ApJ, 736:147, August 2011. doi: 10.1088/0004-637X/736/2/147.

T. H. Greif, V. Bromm, P. C. Clark, S. C. O. Glover, R. J. Smith, R. S. Klessen, N. Yoshida, and V. Springel. Formation and evolution of primordial protostellar systems. MNRAS, 424:399–415, July 2012. doi: 10.1111/j.1365-2966.2012.21212.x.

F. Haardt and P. Madau. Radiative Transfer in a Clumpy Universe. II. The Ultraviolet Extragalactic Background. ApJ, 461:20, April 1996. doi: 10.1086/177035.

Z. Haiman, M. J. Rees, and A. Loeb. H 2 Cooling of Primordial Gas Triggered by UV Irradiation. ApJ, 467:522, August 1996. doi: 10.1086/177628.

A. Heger and S. E. Woosley. The Nucleosynthetic Signature of Population III. ApJ, 567: 532–543, March 2002. doi: 10.1086/338487.

S. Hirano and V. Bromm. Formation and survival of Population III stellar systems. MNRAS, 470:898–914, September 2017. doi: 10.1093/mnras/stx1220.

S. Hirano, T. Hosokawa, N. Yoshida, H. Umeda, K. Omukai, G. Chiaki, and H. W. Yorke. One Hundred First Stars: Protostellar Evolution and the Final Masses. ApJ, 781:60, February 2014. doi: 10.1088/0004-637X/781/2/60.

H. Hirashita. Dust growth in the interstellar medium: how do accretion and coagulation interplay? MNRAS, 422:1263–1271, May 2012. doi: 10.1111/j.1365-2966.2012.20702.x.

H. Hirashita and Z.-Y. Li. Condition for the formation of micron-sized dust grains in dense molecular cloud cores. MNRAS, 434:L70–L74, July 2013. doi: 10.1093/mnrasl/slt081.

H. Hirashita, A. Ferrara, P. Dayal, and M. Ouchi. Constraining dust formation in high-redshift young galaxies. MNRAS, 443:1704–1712, September 2014a. doi: 10.1093/mnras/stu1290.

H. Hirashita, A. Ferrara, P. Dayal, and M. Ouchi. Constraining dust formation in high-redshift young galaxies. MNRAS, 443:1704–1712, September 2014b. doi: 10.1093/mnras/stu1290.

H. Hirashita, T. Nozawa, R. S. Asano, and T. Lee. Revisiting the lifetime estimate of large presolar grains in the interstellar medium. Planet. Space Sci., 133:17–22, November 2016. doi: 10.1016/j.pss.2016.02.006.

H. Hoekstra, Y. Mellier, L. van Waerbeke, E. Semboloni, L. Fu, M. J. Hudson, L. C. Parker, I. Tereno, and K. Benabed. First Cosmic Shear Results from the Canada-France-Hawaii Telescope Wide Synoptic Legacy Survey. ApJ, 647:116–127, August 2006. doi: 10.1086/503249.

T. Hosokawa, K. Omukai, N. Yoshida, and H. W. Yorke. Protostellar Feedback Halts the Growth of the First Stars in the Universe. *Science*, 334:1250, December 2011. doi: 10.1126/science.1207433.

T. Hosokawa, S. Hirano, R. Kuiper, H. W. Yorke, K. Omukai, and N. Yoshida. Formation of Massive Primordial Stars: Intermittent UV Feedback with Episodic Mass Accretion. ApJ, 824:119, June 2016. doi: 10.3847/0004-637X/824/2/119.

J. H. Howell, L. Armus, J. M. Mazzarella, A. S. Evans, J. A. Surace, D. B. Sanders, A. Petric, P. Appleton, G. Bothun, C. Bridge, B. H. P. Chan, V. Charmandaris, D. T. Frayer, S. Haan, H. Inami, D.-C. Kim, S. Lord, B. F. Madore, J. Melbourne, B. Schulz, V. U, T. Vavilkin, S. Veilleux, and K. Xu. The great observatories all-sky lirg survey: Comparison of ultraviolet and far-infrared properties. ApJ, 715:572, 2010.

R. Hultman Kramer, Z. Haiman, and P. Madau. Delayed Enrichment by Unseen Galaxies: Explaining the Rapid Rise in IGM CIV Absorption from z = 6-5. *ArXiv e-prints*, July 2010.

J. A. Hummel, A. H. Pawlik, M. Milosavljević, and V. Bromm. The Source Density and Observability of Pair-instability Supernovae from the First Stars. ApJ, 755:72, August 2012. doi: 10.1088/0004-637X/755/1/72.

A. Hutter, P. Dayal, A. M. Partl, and V. Müller. The visibility of Lyman α emitters: constraining reionization, ionizing photon escape fractions and dust. MNRAS, 441:2861–2877, July 2014. doi: 10.1093/mnras/stu791.

G. D. Illingworth, D. Magee, P. A. Oesch, R. J. Bouwens, I. Labbé, M. Stiavelli, P. G. van Dokkum, M. Franx, M. Trenti, C. M. Carollo, and V. Gonzalez. The HST eXtreme Deep Field (XDF): Combining All ACS and WFC3/IR Data on the HUDF Region into the Deepest Field Ever. ApJS, 209:6, November 2013. doi: 10.1088/0067-0049/209/1/6.

J. Jaacks, R. Thompson, S. L. Finkelstein, and V. Bromm. Baseline Metal Enrichment from Population III Star Formation in Cosmological Volume Simulations. *ArXiv e-prints*, May 2017.

T. Jena, M. L. Norman, D. Tytler, D. Kirkman, N. Suzuki, A. Chapman, C. Melis, P. Paschos, B. O'Shea, G. So, D. Lubin, W.-C. Lin, D. Reimers, E. Janknecht, and C. Fechner. A concordance model of the Lyman α forest at z= 1.95. MNRAS, 361: 70–96, July 2005. doi: 10.1111/j.1365-2966.2005.09095.x.

M. Jeon, V. Bromm, A. H. Pawlik, and M. Milosavljević. The first galaxies: simulating their feedback-regulated assembly. MNRAS, 452:1152–1170, September 2015. doi: 10.1093/mnras/stv1353.

J. L. Johnson. Population III star clusters in the reionized Universe. MNRAS, 404:1425–1436, May 2010. doi: 10.1111/j.1365-2966.2010.16351.x.

J. L. Johnson, T. H. Greif, and V. Bromm. Local Radiative Feedback in the Formation of the First Protogalaxies. ApJ, 665:85–95, August 2007. doi: 10.1086/519212.

A. P. Jones, A. G. G. M. Tielens, D. J. Hollenbach, and C. F. McKee. Grain destruction in shocks in the interstellar medium. ApJ, 433:797–810, October 1994. doi: 10.1086/174689.

N. Kanekar, J. Wagg, R. Ram Chary, and C. L. Carilli. A Search for C II 158 μm Line Emission in HCM 6A, a Lyα Emitter at z = 6.56. ApJ, 771:L20, July 2013. doi: 10.1088/2041-8205/771/2/L20.

Z. Khakhaleva-Li and N. Y. Gnedin. Cosmic Reionization On Computers. Ultraviolet Continuum Slopes and Dust Opacities in High Redshift Galaxies. ApJ, 820:133, April 2016a. doi: 10.3847/0004-637X/820/2/133.

Z. Khakhaleva-Li and N. Y. Gnedin. Cosmic reionization on computers. ultraviolet continuum slopes and dust opacities in high redshift galaxies. ApJ, 820:133, 2016b.

T. D. Kitching, A. F. Heavens, A. N. Taylor, M. L. Brown, K. Meisenheimer, C. Wolf, M. E. Gray, and D. J. Bacon. Cosmological constraints from COMBO-17 using 3D weak lensing. MNRAS, 376:771–778, April 2007. doi: 10.1111/j.1365-2966.2007.11473.x.

K. K. Knudsen, D. Watson, D. Frayer, L. Christensen, A. Gallazzi, M. J. Michałowski, J. Richard, and J. Zavala. A merger in the dusty, z = 7.5 galaxy A1689-zD1? MNRAS, 466:138–146, April 2017. doi: 10.1093/mnras/stw3066.

M. Köhler, N. Ysard, and A. P. Jones. Dust evolution in the transition towards the denser ISM: impact on dust temperature, opacity, and spectral index. A&A, 579:A15, July 2015. doi: 10.1051/0004-6361/201525646.

E. Komatsu, J. Dunkley, M. R. Nolta, C. L. Bennett, B. Gold, G. Hinshaw, N. Jarosik, D. Larson, M. Limon, L. Page, D. N. Spergel, M. Halpern, R. S. Hill, A. Kogut, S. S. Meyer, G. S. Tucker, J. L. Weiland, E. Wollack, and E. L. Wright. Five-Year Wilkinson Microwave Anisotropy Probe Observations: Cosmological Interpretation. ApJS, 180: 330–376, February 2009. doi: 10.1088/0067-0049/180/2/330.

M. R. Krumholz, A. K. Leroy, and C. F. McKee. Which Phase of the Interstellar Medium Correlates with the Star Formation Rate? ApJ, 731:25, April 2011. doi: 10.1088/0004-637X/731/1/25.

M. R. Krumholz, A. Dekel, and C. F. McKee. A universal, local star formation law in galactic clouds, nearby galaxies, high-redshift disks, and starbursts. ApJ, 745:69, 2012.

T.-M. Kuo and H. Hirashita. Impact of grain size distributions on the dust enrichment in high-redshift quasars. MNRAS, 424:L34–L38, July 2012. doi: 10.1111/j.1745-3933.2012.01282.x.

N. Laporte, A. Streblyanska, S. Kim, R. Pelló, F. E. Bauer, D. Bina, G. Brammer, M. A. De Leo, L. Infante, and I. Pérez-Fournon. Frontier Fields: Combining HST, VLT, and Spitzer data to explore the z ∼ 8 Universe behind the lensing cluster MACSJ0416.1-2403. A&A, 575:A92, March 2015. doi: 10.1051/0004-6361/201425040.

N. Laporte, F. E. Bauer, P. Troncoso-Iribarren, X. Huang, J. González-López, S. Kim, T. Anguita, M. Aravena, L. F. Barrientos, R. Bouwens, L. Bradley, G. Brammer, M. Carrasco, R. Carvajal, D. Coe, R. Demarco, R. S. Ellis, H. Ford, H. Francke, E. Ibar, L. Infante, R. Kneissl, A. M. Koekemoer, H. Messias, A. Muñoz Arancibia, N. Nagar, N. Padilla, R. Pelló, M. Postman, D. Quénard, C. Romero-Cañizales, E. Treister, E. Villard, W. Zheng, and A. Zitrin. The ALMA Frontier Fields Survey. II. Multiwavelength Photometric analysis of 1.1 mm continuum sources in Abell 2744, MACSJ0416.1-2403 and MACSJ1149.5+2223. A&A, 604:A132, August 2017a. doi: 10.1051/0004-6361/201730628.

N. Laporte, R. S. Ellis, F. Boone, F. E. Bauer, D. Quénard, G. W. Roberts-Borsani, R. Pelló, I. Pérez-Fournon, and A. Streblyanska. Dust in the Reionization Era: ALMA Observations of a z = 8.38 Gravitationally Lensed Galaxy. ApJ, 837:L21, March 2017b. doi: 10.3847/2041-8213/aa62aa.

C. Leitherer, D. Schaerer, J. D. Goldader, R. M. G. Delgado, C. Robert, D. F. Kune, D. F. de Mello, D. Devost, and T. M. Heckman. Starburst99: Synthesis Models for Galaxies with Active Star Formation. ApJS, 123:3–40, July 1999. doi: 10.1086/313233.

S. Lepp and J. M. Shull. Molecules in the early universe. ApJ, 280:465–469, May 1984. doi: 10.1086/162013.

R. C. Livermore, S. L. Finkelstein, and J. M. Lotz. Directly Observing the Galaxies Likely Responsible for Reionization. *ArXiv e-prints*, April 2016.

P. Madau and M. Dickinson. Cosmic Star-Formation History. ARA&A, 52:415–486, August 2014. doi: 10.1146/annurev-astro-081811-125615.

P. Madau, A. Ferrara, and M. J. Rees. Early Metal Enrichment of the Intergalactic Medium by Pregalactic Outflows. ApJ, 555:92–105, July 2001. doi: 10.1086/321474.

U. Maio and M. Viel. The first billion years of a warm dark matter universe. MNRAS, 446: 2760–2775, January 2015. doi: 10.1093/mnras/stu2304.

U. Maio, K. Dolag, B. Ciardi, and L. Tornatore. Metal and molecule cooling in simulations of structure formation. MNRAS, 379:963–973, August 2007. doi: 10.1111/j.1365-2966.2007.12016.x.

U. Maio, B. Ciardi, N. Yoshida, K. Dolag, and L. Tornatore. The onset of star formation in primordial haloes. A&A, 503:25–34, August 2009. doi: 10.1051/0004-6361/200912234.

U. Maio, B. Ciardi, K. Dolag, L. Tornatore, and S. Khochfar. The transition from population III to population II-I star formation. MNRAS, 407:1003–1015, September 2010. doi: 10.1111/j.1365-2966.2010.17003.x.

U. Maio, S. Khochfar, J. L. Johnson, and B. Ciardi. The interplay between chemical and mechanical feedback from the first generation of stars. MNRAS, 414:1145–1157, June 2011. doi: 10.1111/j.1365-2966.2011.18455.x.

R. Maiolino, R. Schneider, E. Oliva, S. Bianchi, A. Ferrara, F. Mannucci, M. Pedani, and M. Roca Sogorb. A supernova origin for dust in a high-redshift quasar. Nature, 431:533, 2004.

R. Maiolino, S. Carniani, A. Fontana, L. Vallini, L. Pentericci, A. Ferrara, E. Vanzella, A. Grazian, S. Gallerani, M. Castellano, S. Cristiani, G. Brammer, P. Santini, J. Wagg, and R. Williams. The assembly of 'normal' galaxies at z > 7 probed by ALMA. MNRAS, 452:54–68, September 2015. doi: 10.1093/mnras/stv1194.

M. Mancini, R. Schneider, L. Graziani, R. Valiante, P. Dayal, U. Maio, B. Ciardi, and L. K. Hunt. The dust mass in z > 6 normal star-forming galaxies. MNRAS, 451:L70–L74, July 2015. doi: 10.1093/mnrasl/slv070.

M. Mancini, R. Schneider, L. Graziani, R. Valiante, P. Dayal, U. Maio, and B. Ciardi. Interpreting the evolution of galaxy colours from z = 8 to 5. MNRAS, 462:3130–3145, November 2016. doi: 10.1093/mnras/stw1783.

S. Marassi, G. Chiaki, R. Schneider, M. Limongi, K. Omukai, T. Nozawa, A. Chieffi, and N. Yoshida. The Origin of the Most Iron-poor Star. ApJ, 794:100, October 2014. doi: 10.1088/0004-637X/794/2/100.

S. Marassi, R. Schneider, M. Limongi, A. Chieffi, M. Bocchio, and S. Bianchi. The metal and dust yields of the first massive stars. MNRAS, 454:4250–4266, December 2015. doi: 10.1093/mnras/stv2267.

M. Matsuura, E. Dwek, M. Meixner, M. Otsuka, B. Babler, M. J. Barlow, J. Roman-Duval, C. Engelbracht, K. Sandstrom, M. Lakićević, J. T. van Loon, G. Sonneborn, G. C. Clayton, K. S. Long, P. Lundqvist, T. Nozawa, K. D. Gordon, S. Hony, P. Panuzzo, K. Okumura, K. A. Misselt, E. Montiel, and M. Sauvage. Herschel Detects a Massive Dust Reservoir in Supernova 1987A. *Science*, 333:1258, September 2011. doi: 10.1126/science.1205983.

P. McDonald, U. Seljak, R. Cen, D. Shih, D. H. Weinberg, S. Burles, D. P. Schneider, D. J. Schlegel, N. A. Bahcall, J. W. Briggs, J. Brinkmann, M. Fukugita, Ž. Ivezić, S. Kent, and D. E. Vanden Berk. The Linear Theory Power Spectrum from the Lyα Forest in the Sloan Digital Sky Survey. ApJ, 635:761–783, December 2005. doi: 10.1086/497563.

C. McKee. Dust Destruction in the Interstellar Medium. In L. J. Allamandola and A. G. G. M. Tielens, editors, *Interstellar Dust*, volume 135 of *IAU Symposium*, page 431, 1989.

C. F. McKee and J. C. Tan. The Formation of the First Stars. II. Radiative Feedback Processes and Implications for the Initial Mass Function. ApJ, 681:771-797, July 2008. doi: 10.1086/587434.

C. F. McKee, D. J. Hollenbach, G. C. Seab, and A. G. G. M. Tielens. The structure of the time-dependent interstellar shocks and grain destruction in the interstellar medium. ApJ, 318:674–701, July 1987. doi: 10.1086/165403.

R. McKinnon, P. Torrey, M. Vogelsberger, C. C. Hayward, and F. Marinacci. Simulating the dust content of galaxies: successes and failures. MNRAS, 468:1505–1521, June 2017. doi: 10.1093/mnras/stx467.

D. J. McLeod, R. J. McLure, J. S. Dunlop, B. E. Robertson, R. S. Ellis, and T. A. Targett. New redshift z ≃ 9 galaxies in the hubble frontier fields: implications for early evolution of the uv luminosity density. MNRAS, 450:3032, 2015.

D. J. McLeod, R. J. McLure, and J. S. Dunlop. The z = 9-10 galaxy population in the hubble frontier fields and clash surveys: The z=9 lf and further evidence for a smooth decline in uv luminosity at z ≥ 8. *ArXiv e-prints*, 1602.05199, 2016.

R. J. McLure, M. Cirasuolo, J. S. Dunlop, S. Foucaud, and O. Almaini. The luminosity function, halo masses and stellar masses of luminous Lyman-break galaxies at redshifts 5 < z < 6. MNRAS, 395:2196–2209, June 2009. doi: 10.1111/j.1365-2966.2009.14677.x.

R. J. McLure, J. S. Dunlop, M. Cirasuolo, A. M. Koekemoer, E. Sabbi, D. P. Stark, T. A. Targett, and R. S. Ellis. Galaxies at z = 6-9 from the WFC3/IR imaging of the Hubble Ultra Deep Field. MNRAS, 403:960–983, April 2010. doi: 10.1111/j.1365-2966.2009.16176.x.

R. J. McLure, J. S. Dunlop, R. A. A. Bowler, E. Curtis-Lake, M. Schenker, R. S. Ellis, B. E. Robertson, A. M. Koekemoer, A. B. Rogers, Y. Ono, M. Ouchi, S. Charlot, V. Wild, D. P. Stark, S. R. Furlanetto, M. Cirasuolo, and T. A. Targett. A new multifield determination of the galaxy luminosity function at z = 7-9 incorporating the 2012 hubble ultra-deep field imaging. MNRAS, 432:2696, 2013.

G. R. Meurer, T. M. Heckman, and D. Calzetti. Dust Absorption and the Ultraviolet Luminosity Density at z ∼ 3 as Calibrated by Local Starburst Galaxies. ApJ, 521:64–80, August 1999. doi: 10.1086/307523.

M. J. Michałowski. Dust production 680–850 million years after the Big Bang. A&A, 577: A80, 2015.

M. J. Michałowski, E. J. Murphy, J. Hjorth, D. Watson, C. Gall, and J. S. Dunlop. Dust grain growth in the interstellar medium of 5 < z < 6.5 quasars. A&A, 522:A15, November 2010. doi: 10.1051/0004-6361/201014902.

J. Miralda-Escudé. On the Evolution of the Ionizing Emissivity of Galaxies and Quasars

Required by the Hydrogen Reionization. ApJ, 597:66–73, November 2003. doi: 10.1086/378286.

M. Mori, A. Ferrara, and P. Madau. Early Metal Enrichment by Pregalactic Outflows. II. Three-dimensional Simulations of Blow-Away. ApJ, 571:40–55, May 2002. doi: 10.1086/339913.

D. J. Mortlock, S. J. Warren, B. P. Venemans, M. Patel, P. C. Hewett, R. G. McMahon, C. Simpson, T. Theuns, E. A. Gonzáles-Solares, A. Adamson, S. Dye, N. C. Hambly, P. Hirst, M. J. Irwin, E. Kuiper, A. Lawrence, and H. J. A. Röttgering. A luminous quasar at a redshift of z = 7.085. Nature, 474:616–619, June 2011. doi: 10.1038/nature10159.

A. L. Muratov, O. Y. Gnedin, N. Y. Gnedin, and M. Zemp. Revisiting the First Galaxies: The Effects of Population III Stars on their Host Galaxies. ApJ, 772:106, August 2013. doi: 10.1088/0004-637X/772/2/106.

N. Murray. Star formation efficiencies and lifetimes of giant molecular clouds in the milky way. ApJ, 729:133, 2011.

A. Nanni, A. Bressan, P. Marigo, and L. Girardi. Evolution of thermally pulsing asymptotic giant branch stars - II. Dust production at varying metallicity. MNRAS, 434:2390–2417, September 2013. doi: 10.1093/mnras/stt1175.

D. Narayanan, R. Dave, B. Johnson, R. Thompson, C. Conroy, and J. E. Geach. The IRX-Beta Dust Attenuation Relation in Cosmological Galaxy Formation Simulations. *ArXiv e-prints*, May 2017.

J. F. Navarro, C. S. Frenk, and S. D. M. White. The Structure of Cold Dark Matter Halos. ApJ, 462:563, May 1996. doi: 10.1086/177173.

J. F. Navarro, C. S. Frenk, and S. D. M. White. A Universal Density Profile from Hierarchical Clustering. ApJ, 490:493–508, December 1997. doi: 10.1086/304888.

T. Nozawa, T. Kozasa, H. Umeda, K. Maeda, and K. Nomoto. Dust in the Early Universe: Dust Formation in the Ejecta of Population III Supernovae. ApJ, 598:785–803, December 2003. doi: 10.1086/379011.

T. Nozawa, T. Kozasa, and A. Habe. Dust destruction in the high-velocity shocks driven by supernovae in the early universe. ApJ, 648:435, 2006.

P. A. Oesch, R. J. Bouwens, G. D. Illingworth, C. M. Carollo, M. Franx, I. Labbé, D. Magee, M. Stiavelli, M. Trenti, and P. G. van Dokkum. z ∼ 7 Galaxies in the HUDF: First Epoch WFC3/IR Results. ApJ, 709:L16–L20, January 2010. doi: 10.1088/2041-8205/709/1/L16.

P. A. Oesch, I. Labbé, R. J. Bouwens, G. D. Illingworth, V. Gonzalez, M. Franx, M. Trenti, B. P. Holden, P. G. van Dokkum, and D. Magee. A Rest-frame Optical View on z ∼ 4 Galaxies. I. Color and Age Distributions from Deep IRAC Photometry of the IUDF10 and GOODS Surveys. ApJ, 772:136, August 2013. doi: 10.1088/0004-637X/772/2/136.

P. A. Oesch, R. J. Bouwens, G. D. Illingworth, I. Labbé, R. Smit, M. Franx, P. G. van Dokkum, I. Momcheva, M. L. N. Ashby, G. G. Fazio, J.-S. Huang, S. P. Willner, V. Gonzalez, D. Magee, M. Trenti, G. B. Brammer, R. E. Skelton, and L. R. Spitler. The most luminous z ∼ 9-10 galaxy candidates yet found: The luminosity function, cosmic star-formation rate, and the first mass density estimate at 500 myr. ApJ, 786:108, 2014.

P. A. Oesch, G. Brammer, P. G. van Dokkum, G. D. Illingworth, R. J. Bouwens, I. Labbe, M. Franx, I. Momcheva, M. L. N. Ashby, G. G. Fazio, V. Gonzalez, B. Holden, D. Magee, R. E. Skelton, R. Smit, L. R. Spitler, M. Trenti, and S. P. Willner. A remarkably luminous galaxy at z=11.1 measured with hubble space telescope grism spectroscopy. *ArXiv e-prints*, 1603.00461, 2016.

K. Omukai. Protostellar Collapse with Various Metallicities. ApJ, 534:809–824, May 2000. doi: 10.1086/308776.

K. Omukai, T. Tsuribe, R. Schneider, and A. Ferrara. Thermal and Fragmentation Properties of Star-forming Clouds in Low-Metallicity Environments. ApJ, 626:627–643, June 2005. doi: 10.1086/429955.

K. Omukai, T. Hosokawa, and N. Yoshida. Low-metallicity Star Formation: Prestellar Collapse and Protostellar Accretion in the Spherical Symmetry. ApJ, 722:1793–1815, October 2010. doi: 10.1088/0004-637X/722/2/1793.

K. Ota, F. Walter, K. Ohta, B. Hatsukade, C. L. Carilli, E. da Cunha, J. González-López, R. Decarli, J. A. Hodge, H. Nagai, E. Egami, L. Jiang, M. Iye, N. Kashikawa, D. A. Riechers, F. Bertoldi, P. Cox, R. Neri, and A. Weiss. ALMA Observation of 158 μm [C II] Line and Dust Continuum of a z = 7 Normally Star-forming Galaxy in the Epoch of Reionization. ApJ, 792:34, September 2014. doi: 10.1088/0004-637X/792/1/34.

M. Otsuka, J. T. van Loon, K. S. Long, M. Meixner, M. Matsuura, W. T. Reach, J. Roman-Duval, K. Gordon, M. Sauvage, S. Hony, K. Misselt, C. Engelbracht, P. Panuzzo, K. Okumura, P. M. Woods, F. Kemper, and G. C. Sloan. Dust in the bright supernova remnant N49 in the LMC. A&A, 518:L139, July 2010. doi: 10.1051/0004-6361/201014642.

M. Ouchi, R. Ellis, Y. Ono, K. Nakanishi, K. Kohno, R. Momose, Y. Kurono, M. L. N. Ashby, K. Shimasaku, S. P. Willner, G. G. Fazio, Y. Tamura, and D. Iono. An Intensely Star-forming Galaxy at z $\sim$ 7 with Low Dust and Metal Content Revealed by Deep ALMA and HST Observations. ApJ, 778:102, December 2013. doi: 10.1088/0004-637X/778/2/102.

R. A. Overzier, T. M. Heckman, J. Wang, L. Armus, V. Buat, J. Howell, G. Meurer, M. Seibert, B. Siana, A. Basu-Zych, S. Charlot, T. S. Gonçalves, D. C. Martin, J. D. Neill, R. M. Rich, S. Salim, and D. Schiminovich. Dust attenuation in uv-selected starbursts at high redshift and their local counterparts: Implications for the cosmic star formation rate density. ApJ, 726:L7, 2011.

P. Padovani and F. Matteucci. Stellar Mass Loss in Elliptical Galaxies and the Fueling of Active Galactic Nuclei. ApJ, 416:26, October 1993. doi: 10.1086/173212.

F. Palla, D. Galli, and J. Silk. Deuterium in the Universe. ApJ, 451:44, September 1995. doi: 10.1086/176198.

A. Pallottini, A. Ferrara, S. Gallerani, S. Salvadori, and V. D'Odorico. Simulating cosmic metal enrichment by the first galaxies. MNRAS, 440:2498–2518, May 2014. doi: 10.1093/mnras/stu451.

T. Pan, D. Kasen, and A. Loeb. Pair-instability supernovae at the epoch of reionization. MNRAS, 422:2701–2711, May 2012. doi: 10.1111/j.1365-2966.2012.20837.x.

P. J. E. Peebles. *Principles of Physical Cosmology*. 1993.

Y. C. Pei. Interstellar dust from the Milky Way to the Magellanic Clouds. ApJ, 395: 130–139, August 1992. doi: 10.1086/171637.

D. A. Perley, J. S. Bloom, C. R. Klein, S. Covino, T. Minezaki, P. Woźniak, W. T. Vestrand, G. G. Williams, P. Milne, N. R. Butler, A. C. Updike, T. Krühler, P. Afonso, A. Antonelli, L. Cowie, P. Ferrero, J. Greiner, D. H. Hartmann, Y. Kakazu, A. Küpcü Yoldaş, A. N. Morgan, P. A. Price, J. X. Prochaska, and Y. Yoshii. Evidence for supernova-synthesized dust from the rising afterglow of grb071025 at z $\sim$ 5. MNRAS, 406:2473, 2010.

M. Pettini, M. Kellogg, C. C. Steidel, M. Dickinson, K. L. Adelberger, and M. Giavalisco. Infrared observations of nebular emission lines from galaxies at z $\sim=$ 3. ApJ, 508:539, 1998.

Planck Collaboration, P. A. R. Ade, N. Aghanim, M. Arnaud, M. Ashdown, J. Aumont, C. Baccigalupi, A. J. Banday, R. B. Barreiro, J. G. Bartlett, and et al. Planck 2015 results. XIII. Cosmological parameters. A&A, 594:A13, September 2016. doi: 10.1051/0004-6361/201525830.

G. Popping, R. S. Somerville, and M. Galametz. The dust content of galaxies from z = 0 to z = 9. MNRAS, 471:3152–3185, November 2017. doi: 10.1093/mnras/stx1545.

N. A. Reddy, D. K. Erb, M. Pettini, C. C. Steidel, and A. E. Shapley. Dust obscuration and metallicity at high redshift: New inferences from uv, hα, and 8 μm observations of z $\sim$ 2 star-forming galaxies. ApJ, 712:1070, 2010.

T. H. Reiprich and H. Böhringer. Constraining Cosmological Models with the Brightest Galaxy Clusters in the X-Ray Sky. In M. Gilfanov, R. Sunyeav, and E. Churazov, editors, *Lighthouses of the Universe: The Most Luminous Celestial Objects and Their Use for Cosmology*, page 84, 2002. doi: 10.1007/10856495_12.

M. Ricotti, N. Y. Gnedin, and J. M. Shull. The Fate of the First Galaxies. III. Properties of Primordial Dwarf Galaxies and Their Impact on the Intergalactic Medium. ApJ, 685: 21-39, September 2008. doi: 10.1086/590901.

J. S. Ritter, A. Sluder, C. Safranek-Shrader, M. Milosavljević, and V. Bromm. Metal transport and chemical heterogeneity in early star forming systems. MNRAS, 451:1190–1198, August 2015. doi: 10.1093/mnras/stv982.

J. S. Ritter, C. Safranek-Shrader, M. Milosavljević, and V. Bromm. Towards ab initio extremely metal-poor stars. MNRAS, 463:3354–3364, December 2016. doi: 10.1093/mnras/stw2220.

A. B. Rogers, R. J. McLure, J. S. Dunlop, R. A. A. Bowler, E. F. Curtis-Lake, P. Dayal, S. M. Faber, H. C. Ferguson, S. L. Finkelstein, N. A. Grogin, N. P. Hathi, D. Kocevski, A. M. Koekemoer, and P. Kurczynski. The colour distribution of galaxies at redshift five. MNRAS, 440:3714–3725, June 2014. doi: 10.1093/mnras/stu558.

C. E. Rydberg, E. Zackrisson, and P. Scott. Can the James Webb Space Telescope detect isolated population III stars? In M. Raue, T. Kneiske, D. Horns, D. Elsaesser, and P. Hauschildt, editors, *Cosmic Radiation Fields: Sources in the early Universe (CRF 2010)*, page 26, 2010.

Y. Sakurai, E. I. Vorobyov, T. Hosokawa, N. Yoshida, K. Omukai, and H. W. Yorke. Supermassive star formation via episodic accretion: protostellar disc instability and radiative feedback efficiency. MNRAS, 459:1137–1145, June 2016. doi: 10.1093/mnras/stw637.

S. Salvadori, R. Schneider, and A. Ferrara. Cosmic stellar relics in the Galactic halo. MNRAS, 381:647–662, October 2007. doi: 10.1111/j.1365-2966.2007.12133.x.

R. Salvaterra, A. Ferrara, and P. Dayal. Simulating high-redshift galaxies. MNRAS, 414: 847–859, June 2011. doi: 10.1111/j.1365-2966.2010.18155.x.

R. Salvaterra, U. Maio, B. Ciardi, and M. A. Campisi. Simulating high-z gamma-ray burst host galaxies. MNRAS, 429:2718, 2013.

F. Santoro and J. M. Shull. Critical Metallicity and Fine-Structure Emission of Primordial Gas Enriched by the First Stars. ApJ, 643:26–37, May 2006. doi: 10.1086/501518.

A. Sarangi and I. Cherchneff. The Chemically Controlled Synthesis of Dust in Type II-P Supernovae. ApJ, 776:107, October 2013. doi: 10.1088/0004-637X/776/2/107.

C. Scannapieco, P. B. Tissera, S. D. M. White, and V. Springel. Feedback and metal enrichment in cosmological smoothed particle hydrodynamics simulations - I. A model for chemical enrichment. MNRAS, 364:552–564, December 2005. doi: 10.1111/j.1365-2966.2005.09574.x.

D. Schaerer and S. de Barros. The impact of nebular emission on the ages of z∼6 galaxies. A&A, 502:423–426, August 2009. doi: 10.1051/0004-6361/200911781.

D. Schaerer, K. Nakajima, M. Dessauges-Zavadsky, G. Walth, W. Rujopakarn, J. Richard, and E. Egami. Spatially-resolved dust, molecular gas, and star formation maps of an exceptional strongly lensed giant arc at z=2. *IAU General Assembly*, 22:58419, August 2015.

R. Schneider, A. Ferrara, P. Natarajan, and K. Omukai. First Stars, Very Massive Black Holes, and Metals. ApJ, 571:30–39, May 2002. doi: 10.1086/339917.

R. Schneider, A. Ferrara, and R. Salvaterra. Dust formation in very massive primordial supernovae. MNRAS, 351:1379–1386, July 2004. doi: 10.1111/j.1365-2966.2004.07876.x.

R. Schneider, K. Omukai, A. K. Inoue, and A. Ferrara. Fragmentation of star-forming clouds enriched with the first dust. MNRAS, 369:1437–1444, July 2006. doi: 10.1111/j.1365-2966.2006.10391.x.

R. Schneider, K. Omukai, S. Bianchi, and R. Valiante. The first low-mass stars: critical metallicity or dust-to-gas ratio? MNRAS, 419:1566–1575, January 2012a. doi: 10.1111/j.1365-2966.2011.19818.x.

R. Schneider, K. Omukai, S. Bianchi, and R. Valiante. The first low-mass stars: critical metallicity or dust-to-gas ratio? MNRAS, 419:1566–1575, January 2012b. doi: 10.1111/j.1365-2966.2011.19818.x.

R. Schneider, R. Valiante, P. Ventura, F. dell'Agli, M. Di Criscienzo, H. Hirashita, and F. Kemper. Dust production rate of asymptotic giant branch stars in the Magellanic Clouds. MNRAS, 442:1440–1450, August 2014. doi: 10.1093/mnras/stu861.

R. Schneider, R. Valiante, P. Ventura, F. dell'Agli, and M. di Criscienzo. Dust in the Early Universe and the Contribution of AGB Stars. In F. Kerschbaum, R. F. Wing, and J. Hron, editors, *Why Galaxies Care about AGB Stars III: A Closer Look in Space and Time*, volume 497 of *Astronomical Society of the Pacific Conference Series*, page 369, August 2015.

R. Schneider, L. Hunt, and R. Valiante. The dust content of the most metal-poor star-forming galaxies. MNRAS, 457:1842, 2016.

I. Shimizu, A. K. Inoue, T. Okamoto, and N. Yoshida. Physical properties of UDF12 galaxies in cosmological simulations. MNRAS, 440:731–745, May 2014. doi: 10.1093/mnras/stu265.

B. Siana, I. Smail, A. M. Swinbank, J. Richard, H. I. Teplitz, K. E. K. Coppin, R. S. Ellis, D. P. Stark, J.-P. Kneib, and A. C. Edge. Detection of far-infrared and polycyclic aromatic hydrocarbon emission from the cosmic eye: Probing the dust and star formation of lyman break galaxies. ApJ, 698:1273, 2009.

L. J. Smith. Stellar Feedback at Low Metallicity: The Gas Dynamics of the Young SMC Cluster NGC 346. In L. Drissen, C. Robert, N. St-Louis, and A. F. J. Moffat, editors, *Proceedings of a Scientific Meeting in Honor of Anthony F. J. Moffat*, volume 465 of *Astronomical Society of the Pacific Conference Series*, page 416, December 2012.

M. Song, S. L. Finkelstein, M. L. N. Ashby, A. Grazian, Y. Lu, C. Papovich, B. Salmon, R. S. Somerville, M. Dickinson, K. Duncan, S. M. Faber, G. G. Fazio, H. C. Ferguson, A. Fontana, Y. Guo, N. Hathi, S.-K. Lee, E. Merlin, and S. P. Willner. The Evolution of the Galaxy Stellar Mass Function at z = 4–8: A Steepening Low-mass-end Slope with Increasing Redshift. ApJ, 825:5, July 2016. doi: 10.3847/0004-637X/825/1/5.

D. N. Spergel, L. Verde, H. V. Peiris, E. Komatsu, M. R. Nolta, C. L. Bennett, M. Halpern, G. Hinshaw, N. Jarosik, A. Kogut, M. Limon, S. S. Meyer, L. Page, G. S. Tucker, J. L. Weiland, E. Wollack, and E. L. Wright. First-Year Wilkinson Microwave Anisotropy Probe (WMAP) Observations: Determination of Cosmological Parameters. ApJS, 148: 175–194, September 2003. doi: 10.1086/377226.

D. N. Spergel, R. Bean, O. Doré, M. R. Nolta, C. L. Bennett, J. Dunkley, G. Hinshaw, N. Jarosik, E. Komatsu, L. Page, H. V. Peiris, L. Verde, M. Halpern, R. S. Hill, A. Kogut, M. Limon, S. S. Meyer, N. Odegard, G. S. Tucker, J. L. Weiland, E. Wollack, and E. L. Wright. Three-Year Wilkinson Microwave Anisotropy Probe (WMAP) Observations: Implications for Cosmology. ApJS, 170:377–408, June 2007. doi: 10.1086/513700.

V. Springel. The cosmological simulation code GADGET-2. MNRAS, 364:1105–1134, December 2005. doi: 10.1111/j.1365-2966.2005.09655.x.

V. Springel and L. Hernquist. Cosmological smoothed particle hydrodynamics simulations: a hybrid multiphase model for star formation. MNRAS, 339:289–311, February 2003. doi: 10.1046/j.1365-8711.2003.06206.x.

A. Stacy, T. H. Greif, and V. Bromm. The first stars: formation of binaries and small multiple systems. MNRAS, 403:45–60, March 2010. doi: 10.1111/j.1365-2966.2009.16113.x.

A. Stacy, T. H. Greif, and V. Bromm. The first stars: mass growth under protostellar feedback. MNRAS, 422:290–309, May 2012. doi: 10.1111/j.1365-2966.2012.20605.x.

A. Stacy, V. Bromm, and A. T. Lee. Building up the Population III initial mass function from cosmological initial conditions. MNRAS, 462:1307–1328, October 2016. doi: 10.1093/mnras/stw1728.

E. R. Stanway, R. G. McMahon, and A. J. Bunker. Near-infrared properties of i-drop galaxies in the Hubble Ultra Deep Field. MNRAS, 359:1184–1192, May 2005. doi: 10.1111/j.1365-2966.2005.08977.x.

T. K. Starkenburg, A. Helmi, and L. V. Sales. Dark influences II. Gas and star formation in minor mergers of dwarf galaxies with dark satellites. A&A, 587:A24, March 2016. doi: 10.1051/0004-6361/201527247.

G. Stratta, R. Maiolino, F. Fiore, and V. D'Elia. Dust properties at z = 6.3 in the host galaxy of grb 050904. ApJ, 661:L9, 2007.

N. Sugiyama. Cosmic Background Anisotropies in Cold Dark Matter Cosmology. ApJS, 100:281, October 1995. doi: 10.1086/192220.

H. Susa. The Mass of the First Stars. ApJ, 773:185, August 2013. doi: 10.1088/0004-637X/773/2/185.

H. Susa, K. Hasegawa, and N. Tominaga. The Mass Spectrum of the First Stars. ApJ, 792: 32, September 2014. doi: 10.1088/0004-637X/792/1/32.

T. T. Takeuchi, V. Buat, S. Heinis, E. Giovannoli, F.-T. Yuan, J. Iglesias-Páramo, K. L. Murata, and D. Burgarella. Star formation and dust extinction properties of local galaxies from the akari-galex all-sky surveys . first results from the most secure multiband sample from the far-ultraviolet to the far-infrared. A&A, 514:A4, 2010.

M. Talia, A. Cimatti, L. Pozzetti, G. Rodighiero, C. Gruppioni, F. Pozzi, E. Daddi, C. Maraston, M. Mignoli, and J. Kurk. The star formation rate cookbook at $1 < z < 3$: Extinction-corrected relations for uv and [oii]λ3727 luminosities. A&A, 582:A80, 2015.

M. Tegmark, A. de Oliveira-Costa, M. J. Devlin, C. B. Netterfield, L. Page, and E. J. Wollack. A High-Resolution Map of the Cosmic Microwave Background around the North Celestial Pole. ApJ, 474:L77–L80, January 1997. doi: 10.1086/310440.

M. Tegmark, M. A. Strauss, M. R. Blanton, K. Abazajian, S. Dodelson, H. Sandvik, X. Wang, D. H. Weinberg, I. Zehavi, N. A. Bahcall, F. Hoyle, D. Schlegel, R. Scoccimarro, M. S. Vogeley, A. Berlind, T. Budavari, A. Connolly, D. J. Eisenstein, D. Finkbeiner, J. A. Frieman, J. E. Gunn, L. Hui, B. Jain, D. Johnston, S. Kent, H. Lin, R. Nakajima, R. C. Nichol, J. P. Ostriker, A. Pope, R. Scranton, U. Seljak, R. K. Sheth, A. Stebbins, A. S. Szalay, I. Szapudi, Y. Xu, J. Annis, J. Brinkmann, S. Burles, F. J. Castander, I. Csabai, J. Loveday, M. Doi, M. Fukugita, B. Gillespie, G. Hennessy, D. W. Hogg, Ž. Ivezić, G. R. Knapp, D. Q. Lamb, B. C. Lee, R. H. Lupton, T. A. McKay, P. Kunszt, J. A. Munn, L. O'Connell, J. Peoples, J. R. Pier, M. Richmond, C. Rockosi, D. P. Schneider, C. Stoughton, D. L. Tucker, D. E. vanden Berk, B. Yanny, and D. G. York. Cosmological parameters from SDSS and WMAP. Phys. Rev. D, 69(10):103501, May 2004. doi: 10.1103/PhysRevD.69.103501.

F.-K. Thielemann, D. Argast, F. Brachwitz, W. R. Hix, P. Höflich, M. Liebendörfer, G. Martinez-Pinedo, A. Mezzacappa, I. Panov, and T. Rauscher. Nuclear cross sec-

tions, nuclear structure and stellar nucleosynthesis. *Nuclear Physics A*, 718:139–146, May 2003. doi: 10.1016/S0375-9474(03)00704-8.

V. Tilvi, C. Papovich, K.-V. H. Tran, I. Labbé, L. R. Spitler, C. M. S. Straatman, S. E. Persson, A. Monson, K. Glazebrook, R. F. Quadri, P. van Dokkum, M. L. N. Ashby, S. M. Faber, G. G. Fazio, S. L. Finkelstein, H. C. Ferguson, N. A. Grogin, G. G. Kacprzak, D. D. Kelson, A. M. Koekemoer, D. Murphy, P. J. McCarthy, J. A. Newman, B. Salmon, and S. P. Willner. Discovery of Lyman Break Galaxies at z $\sim$ 7 from the zFourGE Survey. ApJ, 768:56, May 2013. doi: 10.1088/0004-637X/768/1/56.

P. Todini and A. Ferrara. Dust formation in primordial Type II supernovae. MNRAS, 325: 726–736, August 2001. doi: 10.1046/j.1365-8711.2001.04486.x.

L. Tornatore, S. Borgani, K. Dolag, and F. Matteucci. Chemical enrichment of galaxy clusters from hydrodynamical simulations. MNRAS, 382:1050–1072, December 2007a. doi: 10.1111/j.1365-2966.2007.12070.x.

L. Tornatore, A. Ferrara, and R. Schneider. Population III stars: hidden or disappeared? MNRAS, 382:945–950, December 2007b. doi: 10.1111/j.1365-2966.2007.12215.x.

M. J. Turk, J. S. Oishi, T. Abel, and G. L. Bryan. Magnetic Fields in Population III Star Formation. ApJ, 745:154, February 2012. doi: 10.1088/0004-637X/745/2/154.

R. Valiante, R. Schneider, S. Bianchi, and A. C. Andersen. Stellar sources of dust in the high-redshift Universe. MNRAS, 397:1661–1671, August 2009. doi: 10.1111/j.1365-2966.2009.15076.x.

R. Valiante, R. Schneider, S. Salvadori, and S. Bianchi. The origin of the dust in high-redshift quasars: the case of SDSS J1148+5251. MNRAS, 416:1916–1935, September 2011. doi: 10.1111/j.1365-2966.2011.19168.x.

R. Valiante, R. Schneider, R. Maiolino, S. Salvadori, and S. Bianchi. Quasar feedback in the early Universe: the case of SDSS J1148+5251. MNRAS, 427:L60–L64, November 2012. doi: 10.1111/j.1745-3933.2012.01345.x.

R. Valiante, R. Schneider, S. Salvadori, and S. Gallerani. High-redshift quasars host galaxies: is there a stellar mass crisis? MNRAS, 444:2442–2455, November 2014. doi: 10.1093/mnras/stu1613.

L. Vallini, P. Dayal, and A. Ferrara. Molecular hydrogen in Lyman alpha emitters. MNRAS, 421:3266–3276, April 2012. doi: 10.1111/j.1365-2966.2012.20551.x.

L. B. van den Hoek and M. A. T. Groenewegen. New theoretical yields of intermediate mass stars. A&AS, 123:305–328, June 1997. doi: 10.1051/aas:1997162.

G. A. Vázquez and C. Leitherer. Optimization of Starburst99 for Intermediate-Age and Old Stellar Populations. ApJ, 621:695–717, March 2005. doi: 10.1086/427866.

B. P. Venemans, G. A. Verdoes Kleijn, J. Mwebaze, E. A. Valentijn, E. Bañados, R. Decarli, J. T. A. de Jong, J. R. Findlay, K. H. Kuijken, F. La Barbera, J. P. McFarland, R. G. McMahon, N. Napolitano, G. Sikkema, and W. J. Sutherland. First discoveries of z $\sim$ 6 quasars with the Kilo-Degree Survey and VISTA Kilo-Degree Infrared Galaxy survey. MNRAS, 453:2259–2266, November 2015. doi: 10.1093/mnras/stv1774.

P. Ventura, M. D. Criscienzo, R. Schneider, R. Carini, R. Valiante, F. D'Antona, S. Gallerani, R. Maiolino, and A. Tornambé. Dust formation around AGB and SAGB stars: a trend with metallicity? MNRAS, 424:2345–2357, August 2012a. doi: 10.1111/j.1365-2966.2012.21403.x.

P. Ventura, M. di Criscienzo, R. Schneider, R. Carini, R. Valiante, F. D'Antona, S. Gallerani, R. Maiolino, and A. Tornambé. The transition from carbon dust to silicate production in low-metallicity asymptotic giant branch and super-asymptotic giant branch stars. MNRAS, 420:1442–1456, February 2012b. doi: 10.1111/j.1365-2966.2011.20129.x.

P. Ventura, F. Dell'Agli, R. Schneider, M. Di Criscienzo, C. Rossi, F. La Franca, S. Gallerani, and R. Valiante. Dust from asymptotic giant branch stars: relevant factors and modelling uncertainties. MNRAS, 439:977–989, March 2014. doi: 10.1093/mnras/stu028.

E. I. Vorobyov, A. L. DeSouza, and S. Basu. The Burst Mode of Accretion in Primordial Protostars. ApJ, 768:131, May 2013. doi: 10.1088/0004-637X/768/2/131.

K. Wada and A. Venkatesan. Feedback from the First Supernovae in Protogalaxies: The Fate of the Generated Metals. ApJ, 591:38–42, July 2003. doi: 10.1086/375335.

L. Wang, D. Baade, E. Baron, S. Bernard, V. Bromm, P. Brown, G. Clayton, J. Cooke, D. Croton, C. Curtin, M. Drout, M. Doi, I. Dominguez, S. Finkelstein, A. Gal-Yam, P. Geil, A. Heger, P. Hoeflich, J. Jian, K. Krisciunas, A. Koekemoer, R. Lunnan, K. Maeda, J. Maund, M. Modjaz, J. Mould, K. Nomoto, P. Nugent, F. Patat, F. Pacucci, M. Phillips, A. Rest, E. Regos, D. Sand, B. Sparks, J. Spyromilio, L. Staveley-Smith, N. Suntzeff, S. Uddin, B. Villarroel, J. Vinko, D. Whalen, J. Wheeler, M. Wood-Vasey, Y. Yang, and B. Yue. A First Transients Survey with JWST: the FLARE project. *ArXiv e-prints*, October 2017.

D. Waters, S. Wilkins, T. Di Matteo, Y. Feng, R. Croft, and D. Nagai. Monsters in the dark: Predictions for luminous galaxies in the early universe from the bluetides simulation. *ArXiv e-prints*, 2016.

D. Watson, L. Christensen, K. K. Knudsen, J. Richard, A. Gallazzi, and M. J. Michałowski. A dusty, normal galaxy in the epoch of reionization. Nature, 519:327–330, March 2015. doi: 10.1038/nature14164.

J. C. Weingartner and B. T. Draine. Dust Grain-Size Distributions and Extinction in the Milky Way, Large Magellanic Cloud, and Small Magellanic Cloud. ApJ, 548:296–309, February 2001. doi: 10.1086/318651.

Z. L. Wen, J. L. Han, and F. S. Liu. Mass function of rich galaxy clusters and its constraint on σ_8. MNRAS, 407:533–543, September 2010. doi: 10.1111/j.1365-2966.2010.16930.x.

D. Whalen, B. van Veelen, B. W. O'Shea, and M. L. Norman. The Destruction of Cosmological Minihalos by Primordial Supernovae. ApJ, 682:49-67, July 2008. doi: 10.1086/589643.

D. J. Whalen, W. Even, L. H. Frey, J. Smidt, J. L. Johnson, C. C. Lovekin, C. L. Fryer, M. Stiavelli, D. E. Holz, A. Heger, S. E. Woosley, and A. L. Hungerford. Finding the First Cosmic Explosions. I. Pair-instability Supernovae. ApJ, 777:110, November 2013. doi: 10.1088/0004-637X/777/2/110.

S. D. M. White, G. Efstathiou, and C. S. Frenk. The amplitude of mass fluctuations in the universe. MNRAS, 262:1023–1028, June 1993. doi: 10.1093/mnras/262.4.1023.

S. M. Wilkins, A. J. Bunker, E. Stanway, S. Lorenzoni, and J. Caruana. The ultraviolet properties of star-forming galaxies - I. HST WFC3 observations of very high redshift galaxies. MNRAS, 417:717–729, October 2011. doi: 10.1111/j.1365-2966.2011.19315.x.

S. M. Wilkins, V. Gonzalez-Perez, C. G. Lacey, and C. M. Baugh. Predictions for the intrinsic UV continuum properties of star-forming galaxies and the implications for inferring dust extinction. MNRAS, 424:1522–1529, August 2012. doi: 10.1111/j.1365-2966.2012.21344.x.

S. M. Wilkins, A. Bunker, W. Coulton, R. Croft, T. D. Matteo, N. Khandai, and Y. Feng. Interpreting the observed UV continuum slopes of high-redshift galaxies. MNRAS, 430: 2885–2890, April 2013. doi: 10.1093/mnras/stt096.

S. M. Wilkins, Y. Feng, T. Di-Matteo, R. Croft, E. R. Stanway, A. Bunker, D. Waters, and C. Lovell. The photometric properties of galaxies in the early Universe. MNRAS, 460: 3170–3178, August 2016. doi: 10.1093/mnras/stw1154.

C. J. Willott, L. Albert, D. Arzoumanian, J. Bergeron, D. Crampton, P. Delorme, J. B. Hutchings, A. Omont, C. Reylé, and D. Schade. Eddington-limited Accretion and the Black Hole Mass Function at Redshift 6. AJ, 140:546–560, August 2010. doi: 10.1088/0004-6256/140/2/546.

S. E. Woosley and T. A. Weaver. The Evolution and Explosion of Massive Stars. II. Explosive Hydrodynamics and Nucleosynthesis. ApJS, 101:181, November 1995. doi: 10.1086/192237.

X.-B. Wu, F. Wang, X. Fan, W. Yi, W. Zuo, F. Bian, L. Jiang, I. D. McGreer, R. Wang, J. Yang, Q. Yang, D. Thompson, and Y. Beletsky. An ultraluminous quasar with a twelve-billion-solar-mass black hole at redshift 6.30. Nature, 518:512–515, February 2015. doi: 10.1038/nature14241.

J. S. B. Wyithe and R. Cen. The Extended Star Formation History of the First Generation of Stars and the Reionization of Cosmic Hydrogen. ApJ, 659:890–907, April 2007. doi: 10.1086/511948.

H. Xu, K. Ahn, M. L. Norman, J. H. Wise, and B. W. O'Shea. X-Ray Background at High Redshifts from Pop III Remnants: Results from Pop III Star Formation Rates in the Renaissance Simulations. ApJ, 832:L5, November 2016a. doi: 10.3847/2041-8205/832/1/L5.

H. Xu, M. L. Norman, B. W. O'Shea, and J. H. Wise. Late Pop III Star Formation During the Epoch of Reionization: Results from the Renaissance Simulations. ApJ, 823:140, June 2016b. doi: 10.3847/0004-637X/823/2/140.

H. Xu, M. L. Norman, B. W. O'Shea, and J. H. Wise. Late Pop III Star Formation During the Epoch of Reionization: Results from the Renaissance Simulations. ApJ, 823:140, June 2016c. doi: 10.3847/0004-637X/823/2/140.

N. Yoshida, T. Abel, L. Hernquist, and N. Sugiyama. Simulations of Early Structure Formation: Primordial Gas Clouds. ApJ, 592:645–663, August 2003. doi: 10.1086/375810.

N. Yoshida, V. Bromm, and L. Hernquist. The Era of Massive Population III Stars: Cosmological Implications and Self-Termination. ApJ, 605:579–590, April 2004. doi: 10.1086/382499.

N. Yoshida, K. Omukai, L. Hernquist, and T. Abel. Formation of Primordial Stars in a ΛCDM Universe. ApJ, 652:6–25, November 2006. doi: 10.1086/507978.

T. Zafar, D. J. Watson, D. Malesani, P. M. Vreeswijk, J. P. U. Fynbo, J. Hjorth, A. J. Levan, and M. J. Michałowski. No evidence for dust extinction in grb 050904 at z ∼ 6.3. A&A, 515(A94), 2010.

J. A. Zavala, M. J. Michałowski, I. Aretxaga, G. W. Wilson, D. H. Hughes, A. Montaña, J. S. Dunlop, A. Pope, D. Sánchez-Argüelles, M. S. Yun, and M. Zeballos. Early science with the large millimeter telescope: dust constraints in a z ~ 9.6 galaxy. MNRAS, 453: L88, 2015.

S. Zhukovska. Dust origin in late-type dwarf galaxies: ISM growth vs. type II supernovae. A&A, 562:A76, February 2014. doi: 10.1051/0004-6361/201322989.

S. Zhukovska, H.-P. Gail, and M. Trieloff. Evolution of interstellar dust and stardust in the solar neighbourhood. A&A, 479:453–480, February 2008. doi: 10.1051/0004-6361:20077789.

S. Zhukovska, C. Dobbs, E. B. Jenkins, and R. S. Klessen. Modeling Dust Evolution in Galaxies with a Multiphase, Inhomogeneous ISM. ApJ, 831:147, November 2016. doi: 10.3847/0004-637X/831/2/147.

A. Zitrin, I. Labbé, S. Belli, R. Bouwens, R. S. Ellis, G. Roberts-Borsani, D. P. Stark, P. A. Oesch, and R. Smit. Lymanα Emission from a Luminous z = 8.68 Galaxy: Implications for Galaxies as Tracers of Cosmic Reionization. ApJ, 810:L12, September 2015. doi: 10.1088/2041-8205/810/1/L12.